

MASS TRANSFER AND KINETICS IN OXYGEN DELIGNIFICATION

A THESIS SUBMITTED TO
THE GRADUATE SCHOOL OF NATURAL AND APPLIED SCIENCES
OF
MIDDLE EAST TECHNICAL UNIVERSITY

BY

İSMAİL DOĞAN

IN PARTIAL FULFILLMENT OF THE REQUIREMENTS
FOR
THE DEGREE OF DOCTOR OF PHILOSOPHY
IN
CHEMICAL ENGINEERING

NOVEMBER 2004

Approval of the Graduate School of Natural and Applied Sciences

Prof. Dr. Canan Özgen
Director

I certify that this thesis satisfies all the requirements as a thesis for the degree of Doctor of Philosophy.

Prof. Dr. Timur Doğu
Head of Department

This is to certify that we have read this thesis and that in our opinion it is fully adequate, in scope and quality, as a thesis for the degree of Doctor of Philosophy.

Prof. Dr. Güniz Gürüz
Co-Supervisor

Prof. Dr. Hayrettin Yücel
Supervisor

Examining Committee Members

Prof. Dr. Ali Çulfaz (METU,CHE)

Prof. Dr. Hayrettin Yücel (METU,CHE)

Prof. Dr. Ülkü Yetiş (METU,ENVE)

Prof. Dr. Nurcan Baç (METU,CHE)

Prof. Dr. Tunçer Özdamar (AU,CHE)

I hereby declare that all information in this document has been obtained and presented in accordance with academic rules and ethical conduct. I also declare that, as required by these rules and conduct, I have fully cited and referenced all material and results that are not original to this work.

Name, Last Name : İsmail Doğan

Signature :

ABSTRACT

MASS TRANSFER AND KINETICS IN OXYGEN DELIGNIFICATION

Dođan, İsmail

Ph.D., Department of Chemical Engineering

Supervisor : Prof. Dr. Hayrettin Yücel

Co-Supervisor : Prof. Dr. Güniz Gürüz

November 2004, 147 pages

In this study, the kinetic analysis of oxygen delignification of Turkish southern hardwood Kraft pulp was carried out. Kraft pulp was obtained from Mopak Dalaman pulp and paper mill. The kinetic rate data were collected in a 1 L high pressure batch reactor. The delignification experiments were carried out under a wide range of industrially significant conditions of temperature (90, 100 and 110 °C), alkali charge (1, 3, 5% on oven dry pulp), and oxygen partial pressure (0.5, 3.5, 6.5 bar).

In order to achieve this objective, the study is separated into different stages. In the first stage of the work, the mass transfer effects were examined for different pulp consistencies. It was seen that the inter-fiber mass transfer resistances become negligible at the consistencies below 1%. Therefore, the experiments were performed at 0.5% consistency. In the following stage, the kinetics of oxygen delignification was studied and the governing rate equations were derived. Then, the kinetics of the carbohydrate degradation was analyzed in order to determine the extent of delignification without the reduction in the pulp strength. The delignification and the carbohydrate degradation rate during oxygen delignification increase with increasing in alkali concentration, oxygen

partial pressure and temperature. However, the most effective parameters are the alkali concentration and temperature. The dimensionless terms for Kappa number, intrinsic viscosity and reaction time were used in order to generalize the results and to make them independent of the initial Kappa number, the intrinsic viscosity, experimental conditions and pulping conditions prior to oxygen delignification. These dimensionless parameters were fitted to nonlinear equations from which the control of the oxygen delignification towers can be done with a simple equation. The same approach was also used for the reported studies in the literature which allowed the comparison with the results of this study.

In the final stage of the study, the simulation of the oxygen delignification unit preceding the CEHDED bleach plant is performed, in order to see the effect of oxygen delignification on the amount of total wastes coming out from the bleach plant. When an oxygen delignification unit is added to the existing CEHDED bleach plant, the amount of pollutants are decreased by 17.96% with output brightness of 92.95. When the overall process parameter optimization of the CEHDED bleach plant is done with oxygen delignification unit, the total amount of dissolved solids coming out from the six washers are decreased by 25.97% with output brightness of 89.5.

In order to reduce the pollution load and chemical consumption in Mopak Dalaman pulp and paper mill, management has decided to install an oxygen delignification unit to the plant. Therefore, the rate equations obtained from this study can form a basis for the design and optimization of oxygen reactor in the mill.

Keyword: Oxygen Delignification Kinetics, Rate Equations, Carbohydrate Degredation Kinetics, OCEHDED Simulation, Effluent Reduction

ÖZ

OKSİJENLE BEYAZLATMA KİNETİĞİ VE KÜTLE TRANSFERİ

Dođan, İsmail

Doktora, Kimya Mühendisliđi Bölümü

Tez Yöneticisi : Prof. Dr. Hayrettin Yücel

Ortak Tez Yöneticisi : Prof. Dr. Güniz Gürüz

Kasım 2004, 147 sayfa

Bu çalışmada, Türkiyenin güneyinde üretilen Kraft kısa elyaflı odun hamurunun oksijenle beyazlatma kinetiđi çalışılmıştır. Kraft seluloz hamuru Mopak Dalaman kağıt fabrikasından sağlanmışır. Kinetik analiz verileri yüksek basınca dayanıklı 1 litrelik kesikli reaktörde yapılan deneylerde elde edilmiştir. Delignifikasyon deneyleri endüstrinin kullandığı geniş sıcaklık (90, 100 ve 110 °C), alkali yükü (%1, 3 ve 5 kuru hamur miktarına göre) ve oksijen kısmi basınc (0.5, 3.5 ve 6.5 bar) aralıklarında gerçekleştirilmiştir.

Yukardaki amaca ulaşabilmek için, çalışma birçok aşamada gerçekleştirilmiştir. Bu çalışmanın ilk aşamasında, kütle transferi etkileri deđişik hamur yüzdelerinde incelenmiştir. Fiberler arası kütle transferi direncinin %1 lik hamur yüzdesinin altında azaldığı belirlenmiş ve deneyler %0.5 lik hamur yüzdesinde gerçekleştirilmiştir. Bunu izleyen aşamada, oksijenle beyazlatma kinetiđi çalışılmışır ve ilgili hız denklemleri çıkarılmışır. Daha sonra, hamurun dayanıklılıđını azaltmadan delignifikasyon miktarının ne kadar arttırılabileceđini belirlemek amacıyla, karbonhidrat degradasyon kinetiđinin analizi yapılmıştır.

Oksijenle beyazlatmada, delignifikasyon ve karbonhidrat degradasyon hızının artan alkali konsantrasyonu, oksijen kısmi basıncı ve sıcaklıkla arttığı gözlemlenmiştir. Fakat, en etkili parametreler alkali konsantrasyonu ve sıcaklıktır. Elde edilen sonuçları genelleştirmek ve giriş Kappa sayısı, içsel viskosite, deneysel koşullar ve oksijenle beyazlatma öncesi hamur özelliklerinden bağımsız kılmak amacı ile, Kappa sayısı, içsel viskosite ve reaksiyon zamanı için boyutsuz terimler tanımlanmıştır. Bu boyutsuz terimler doğrusal olmayan denklemlerin fonksiyonu olarak ifade edilmiştir. Bu sayede oksijenle beyazlatma kulelerinin kontrolü basit bir denklemle gerçekleştirilebilecektir.

Bu çalışmanın son bölümünde, oksijen delignifikasyon ünitesinin beyazlatma ünitesinden çıkan toplam kirletici miktarı üzerindeki etkisini görmek amacıyla, oksijen delignifikasyon ünitesinin CEHDED beyazlatma bölümüne eklenmiş şekli ile simülasyonu gerçekleştirilmiştir. Bu durumda elde edilen sonuçlar toplam kirletici miktarında %17.96'lık bir azalma, hamur beyazlığında 92.95'lik bir çıktıyla sağlanmıştır. Oksijen delignifikasyonlu CEHDED beyazlatma ünitesinde yapılan proses parametreleri optimizasyonu ile ise 89.5'luk hamur beyazlık değeri ile altı yıkayıcıdan çıkan toplam kirletici miktarında %25.97'lik bir azalma sağlanmıştır.

Mopak Dalaman kağıt fabrikasında yönetim, kirletici ve kullanılan kimyasal miktarını azaltmak amacıyla, oksijen delignifikasyon ünitesinin kurulmasına karar vermiştir. Bu nedenle, bu çalışmada elde edilen hız denklemleri oksijen reaktörünün tasarımında ve optimizasyonunda bir kaynak teşkil edecektir.

Anahtar Kelimeler: Oksijen Delignifikasyon Kinetiği, Hız Denklemleri, Karbonhidrat Degradasyon Kinetiği, OCEHDED Simülasyonu, Kirletici Azaltılması

To My Mother and Almila Bahar

ACKNOWLEDGEMENTS

I extend my sincerest appreciation and thanks to my thesis supervisors, Prof. Dr. Güniz Gürüz and Prof. Dr. Hayrettin Yücel for their guidance, kind support, encouragement and valuable discussions throughout the course of this research, without whom this work would not have been possible.

I would like to thank Prof. Dr. Ali Çulfaz and Prof. Dr. Ülkü Yetiş for their precious discussions and comments during the progress of this work. I am also grateful to the members of my thesis examining committee members Prof. Dr. Nurcan Baç and Prof. Dr. Tunçer Özdamar.

I also thank to MOPAK Dalaman pulp and paper mill management to supply the necessary pulp for this study. I would like to thank engineers and technicians working in the bleaching unit, for their valuable advices and help to perform this study.

I would like to thank the staff in the machinery shop, Süleyman N. Kuşhan, Adil Demir, Ertuğrul Özdemir, Nevzat Bekçi and İsa Çağlar for the construction of the experimental setup. Also, I want to thank Kerime Güney for the assistance and support in performing the analyses in the laboratory.

I would like to thank my colleagues and also my friends, Yusuf Göğebakan, Işıl Ayrancı, Yalçın Yıldız and Işık Aşar for their support and for providing an enjoyable working atmosphere.

Finally, my heartfelt thanks to my mother and my fiancé Almıla Bahar for their love and support.

TABLE OF CONTENTS

ABSTRACT	iv
ÖZ.....	vi
DEDICATION.....	viii
ACKNOWLEDGEMENTS	ix
TABLE OF CONTENTS	x
LIST OF TABLES	xiii
LIST OF FIGURES	xvii
NOMENCLATURE.....	xxiii
CHAPTER	
INTRODUCTION	1
1.1 Wood.....	1
1.2 Pulping and Bleaching	2
1.3 Oxygen Delignification.....	4
1.4 Objective and Scope of the Work	5
LITERATURE SURVEY	8
2.1 Oxygen Delignification Chemistry.....	8
2.1.1 Oxygen Chemistry	8
2.1.2 Lignin Reactions	10
2.1.3 Carbohydrate Reactions.....	12
2.1.4 Selectivity and Protectors	13
2.2 Mass Transfer	14
2.3 The Rate of Oxygen Delignification.....	15
2.4 The Kinetic Analysis of Carbohydrate Degradation	21
EXPERIMENTAL PROCEDURE	23
3.1 Pulp Preparation and Experimental Setup.....	23
3.2 Experimental Conditions	24

3.3 Experimental Procedure.....	25
3.4 Pulp and Liquor Analyses	26
RESULTS AND DISCUSSION	27
4.1 The Analysis of Mass Transfer	27
4.2 The results of Oxygen Delignification Experiments.....	30
4.3 The Kinetic Analysis of Carbohydrate Degradation	36
4.4 Comparison with Literature Data.....	50
4.5 The Method of Dimensionless Parameters	51
4.6 Simulation of CEHDED Bleach Plant with Oxygen Delignification Tower	56
4.6.1 Mathematical Models of the Unit Operations	57
4.6.2 Kinetic Models.....	59
4.6.3 Oxygen Delignification Unit Simulation and Case Studies Performed	61
4.6.3.1 Bleaching Chemicals	64
4.6.3.2 Retention Tower Reaction Temperature	65
4.6.3.3 Retention Time in the Tower	66
4.6.3.4 Consistency in the Tower.....	67
4.6.3.5 Wash Water Flow Rate in the Washer	67
4.6.3.6 Overall Optimization	68
CONCLUSIONS AND RECOMMENDATIONS	69
5.1 Conclusions	69
5.2 Recommendations	71
REFERENCES	72
STANDARDS	75
A.1 Kappa number of pulp (Tappi T236).....	75
A.2 Viscosity of pulp (ASTM D 1795 or Tappi T230).....	77
A.3 Determination of Residual Alkali (Tappi T625)	79
DELIGNIFICATION KINETICS CALCULATION PROCEDURE	80
B.1 Estimation of Rate Order q and Rate Constant k	80
B.1 .1 Integral Method	80
B.2 Estimation of A , E_a , m and n	111
CARBOHYDRATE DEGRADATION KINETICS CALCULATION PROCEDURE	113
C.1 Estimation of Rate Constant k_1 and k_2	113
C.2 Estimation of A_1 , E_{A1} , a , b , A_2 , E_{A2} , c , d	143
CURRICULUM VITAE.....	146

LIST OF TABLES

Table 3.1 Range of process variables.....	24
Table 4.1 The mathematical models used to simulate the mixer in bleach plant.....	57
Table 4.2 The CSTR and PFR model equations to represent the retention tower.....	58
Table 4.4 The kinetic expressions used in the model	60
Table 4.5 The input data for simulation of CEHDED bleach plant	62
Table 4.6 The simulation results with and without oxygen delignification.....	63
Table 4.7 The range of the process parameters studied in process parameter optimization.....	64
Table 4.8 The optimization of the bleaching chemicals for each stage	65
Table 4.9 The optimization of the reaction temperature for each stage	66
Table 4.10 The optimization of the retention time for each stage	66
Table 4.11 The optimization of the consistency for each stage.....	67
Table 4.12 The optimization of the wash water flow rates in the washers.....	68
Table A.1 Correction factor d , expressed as a function of V_1	76
Table B.1 Value for q and k estimated from the integral method for 0.5 bar, 0.05 g/L NaOH and 90 °C experiment	82
Table B.2 Value for q and k estimated from the integral method for 0.5 bar, 0.15 g/L NaOH and 90 °C experiment	83
Table B.3 Value for q and k estimated from the integral method for 0.5 bar, 0.25 g/L NaOH and 90 °C experiment	84
Table B.4 Value for q and k estimated from the integral method for 0.5 bar, 0.05 g/L NaOH and 100 °C experiment	85
Table B.5 Value for q and k estimated from the integral method for 0.5 bar, 0.15 g/L NaOH and 100 °C experiment	86
Table B.6 Value for q and k estimated from the integral method for 0.5 bar, 0.25 g/L NaOH and 100 °C experiment	87
Table B.7 Value for q and k estimated from the integral method for 0.5 bar, 0.05 g/L NaOH and 110 °C experiment	88

Table B.8 Value for q and k estimated from the integral method for 0.5 bar, 0.15 g/L NaOH and 110 °C experiment	89
Table B.9 Value for q and k estimated from the integral method for 0.5 bar, 0.25 g/L NaOH and 110 °C experiment	90
Table B.10 Value for q and k estimated from the integral method for 3.5 bar, 0.05 g/L NaOH and 90 °C experiment	91
Table B.11 Value for q and k estimated from the integral method for 3.5 bar, 0.15 g/L NaOH and 90 °C experiment	92
Table B.12 Value for q and k estimated from the integral method for 3.5 bar, 0.25 g/L NaOH and 90 °C experiment	93
Table B.13 Value for q and k estimated from the integral method for 3.5 bar, 0.05 g/L NaOH and 100 °C experiment	94
Table B.14 Value for q and k estimated from the integral method for 3.5 bar, 0.15 g/L NaOH and 100 °C experiment	95
Table B.15 Value for q and k estimated from the integral method for 3.5 bar, 0.25 g/L NaOH and 100 °C experiment	96
Table B.16 Value for q and k estimated from the integral method for 3.5 bar, 0.05 g/L NaOH and 110 °C experiment	97
Table B.17 Value for q and k estimated from the integral method for 3.5 bar, 0.15 g/L NaOH and 110 °C experiment	98
Table B.18 Value for q and k estimated from the integral method for 3.5 bar, 0.25 g/L NaOH and 110 °C experiment	99
Table B.19 Value for q and k estimated from the integral method for 6.5 bar, 0.05 g/L NaOH and 90 °C experiment	100
Table B.20 Value for q and k estimated from the integral method for 6.5 bar, 0.15 g/L NaOH and 90 °C experiment	101
Table B.21 Value for q and k estimated from the integral method for 6.5 bar, 0.25 g/L NaOH and 90 °C experiment	102
Table B.22 Value for q and k estimated from the integral method for 6.5 bar, 0.05 g/L NaOH and 100 °C experiment	103
Table B.23 Value for q and k estimated from the integral method for 6.5 bar, 0.15 g/L NaOH and 100 °C experiment	104
Table B.24 Value for q and k estimated from the integral method for 6.5 bar, 0.25 g/L NaOH and 100 °C experiment	105
Table B.25 Value for q and k estimated from the integral method for 6.5 bar, 0.05 g/L NaOH and 110 °C experiment	106
Table B.26 Value for q and k estimated from the integral method for 6.5 bar, 0.15 g/L NaOH and 110 °C experiment	107

Table B.27 Value for q and k estimated from the integral method for 6.5 bar, 0.25 g/L NaOH and 110 °C experiment	108
Table B.28 Best values of k and q for 27 set of experiments	109
Table B.29 Values of k for $q= 7.9$	110
Table C.1 Value of k_1 0.5 bar, 0.05 g/L NaOH and 90 °C experiment	115
Table C.2 Value of k_2 0.5 bar, 0.05 g/L NaOH and 90 °C experiment	115
Table C.3 Value of k_1 for 0.5 bar, 0.15 g/L NaOH and 90 °C experiment.....	116
Table C.4 Value of k_2 for 0.5 bar, 0.15 g/L NaOH and 90 °C experiment.....	116
Table C.5 Value of k_1 for 0.5 bar, 0.25 g/L NaOH and 90 °C experiment.....	117
Table C.6 Value of k_2 for 0.5 bar, 0.25 g/L NaOH and 90 °C experiment.....	117
Table C.7 Value of k_1 for 0.5 bar, 0.05 g/L NaOH and 100 °C experiment.....	118
Table C.8 Value of k_2 for 0.5 bar, 0.05 g/L NaOH and 100 °C experiment.....	118
Table C.9 Value of k_1 for 0.5 bar, 0.15 g/L NaOH and 100 °C experiment.....	119
Table C.10 Value of k_2 for 0.5 bar, 0.15 g/L NaOH and 100 °C experiment	119
Table C.11 Value of k_1 for 0.5 bar, 0.25 g/L NaOH and 100 °C experiment	120
Table C.12 Value of k_2 for 0.5 bar, 0.25 g/L NaOH and 100 °C experiment	120
Table C.13 Value of k_1 for 0.5 bar, 0.05 g/L NaOH and 110 °C experiment	121
Table C.14 Value of k_2 for 0.5 bar, 0.05 g/L NaOH and 110 °C experiment	121
Table C.15 Value of k_1 for 0.5 bar, 0.15 g/L NaOH and 110 °C experiment	122
Table C.16 Value of k_2 for 0.5 bar, 0.15 g/L NaOH and 110 °C experiment	122
Table C.17 Value of k_1 for 0.5 bar, 0.25 g/L NaOH and 110 °C experiment	123
Table C.18 Value of k_2 for 0.5 bar, 0.25 g/L NaOH and 110 °C experiment	123
Table C.19 Value of k_1 for 3.5 bar, 0.05 g/L NaOH and 90 °C experiment.....	124
Table C.20 Value of k_2 for 3.5 bar, 0.05 g/L NaOH and 90 °C experiment.....	124
Table C.21 Value of k_1 for 3.5 bar, 0.15 g/L NaOH and 90 °C experiment.....	125
Table C.22 Value of k_2 for 3.5 bar, 0.15 g/L NaOH and 90 °C experiment.....	125
Table C.23 Value of k_1 for 3.5 bar, 0.25 g/L NaOH and 90 °C experiment.....	126
Table C.24 Value of k_2 for 3.5 bar, 0.25 g/L NaOH and 90 °C experiment.....	126
Table C.25 Value of k_1 for 3.5 bar, 0.05 g/L NaOH and 100 °C experiment	127
Table C.26 Value of k_2 for 3.5 bar, 0.05 g/L NaOH and 100 °C experiment	127
Table C.27 Value of k_1 for 3.5 bar, 0.15 g/L NaOH and 100 °C experiment	128
Table C.28 Value of k_2 for 3.5 bar, 0.15 g/L NaOH and 100 °C experiment	128
Table C.29 Value of k_1 for 3.5 bar, 0.25 g/L NaOH and 100 °C experiment	129
Table C.30 Value of k_2 for 3.5 bar, 0.25 g/L NaOH and 100 °C experiment	129
Table C.31 Value of k_1 for 3.5 bar, 0.05 g/L NaOH and 110 °C experiment	130
Table C.32 Value of k_2 for 3.5 bar, 0.05 g/L NaOH and 110 °C experiment	130
Table C.33 Value of k_1 for 3.5 bar, 0.15 g/L NaOH and 110 °C experiment	131
Table C.34 Value of k_2 for 3.5 bar, 0.15 g/L NaOH and 110 °C experiment	131

Table C.35 Value of k_1 for 3.5 bar, 0.25 g/L NaOH and 110 °C experiment	132
Table C.36 Value of k_2 for 3.5 bar, 0.25 g/L NaOH and 110 °C experiment	132
Table C.37 Value of k_1 for 6.5 bar, 0.05 g/L NaOH and 90 °C experiment	133
Table C.38 Value of k_2 for 6.5 bar, 0.05 g/L NaOH and 90 °C experiment	133
Table C.39 Value of k_1 for 6.5 bar, 0.15 g/L NaOH and 90 °C experiment	134
Table C.40 Value of k_2 for 6.5 bar, 0.15 g/L NaOH and 90 °C experiment	134
Table C.41 Value of k_1 for 6.5 bar, 0.25 g/L NaOH and 90 °C experiment	135
Table C.42 Value of k_2 for 6.5 bar, 0.25 g/L NaOH and 90 °C experiment	135
Table C.43 Value of k_1 for 6.5 bar, 0.05 g/L NaOH and 100 °C experiment	136
Table C.44 Value of k_2 for 6.5 bar, 0.05 g/L NaOH and 100 °C experiment	136
Table C.45 Value of k_1 for 6.5 bar, 0.15 g/L NaOH and 100 °C experiment	137
Table C.46 Value of k_2 for 6.5 bar, 0.15 g/L NaOH and 100 °C experiment	137
Table C.47 Value of k_1 for 6.5 bar, 0.25 g/L NaOH and 100 °C experiment	138
Table C.48 Value of k_2 for 6.5 bar, 0.25 g/L NaOH and 100 °C experiment	138
Table C.49 Value of k_1 for 6.5 bar, 0.05 g/L NaOH and 110 °C experiment	139
Table C.50 Value of k_2 for 6.5 bar, 0.05 g/L NaOH and 110 °C experiment	139
Table C.51 Value of k_1 for 6.5 bar, 0.15 g/L NaOH and 110 °C experiment	140
Table C.52 Value of k_2 for 6.5 bar, 0.15 g/L NaOH and 110 °C experiment	140
Table C.53 Value of k_1 for 6.5 bar, 0.25 g/L NaOH and 110 °C experiment	141
Table C.54 Value of k_2 for 6.5 bar, 0.25 g/L NaOH and 110 °C experiment	141
Table C.55 Values of k_1 and k_2 for 27 set of experiments	142

LIST OF FIGURES

Figure 1.1 Average composition of softwoods and hardwoods.....	1
Figure 1.2 Oxygen delignification stage flowsheet.....	5
Figure 2.1 Stepwise reduction of oxygen (Dence and Reeve, 1996).....	9
Figure 2.2 Initial reactions leading to oxygen delignification (Dence and Reeve, 1996)	10
Figure 2.3 Reactions of intermediate hydroperoxides (Dence and Reeve, 1996)	11
Figure 2.4 Oxidation and cleavage of the cellulose chain (Gratzl, 1990)	13
Figure 2.5 Mass transfer of oxygen to fiber wall (Hsu and Hsieh, 1985a).....	15
Figure 3.1 The experimental setup for ultra low consistency oxygen bleaching.	24
Figure 4.1 The effect of consistency on the change of Kappa number (T = 100 °C, oxygen partial pressure = 6.5 bar and 600 rpm)	27
Figure 4.2 The effect of mixing rate on the change of Kappa number (T = 100 °C, partial oxygen pressure = 6.5 bar).....	28
Figure 4.3 The change in residual alkali concentration with respect to time (T = 100 °C and oxygen partial pressure = 6.5 bar)	29
Figure 4.4 The effect of refining on the change of Kappa number (T = 100 °C and oxygen partial pressure = 6.5 bar).....	30
Figure 4.5 The change in Kappa number with respect to time (T = 90, 100, 110 °C, oxygen partial pressure = 0.5 bar, NaOH concentration = 0.05, 0.15, 0.25 g/L)	32
Figure 4.6 The change in Kappa number with respect to time (T = 90, 100,110 °C, oxygen partial pressure = 3.5 bar, NaOH concentration = 0.05, 0.15, 0.25 g/L)	33
Figure 4.7 The change in Kappa number with respect to time (T = 90, 100, 110 °C, oxygen partial pressure = 6.5 bar, NaOH concentration = 0.05, 0.15, 0.25 g/L)	34
Figure 4.8 The effect of temperature on the change of Kappa number (NaOH concentration = 0.15 g/L and oxygen partial pressure = 6.5).....	35

Figure 4.9 The effect of oxygen partial pressure on the change of Kappa number (T = 100 °C and NaOH concentration = 0.15 g/L)	36
Figure 4.10 Intrinsic viscosity with respect to time (T = 90 °C, oxygen partial pressure = 0.5, 3.5, 6.5 bar and NaOH concentration = 0.05, 0.15, 0.25 g/L)	38
Figure 4.11 Intrinsic viscosity with respect to time (T = 100 °C, oxygen partial pressure = 0.5, 3.5, 6.5 bar and NaOH concentration = 0.05, 0.15, 0.25 g/L)	39
Figure 4.12 Intrinsic viscosity with respect to time (T = 110 °C, oxygen partial pressure = 0.5, 3.5, 6.5 bar and NaOH concentration 0.05, 0.15, 0.25 g/L)	40
Figure 4.13 The two stage zero order power law model for intrinsic viscosity (T = 90 °C, oxygen partial pressure = 0.5, 3.5, 6.5 bar and NaOH concentration = 0.05, 0.15, 0.25 g/L).....	42
Figure 4.14 The two stage zero order power law model for intrinsic viscosity (T = 100 °C, oxygen partial pressure = 0.5, 3.5, 6.5 bar and NaOH concentration 0.05, 0.15, 0.25 g/L).....	43
Figure 4.15 The two stage zero order power law model for intrinsic viscosity (T = 110 °C, oxygen partial pressure = 0.5, 3.5, 6.5 bar and NaOH concentration = 0.05, 0.15, 0.25 g/L).....	44
Figure 4.16 The effect of temperature on the carbohydrate degradation (NaOH concentration = 0.15 g/L and oxygen partial pressure = 6.5 bar)	45
Figure 4.17 The effect of sodium hydroxide concentration on the carbohydrate degradation (T= 100 °C and oxygen partial pressure = 3.5 bar)	45
Figure 4.18 The moles of cellulose chains per ton of pulp with respect to time (T = 90 °C, oxygen partial pressure = 0.5, 3.5, 6.5 bar and NaOH concentration = 0.05, 0.15, 0.25 g/L).....	47
Figure 4.19 The moles of cellulose chains per ton of pulp with respect to time (T = 100 °C, oxygen partial pressure = 0.5, 3.5, 6.5 bar and NaOH concentration = 0.05, 0.15, 0.25 g/L).....	48
Figure 4.20 The moles of cellulose chains per ton of pulp with respect to time (T = 110 °C, oxygen partial pressure = 0.5, 3.5, 6.5 bar and NaOH concentration = 0.05, 0.15, 0.25 g/L).....	49
Figure 4.21 The oxygen delignification kinetics for this study and the previous studies (oxygen partial pressure = 414 kPa, T = 100 °C, NaOH concentration = 4 g/L)	50

Figure 4.22 The carbohydrate degradation kinetics for this study and previous study (1997) (oxygen partial pressure = 414 kPa, T = 100 °C, NaOH concentration = 4 g/L)	51
Figure 4.23 The extent of delignification versus dimensionless time ($\tau=t/t_{0.15}$) for this study	53
Figure 4.24 Extent of delignification versus dimensionless time ($\tau=t/t_{0.20}$) for Agarwal et al. (1999)	54
Figure 4.25 Extent of delignification versus dimensionless time ($\tau=t/t_{0.25}$) for Hsu & Hsieh (1988)	55
Figure 4.26 Extent of delignification versus dimensionless time for Hsu & Hsieh (1988) with different τ	55
Figure 4.27 Extent of carbohydrate degradation as viscosity versus dimensionless time ($\tau=t/t_{0.1}$) for this study	56
Figure 4.28 Process flow diagram of CEHDED bleach plant	57
Figure B.1. Estimation of q and k for 0.5 bar, 0.05 g/L NaOH and 90 °C experiment using the integral method	82
Figure B.3. Estimation of q and k for 0.5 bar, 0.15 g/L NaOH and 90 °C experiment using the integral method	83
Figure B.5. Estimation of q and k for 0.5 bar, 0.25 g/L NaOH and 90 °C experiment using the integral method	84
Figure B.7. Estimation of q and k for 0.5 bar, 0.05 g/L NaOH and 100 °C experiment using the integral method	85
Figure B.9. Estimation of q and k for 0.5 bar, 0.15 g/L NaOH and 100 °C experiment using the integral method	86
Figure B.11. Estimation of q and k for 0.5 bar, 0.25 g/L NaOH and 100 °C experiment using the integral method	87
Figure B.13. Estimation of q and k for 0.5 bar, 0.05 g/L NaOH and 110 °C experiment using the integral method	88
Figure B.15. Estimation of q and k for 0.5 bar, 0.15 g/L NaOH and 110 °C experiment using the integral method	89
Figure B.17. Estimation of q and k for 0.5 bar, 0.25 g/L NaOH and 110 °C experiment using the integral method	90
Figure B.19. Estimation of q and k for 3.5 bar, 0.05 g/L NaOH and 90 °C experiment using the integral method	91
Figure B.21. Estimation of q and k for 3.5 bar, 0.15 g/L NaOH and 90 °C experiment using the integral method	92

Figure B.23. Estimation of q and k for 3.5 bar, 0.25 g/L NaOH and 90 °C experiment using the integral method	93
Figure B.25. Estimation of q and k for 3.5 bar, 0.05 g/L NaOH and 100 °C experiment using the integral method	94
Figure B.27. Estimation of q and k for 3.5 bar, 0.15 g/L NaOH and 100 °C experiment using the integral method	95
Figure B.29. Estimation of q and k for 3.5 bar, 0.25 g/L NaOH and 100 °C experiment using the integral method	96
Figure B.31. Estimation of q and k for 3.5 bar, 0.05 g/L NaOH and 110 °C experiment using the integral method	97
Figure B.33. Estimation of q and k for 3.5 bar, 0.15 g/L NaOH and 110 °C experiment using the integral method	98
Figure B.35. Estimation of q and k for 3.5 bar, 0.25 g/L NaOH and 110 °C experiment using the integral method	99
Figure B.37. Estimation of q and k for 6.5 bar, 0.05 g/L NaOH and 90 °C experiment using the integral method	100
Figure B.39. Estimation of q and k for 6.5 bar, 0.15 g/L NaOH and 90 °C experiment using the integral method	101
Figure B.41. Estimation of q and k for 6.5 bar, 0.25 g/L NaOH and 90 °C experiment using the integral method	102
Figure B.43. Estimation of q and k for 6.5 bar, 0.05 g/L NaOH and 100 °C experiment using the integral method	103
Figure B.45. Estimation of q and k for 6.5 bar, 0.15 g/L NaOH and 100 °C experiment using the integral method	104
Figure B.47. Estimation of q and k for 6.5 bar, 0.25 g/L NaOH and 100 °C experiment using the integral method	105
Figure B.49. Estimation of q and k for 6.5 bar, 0.05 g/L NaOH and 110 °C experiment using the integral method	106
Figure B.51. Estimation of q and k for 6.5 bar, 0.15 g/L NaOH and 110 °C experiment using the integral method	107
Figure B.53. Estimation of q and k for 6.5 bar, 0.25 g/L NaOH and 110 °C experiment using the integral method	108
Figure C.1 Value of k_1 for 0.5 bar, 0.05 g/L NaOH and 90 °C experiment	115
Figure C.2 Value of k_2 for 0.5 bar, 0.05 g/L NaOH and 90 °C experiment	115
Figure C.3 Value of k_1 for 0.5 bar, 0.15 g/L NaOH and 90 °C experiment	116
Figure C.4 Value of k_2 for 0.5 bar, 0.15 g/L NaOH and 90 °C experiment	116
Figure C.5 Value of k_1 for 0.5 bar, 0.25 g/L NaOH and 90 °C experiment	117
Figure C.6 Value of k_2 for 0.5 bar, 0.25 g/L NaOH and 90 °C experiment	117

Figure C.7 Value of k_1 for 0.5 bar, 0.05 g/L NaOH and 100 °C experiment.....	118
Figure C.8 Value of k_2 for 0.5 bar, 0.05 g/L NaOH and 100 °C experiment.....	118
Figure C.9 Value of k_1 for 0.5 bar, 0.15 g/L NaOH and 100 °C experiment.....	119
Figure C.10 Value of k_2 for 0.5 bar, 0.15 g/L NaOH and 100 °C experiment ...	119
Figure C.11 Value of k_1 for 0.5 bar, 0.25 g/L NaOH and 100 °C experiment ...	120
Figure C.12 Value of k_2 for 0.5 bar, 0.25 g/L NaOH and 100 °C experiment ...	120
Figure C.13 Value of k_1 for 0.5 bar, 0.05 g/L NaOH and 110 °C experiment ...	121
Figure C.14 Value of k_2 for 0.5 bar, 0.05 g/L NaOH and 110 °C experiment ...	121
Figure C.15 Value of k_1 for 0.5 bar, 0.15 g/L NaOH and 110 °C experiment ...	122
Figure C.16 Value of k_2 for 0.5 bar, 0.15 g/L NaOH and 110 °C experiment ...	122
Figure C.17 Value of k_1 for 0.5 bar, 0.25 g/L NaOH and 110 °C experiment ...	123
Figure C.18 Value of k_2 for 0.5 bar, 0.25 g/L NaOH and 110 °C experiment ...	123
Figure C.19 Value of k_1 for 3.5 bar, 0.05 g/L NaOH and 90 °C experiment.....	124
Figure C.20 Value of k_2 for 3.5 bar, 0.05 g/L NaOH and 90 °C experiment.....	124
Figure C.21 Value of k_1 for 3.5 bar, 0.15 g/L NaOH and 90 °C experiment.....	125
Figure C.22 Value of k_2 for 3.5 bar, 0.15 g/L NaOH and 90 °C experiment.....	125
Figure C.23 Value of k_1 for 3.5 bar, 0.25 g/L NaOH and 90 °C experiment.....	126
Figure C.24 Value of k_2 for 3.5 bar, 0.25 g/L NaOH and 90 °C experiment.....	126
Figure C.25 Value of k_1 for 3.5 bar, 0.05 g/L NaOH and 100 °C experiment ...	127
Figure C.26 Value of k_2 for 3.5 bar, 0.05 g/L NaOH and 100 °C experiment ...	127
Figure C.27 Value of k_1 for 3.5 bar, 0.15 g/L NaOH and 100 °C experiment ...	128
Figure C.28 Value of k_2 for 3.5 bar, 0.15 g/L NaOH and 100 °C experiment ...	128
Figure C.29 Value of k_1 for 3.5 bar, 0.25 g/L NaOH and 100 °C experiment ...	129
Figure C.30 Value of k_2 for 3.5 bar, 0.25 g/L NaOH and 100 °C experiment ...	129
Figure C.31 Value of k_1 for 3.5 bar, 0.05 g/L NaOH and 110 °C experiment ...	130
Figure C.32 Value of k_2 for 3.5 bar, 0.05 g/L NaOH and 110 °C experiment ...	130
Figure C.33 Value of k_1 for 3.5 bar, 0.15 g/L NaOH and 110 °C experiment ...	131
Figure C.34 Value of k_2 for 3.5 bar, 0.15 g/L NaOH and 110 °C experiment ...	131
Figure C.35 Value of k_1 for 3.5 bar, 0.25 g/L NaOH and 110 °C experiment ...	132
Figure C.36 Value of k_2 for 3.5 bar, 0.25 g/L NaOH and 110 °C experiment ...	132
Figure C.37 Value of k_1 for 6.5 bar, 0.05 g/L NaOH and 90 °C experiment.....	133
Figure C.38 Value of k_2 for 6.5 bar, 0.05 g/L NaOH and 90 °C experiment.....	133
Figure C.39 Value of k_1 for 6.5 bar, 0.15 g/L NaOH and 90 °C experiment.....	134
Figure C.40 Value of k_2 for 6.5 bar, 0.15 g/L NaOH and 90 °C experiment.....	134
Figure C.41 Value of k_1 for 6.5 bar, 0.25 g/L NaOH and 90 °C experiment.....	135
Figure C.42 Value of k_2 for 6.5 bar, 0.25 g/L NaOH and 90 °C experiment.....	135
Figure C.43 Value of k_1 for 6.5 bar, 0.05 g/L NaOH and 100 °C experiment ...	136
Figure C.44 Value of k_2 for 6.5 bar, 0.05 g/L NaOH and 100 °C experiment ...	136

Figure C.45 Value of k_1 for 6.5 bar, 0.15 g/L NaOH and 100 °C experiment ...	137
Figure C.46 Value of k_2 for 6.5 bar, 0.15 g/L NaOH and 100 °C experiment ...	137
Figure C.47 Value of k_1 for 6.5 bar, 0.25 g/L NaOH and 100 °C experiment ...	138
Figure C.48 Value of k_2 for 6.5 bar, 0.25 g/L NaOH and 100 °C experiment ...	138
Figure C.49 Value of k_1 for 6.5 bar, 0.05 g/L NaOH and 110 °C experiment ...	139
Figure C.50 Value of k_2 for 6.5 bar, 0.05 g/L NaOH and 110 °C experiment ...	139
Figure C.51 Value of k_1 for 6.5 bar, 0.15 g/L NaOH and 110 °C experiment ...	140
Figure C.52 Value of k_2 for 6.5 bar, 0.15 g/L NaOH and 110 °C experiment ...	140
Figure C.53 Value of k_1 for 6.5 bar, 0.25 g/L NaOH and 110 °C experiment ...	141
Figure C.54 Value of k_2 for 6.5 bar, 0.25 g/L NaOH and 110 °C experiment ...	141

NOMENCLATURE

A	Frequency factor in Arrhenius' law
C_m	Fibre consistency, % on slurry
E_a	Activation energy of bleaching reaction, kJ/mol
E_N	Norden efficiency factor, dimensionless
f	Chlorine charge factor, %available Cl_2 on o.d. pulp/unbleached kappa number
K	Content of chromophores, expressed as kappa number in delignification stage and light absorption coefficient in brightening stage
k	Rate constant of bleaching reaction
k_1 and k_2	Rate constants of fast and slow bleaching reaction
L	Flow rate of liquor in pulp stream, kg/min
M_n	Moles of cellulose chains per ton of pulp
$[OH^-]$	Sodium hydroxide concentration, g/L
P	Oxygen partial pressure, bar
R	Ideal gas constant, kJ/mol.K
R_∞	Reflectance at 457 nm , % ISO
r	Bleaching reaction rate, ie rate of kappa number decrease in a delignification or rate of light absorption coefficient decrease in a brightening reaction
RW	Wash liquor ratio, dimensionless
S	Light scattering coefficient, m^2/kg
T	Temperature, K
t	Time, min
t_c	Mean residence time in CSTR, min
t_p	Mean residence time in PFR, min
V	Flow rate of liquor in non-pulp stream, kg/min
X_i	Dissolved solids or bleaching chemical content of the pulp stream, %

Y_i Dissolved solids or bleaching chemical content of the non-pulp stream, %

Greek Letters

η Intrinsic viscosity, dl/g
 κ Dimensionless extent of delignification
 τ Dimensionless time
M Dimensionless carbohydrate degradation

Subscripts

0 Initial value
Cl Chlorination
 Cl_2 Chlorine
 ClO_2 Chlorine dioxide
d Drum filter stream
DS Dissolved solids
 D_1 First chlorine dioxide
 E_1 First extraction stage
H Hypochlorination
i Inlet
 OCl^- Hypochlorite
o Outlet
 O_2 Oxygen
r Recycle stream
v Dilution vat stream

Superscripts

a Order in Equation 4.11
b Order in Equation 4.11
c Order in Equation 4.11
d Order in Equation 4.11
m Order in Equation 4.2
n Order in Equation 4.2
o Order in Equation 4.7
p Order in Equation 4.7
q Order in Equation 4.1
r Order in Equation 4.6

Abbreviations:

AOX Adsorbable organic halogen
BOD Biochemical oxygen demand
C Chlorination stage

CEHDED	Chlorination, extraction (NaOH), hypochlorination, chlorine dioxide, extraction (NaOH), chlorine dioxide bleaching sequence
COD	Chemical oxygen demand
D ₁	First chlorine dioxide bleaching stage
D ₂	Second chlorine dioxide bleaching stage
DTPA	Diethylenetriaminepentaacetic acid
ECF	Elemental chlorine free
E ₁	First alkaline extraction stage
E ₂	Second alkaline extraction stage
EOX	Extractable organic halogen
H	Hypochlorination stage
O	Oxygen stage
TCF	Total chlorine free
TDS	Total dissolved solids
TOC	Total organic carbon
TSS	Total suspended solids

CHAPTER 1

INTRODUCTION

1.1 Wood

Wood is the principal source of cellulosic fiber for pulp and paper manufacture. Wood can be simply classified as softwood and hardwood. Both softwoods and hardwoods consist of four major components: cellulose, hemicellulose, lignin and extractives. The relative amounts of the components differ between softwoods and hardwoods and between species. The typical compositions of woods are shown in Figure 1.1 for softwoods (pine, spruce, fir, cedar) and hardwoods (eucalyptus, aspen, birch, beech, oaks) (Smook, 2002).

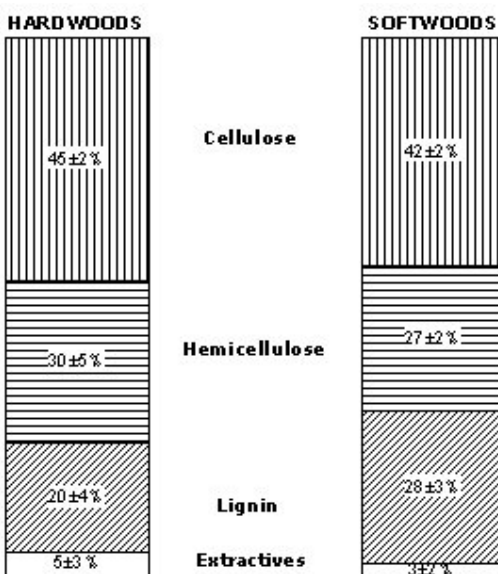


Figure 1.1 Average composition of softwoods and hardwoods.

In plant fibers cellulose is the substance that determines the character of the fiber and permits its use in papermaking. The chemical formula for cellulose is $(C_6H_{10}O_5)_n$, where n is the number of repeating sugar units or the degree of polymerization (DP). The value of n varies with the different sources of cellulose and the treatment received. Most papermaking fibers have a weight-averaged DP in the range of 600-1500. In chemical pulping and bleaching, the objective is to separate the wood fiber without seriously degrading the cellulose chain.

By contrast to cellulose which is a polymer only of glucose, the hemicelluloses are polymers of five different sugars: glucose, mannose, galactose, xylose, arabinose. During the chemical treatment of wood to produce pulp, the amounts, locations and structures of the various hemicelluloses usually change dramatically. The hemicelluloses are more easily degraded and dissolved than cellulose, so their percentage is always less in the pulp than in the original wood.

Lignin is a very complex polymer consisting of phenylpropane units combined in a random formation. Its principle role is to form the middle lamella, the intercellular material which cements the fibers together. The exact structure of lignin is not completely understood because of the random nature of the linkages between the phenylpropane units. The lignin content is usually measured by the Kappa number in bleaching physical chemistry as well as in the industry. The Kappa number is defined as the number of cubic centimeters of 0.1N potassium permanganate solution consumed by 1 gram of moisture-free pulp. It relates linearly to the lignin content for all types and grades of pulps up to yield of 70%.

1.2 Pulping and Bleaching

The objective of chemical pulping and bleaching is using specific amounts of chemicals to remove as much lignin as possible from wood to form pulp without damaging the fiber structure and losing hemicelluloses and cellulose.

The major pulping processes are mechanical, chemical and semichemical. There are many chemical pulping methods used, which are Kraft, sulfite, polysulfide, and anthraquinone. The most popular chemical wood pulping process is the Kraft process because of high pulp strength and wide adaptability.

The objective of Kraft pulping is to chemically separate the fibers in wood and dissolve most of the lignin contained in the fiber wall. In Kraft pulping process, a

mixture of sodium sulfide (Na_2S) and sodium hydroxide (NaOH) is used to pulp the wood. All sorts of woods can be cooked by the Kraft process and the fibers obtained are bleachable and strong. During and after cooking, the dissolved organic material and cooking chemicals are extracted from the undissolved cellulose fibers. The effluent from this process, black liquor, is treated in recovery boiler, where the cooking chemicals are recovered for reuse, and the organic material is burned for energy. The manner in which the Kraft pulping process is executed has a significant effect on pulp bleaching and oxygen delignification.

Bleaching is a chemical process to increase the brightness of the pulp and to make it suitable for the manufacture of printing and tissue grade papers by removal or modification of some of the constituents of the unbleached pulp, including the lignin and its degradation products. For most purposes, it is desired not only to make the pulp whiter and brighter, but also to make it stable so that it will not become yellow or lose strength or brightness in aging.

The chemicals commonly used for pulp bleaching include oxidants (chlorine, C; chlorine dioxide, D; hypochlorite, H; oxygen, O; ozone, Z; and hydrogen peroxide, P) and alkali (sodium hydroxide, E). These chemicals are mixed with pulp suspensions and the mixture is retained at prescribed pH, temperature and concentration conditions for a specified time period. The bleaching reactions that occur are highly complex due to the complexity of lignin and the wide variety of reactive bleaching species present. The progress of bleaching reactions is monitored by measuring Kappa number, pulp brightness and residual chemical. Bleaching chemicals are applied sequentially with intermediate washing between stages, because it is not possible to achieve sufficient removal or decolorization of lignin by the action of any one chemical in a single stage.

Chlorine and hypochlorite were commonly used in bleaching sequences until the early 1990s. These chemicals are low cost and effective bleaching agents, but are known to be major contributors of chlorinated organic compounds (Adsorbable Organic Halides, AOX) to the environment. Hypochlorite has also been identified as a major source of chloroform formation. Elemental chlorine use was largely phased out in the 1990s (Smook, 2002). Bleached pulps processed without elemental chlorine or hypochlorite is known as ECF (Elemental Chlorine Free) pulps.

In order to meet more stringent wastewater standards, few mills in the United States and Europe have gone TCF (Total Chlorine Free) bleaching (Smook, 2002). TCF pulps are bleached without the use of chlorine gas or chlorine compounds (hypochlorite and chlorine dioxide). The elimination of chlorine dioxide has led to the development of a number of sequences using oxygen, ozone, peroxide and other more novel treatments including the use of enzymes, chelants and peracids.

1.3 Oxygen Delignification

Oxygen delignification is defined as the use of oxygen and alkali to remove a substantial fraction of the lignin from the unbleached pulp. This process is becoming increasingly important in modern pulp bleaching technologies. Oxygen delignification kinetics is very important for understanding the reaction mechanism and in the design and control of oxygen delignification reactions.

The most important advantage of installing an oxygen delignification stage is the decrease in chlorinated organic byproducts (AOX) in the bleach plant effluents. In addition, the effluents from an oxygen delignification stage can be recycled to the chemical recovery system. The addition of an oxygen stage causes to a major decrease in biochemical oxygen demand (BOD), chemical oxygen demand (COD) and color. Furthermore, the oxygen delignification unit leads to a decrease in oxidizing chemicals (chlorine, chlorine dioxide, hypochlorite, ozone) in the upcoming bleaching sequences to obtain the target brightness. Thus, savings in the cost of chemicals in the bleach plant can be achieved.

The biggest drawback of an oxygen delignification system is that the selectivity of the process is low compared to chlorine-compound (chlorine, chlorine dioxide) based bleaching so that commercially the delignification has been traditionally limited to about 50%. Another disadvantage is the high capital cost of installing an oxygen delignification system.

Oxygen delignification is practiced commercially using both medium consistency (8%-14%) and high consistency (25%-35%) technologies; although, practically all new systems use medium consistency technology because the capital cost is lower. Figure 1.2 shows a simplified oxygen delignification stage flowsheet. The unbleached pulp discharged from the repulper of the last brown stock washer passes to a steam mixer and is then fed to a feed tank. Alkali, usually sodium

hydroxide or oxidized white liquor and $MgSO_4$ protector, is added to the pulp at the base of the feed tank and is mixed with the pulp. The pulp then goes to one or more medium consistency high shear mixers where oxygen gas is added together with additional steam. The mixers disperse the oxygen in the pulp, which then passes to an upflow pressurized reactor. After a retention time of about one hour, the pulp is blown to a gas separator mounted on a blown tank. Product gases and unreacted oxygen are vented and the pulp enters to the washing system. The washing system is very important in order to remove completely the dissolved materials in the oxygen stage. Then, the pulp is sent to the bleaching unit in order to further bleached to a desired brightness.

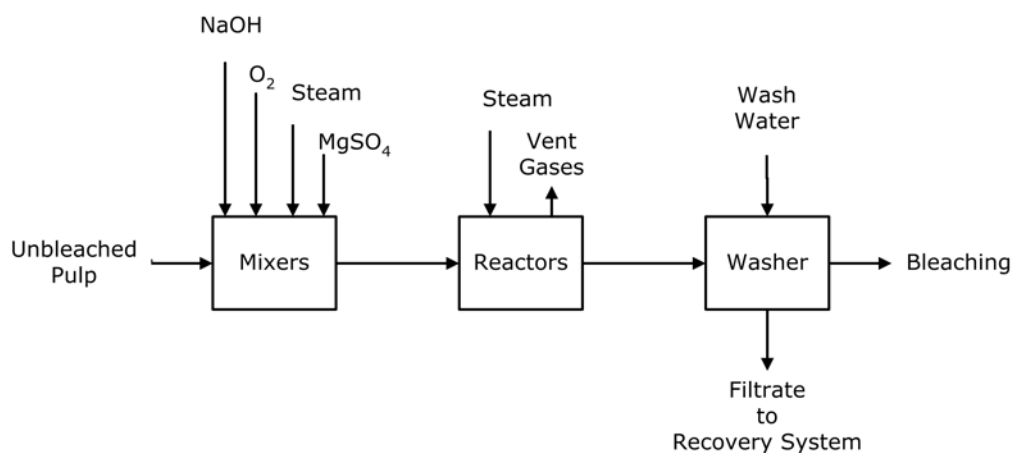


Figure 1.2 Oxygen delignification stage flowsheet

1.4 Objective and Scope of the Work

In this study, the kinetics of oxygen delignification of Turkish southern hardwood Kraft pulp was studied. In order to achieve this objective, the study is composed of different stages. In the first stage of the work, the mass transfer effects were examined for different pulp consistencies. In the following stage, the kinetics of oxygen delignification was studied and the governing mathematical equations were derived. Then, the kinetics of the carbohydrate degradation was analyzed in order to determine the extent of delignification without the reduction in the pulp strength. In the final stage of the study, the simulation of the oxygen delignification unit preceding the CEHDED bleach plant is performed, in order to see the effect of oxygen delignification on the amount of total wastes coming out from the bleach plant.

In oxygen delignification, the two main mass transfer resistances expected to play a role are inter-fiber and intra-fiber mass transfer of oxygen. In order to test the inter-fiber mass transfer effect, the experiments were performed with three different consistency values as 0.5, 1, and 8%. To investigate the significance of intra-fiber diffusion during oxygen delignification, the pulp was refined before being subjected to oxygen delignification. Refining shortens, hydrates and fibrillates the pulp, thus increasing the surface area tremendously. If the intra-fiber mass transfer is significant, then prerefining the pulp is expected to give higher levels of delignification because of the increased surface area.

In the following part of the study, the intrinsic reaction rate of oxygen delignification was examined by performing experiments at 0.5% consistency. The experiments were carried out in order to investigate the effect of the process variables on the Kappa number. Temperature, alkali concentration and oxygen pressure were selected as the major process variables. For the determined range of process variables, the change in Kappa number was studied for different reaction times. With the help of these data, the intrinsic kinetic rate equation was derived for the oxygen delignification.

Another important factor in oxygen delignification is selectivity, defined as the ratio of the delignification rate to that of the carbohydrate degradation rate. It determines how far the delignification can proceed without loss of pulp strength. Therefore, the carbohydrate degradation kinetics was also studied for the Turkish Kraft pulp, where the viscosity of the pulp was considered as the major independent variable. The experimental conditions were kept at the same values as in the kinetic study experiments.

Previously, oxygen delignification kinetics was investigated by a number of different researchers (Olm and Teder, 1979; Hsu and Hsieh, 1987, 1988; Iribarne and Schroeder, 1997; Agarwal et al., 1999). However oxygen delignification is a complex phenomena and show significant variation depending upon the wood species and pulping process used. The manner in which the Kraft pulping process is executed has a significant effect on the oxygen delignification. The amount of reduced lignin remaining in the pulp will depend upon the conditions used in the pulping processes. In addition, variations in the hemicellulose content and structure resulting from different pulping conditions and wood species have a significant effect on oxygen delignification. In this

study, the oxygen delignification kinetics was studied for the southern Turkish hardwood eucalyptus Kraft pulp produced in Mopak Dalaman pulp and paper mill. In the near future, the mill is planning to construct an oxygen delignification unit to be added to the front of the existing CEHDED bleach plant. It is also believed that this study will form a basis for the design of the oxygen delignification tower in the mill.

CHAPTER 2

LITERATURE SURVEY

2.1 Oxygen Delignification Chemistry

Several reviews of the chemistry of oxygen delignification are available in the literature. Argyropoulos (2001) reviewed the research efforts aimed at utilizing oxygen and peroxide for removing the lignin from chemical pulps. Therefore, most of the studies included in the review are towards exploring oxygen and peroxide organic chemistry and their fundamental interactions with the lignocellulosic substrate. Gratzl (1992) has reviewed the inorganic chemistry of dissolved oxygen and the various radicals and other species derived from it. Singh (1987) has presented a comprehensive overview of the chemistry of the various radical species likely to play a role in the oxygen delignification. Reactions of lignin, inferred from the results of model compound studies have been the focus of reviews by Gierer and Imsgard (1977) and Gratzl (1987). A more general review by Gierer (1986) also discusses relevant lignin reactions. Carbohydrate reactions are the subject of papers by Theander (1980) and Sjöström (1980). All three topics have been reviewed by Gratzl (1990).

2.1.1 Oxygen Chemistry

Oxygen is an unusual molecule in that its normal configuration is the triplet state. It contains two electrons that are unpaired. Each of these electrons therefore has an affinity for other electrons of opposite spin. In other words, oxygen is a free radical. Although less reactive than other free radicals, it shares their tendency to react with appropriate substrates at regions of high density. The result is the initial step in a four-step process in which oxygen is reduced to

water and the substrate is oxidized. Figure 2.1 illustrates the process. The product of the first step is a negatively charged ion, called the superoxide anion, $O_2^{\cdot-}$, which can combine with a hydrogen ion to form the hydroperoxy radical $HOO\cdot$. However, because this radical is a weak acid ($pK_a=4.8$), the anion remains uncombined under the alkaline conditions of oxygen delignification (Dence and Reeve, 1996).

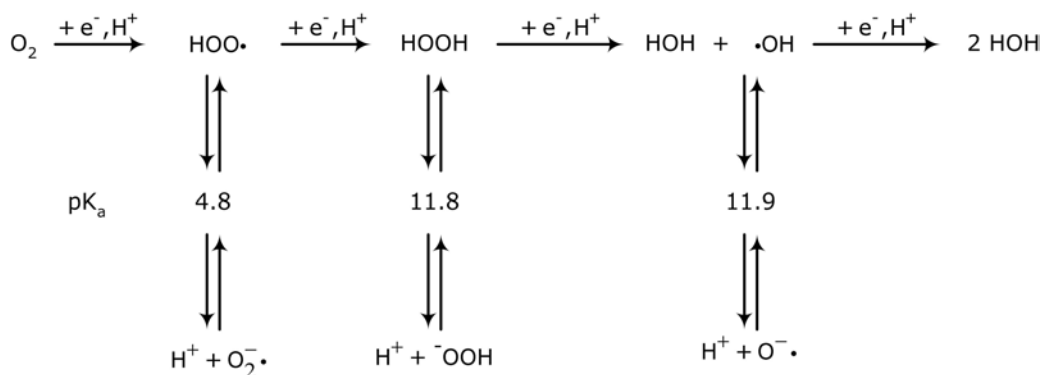


Figure 2.1 Stepwise reduction of oxygen (Dence and Reeve, 1996)

Both the superoxide anion and the hydroperoxy radical have higher oxidation potential than their parent oxygen. In principle, each can readily acquire another electron to form the peroxide dianion, O_2^{2-} , and hydroperoxide anion, HOO^- . In reality, the dianion is probably not sufficiently stable form in appreciable amounts. The hydroperoxide anion is the dissociated form of hydrogen peroxide. Because hydrogen peroxide is a weak acid ($pK_a=11.8$), both it and its anion are present in appreciable amounts under oxygen delignification condition (Dence and Reeve, 1996).

The third step in the stepwise reduction of oxygen occurs when hydrogen peroxide accepts an electron to form a hydroxide ion and a hydroxyl radical, $HO\cdot$. The hydroxyl radical is also a weak acid ($pK_a = 11.9$) that exist in equilibrium with its anion, $^-\dot{O}$. Finally, the hydroxyl radical can acquire another electron to form hydroxide ion or water. The occurrence of hydroxyl radicals in this process is particularly significant because they are extremely reactive and indiscriminate, attacking cellulose as well as lignin (Dence and Reeve, 1996).

2.1.2 Lignin Reactions

In lignin reactions free phenolic hydroxyl groups play a key role. When ionized by addition of alkali, they furnish the high electron density that is needed to initiate reaction with the relatively weakly oxidizing molecular oxygen. This, together with the weakly acidic nature of phenolic hydroxyl groups, explains why strongly alkaline conditions are needed to achieve appreciable delignification rates. The initial step is conversion of the ionized phenolic group to a phenoxy radical by the loss of a single electron to a suitable acceptor; this may be molecular oxygen or one of the many other radical species present. The resulting phenoxy radical is a resonance hybrid of structures in which the odd electron formally resides at the phenolic oxygen, at one of several different atoms in the aromatic ring, or at the β -carbon atom of the side chain. All of these positions are therefore potential sites for the next step of the reaction, conversion to a hydroperoxide. The other reactant can be molecular oxygen, the superoxide anion radical, or the hydroperoxy radical (Dence and Reeve, 1996). Figure 2.2 illustrates these steps.

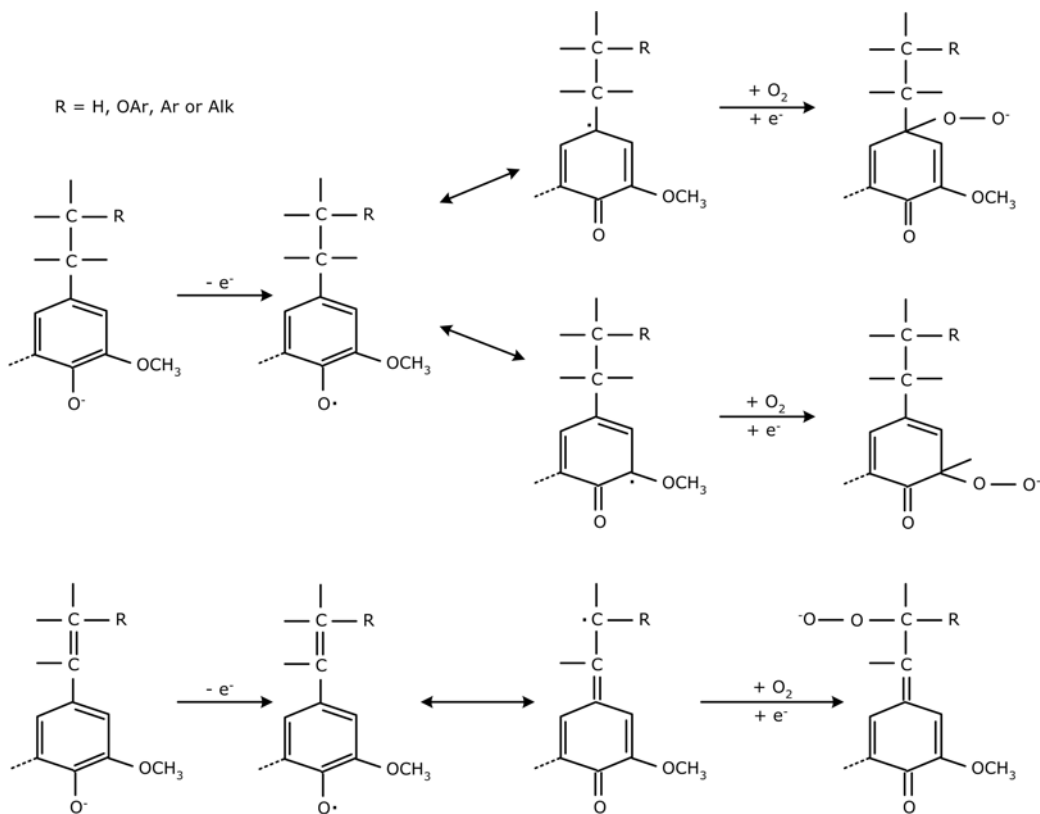


Figure 2.2 Initial reactions leading to oxygen delignification (Dence and Reeve, 1996)

In the alkaline environment of the oxygen delignification process, the hydroperoxide intermediate exists, in part, as the corresponding anion, which can subsequently undergo an intramolecular nucleophilic reaction at an adjacent site. This may be the carbonyl carbon of the quinone methide, a ring carbon conjugated with it, or an adjacent side chain carbon, depending on the location of the hydroperoxy function. These reactions, illustrated in Figure 2.3, lead to the formation of oxirane, muconic acid, and carbonyl structures. The last corresponds to breakage of a bond joining two lignin monomeric units and therefore leads to lignin fragmentation. The others correspond to introduction of hydrophilic groups, imparting polar character. Both types of reactions may be expected to enhance the solubility of the lignin in the alkaline medium.

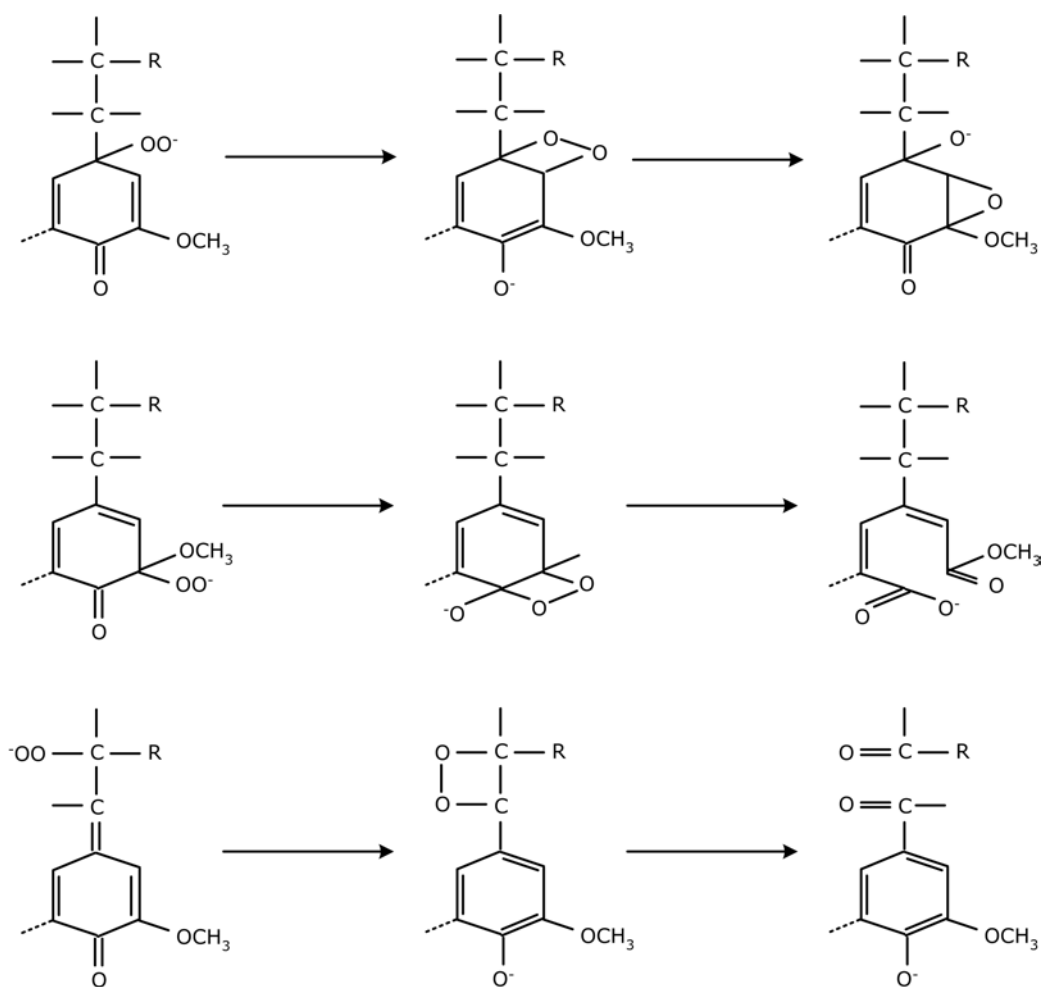


Figure 2.3 Reactions of intermediate hydroperoxides (Dence and Reeve, 1996)

2.1.3 Carbohydrate Reactions

Carbohydrates are attacked during the course of oxygen delignification to a greater extent than during chlorination and alkali extraction. For this reason, delignification is usually limited to removal of no more than about half of the lignin in the pulp entering the oxygen stage.

Reactions that degrade cellulose can be divided into two categories: random chain cleavage, which may occur at any point along the chainlike molecule, and endwise "peeling" by which units on the end of the chain are attacked and successively removed (Sjöström, 1981). Although both types may occur during oxygen delignification, random chain cleavage is the more significant.

Traces of metals that are unavoidably present in unbleached pulps promote random chain cleavage. Transition metals such as iron, manganese, and copper are particularly troublesome. They catalyze the formation of reactive, oxygen based radicals such as hydroxyl radicals that randomly attack the cellulose chain, ultimately leading to chain breakage at the point of attack. The associated decrease in the average length of the cellulose chains manifests itself as decrease in pulp viscosity and, if allowed to proceed far enough, as a decrease in pulp strength.

As illustrated in Figure 2.4, the initial step in the chain cleavage process involves oxidation of a hydroxyl group to a carbonyl group. The ionized enol form of the resulting carbonyl-containing unit then undergoes a beta-elimination reaction, breaking the glycosidic linkage joining the affected unit to the rest of the cellulose chain. The initially formed carbonyl-containing unit does not necessarily have to react as described above to break the cellulose chain. A competing reaction occurs when oxygen attacks its ionized keto form, forming a cyclic carboxylic acid or an open chain structure containing two carboxylic acid groups. In neither case the cellulose chain is broken.

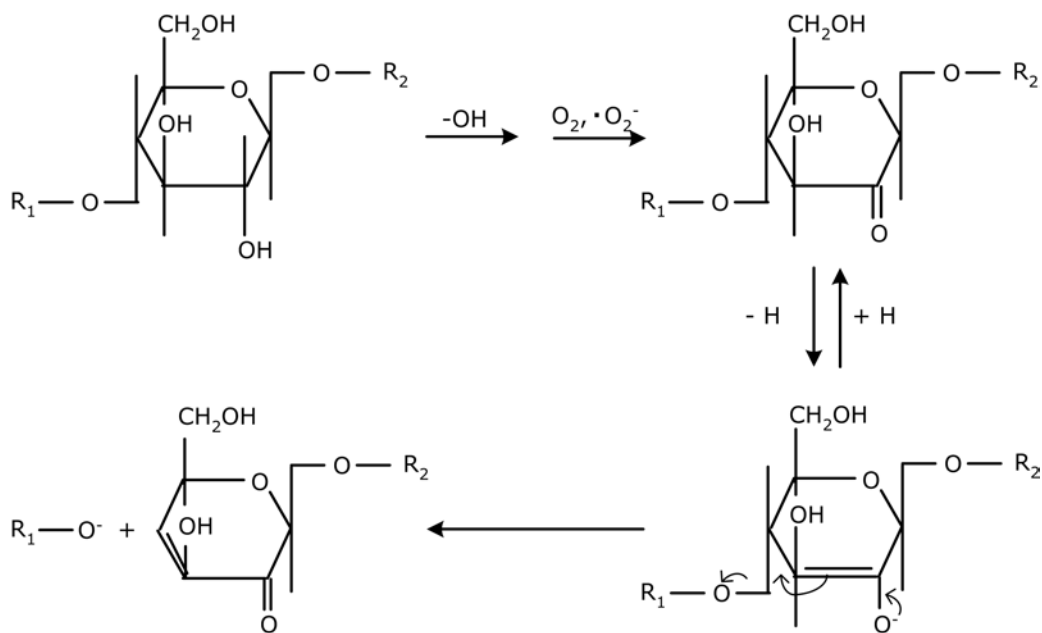


Figure 2.4 Oxidation and cleavage of the cellulose chain (Gatzl, 1990)

The reaction that causes yield loss in alkaline media, the peeling reaction, has usually less importance in oxygen delignification than random chain cleavage. For an end unit to be susceptible to removal by the peeling reaction, it must contain a carbonyl group. Because the occurrence of the reaction leaves behind a new end unit containing a carbonyl group, the process is self propagating and continues until all the cellulose is dissolved. This is prevented by the occurrence of a competing reaction, termed as the stopping reaction that converts the end unit to one that does not contain a carbonyl group (Dence and Reeve, 1996).

2.1.4 Selectivity and Protectors

Selectivity can be defined as the ratio of the attack on lignin to the attack on carbohydrate. It is affected by the choice of process conditions and by the presence of pulp contaminants. Of the factors governing selectivity in oxygen delignification, one of the most important is the transition metal content of the pulp, because these metals catalyze the generation of harmful radical species. Most pulps contain appreciable quantities of iron, copper, and manganese, all of which have this effect. One approach for dealing with transition metals is to remove them by acid washing before the oxygen stage; another is to add compounds to the pulp that inhibit carbohydrate degradation. These compounds are called carbohydrate protectors.

The protector of greatest commercial importance is the magnesium ion. The discovery of its effectiveness in 1963 by Robert and co-workers provided a great impetus for the development of oxygen delignification. Since then a considerable number of compounds have been found effective, but none is as economical as magnesium sulfate or its heptahydrate, Epsom salt. It is believed to function by precipitating as magnesium hydroxide, which adsorbs the metal ions, making them unavailable for catalysis of peroxide decomposition or by forming complexes with them (Gilbert et al., 1973).

2.2 Mass Transfer

Oxygen delignification is a heterogeneous reaction involving three phases solid (fiber), liquid (aqueous alkali solution), and gas (oxygen). The diagram of the microscopic bleaching process for a single fiber is shown in Figure 2.5. The mass transfer of oxygen gas is described as follows (Hsu and Hsieh, 1985a):

- Oxygen transfer from the gas phase through a gas film into the gas-liquid interfacial boundary.
- Oxygen transfer from the interfacial boundary through a liquid film into the bulk liquid phase.
- Diffusion and convection of oxygen molecules from the bulk phase into the liquid layer surrounding the fiber.
- Diffusion of OH^- ions and oxygen molecules through the liquid layer to the fiber.
- Interfiber mass transfer for the multifiber structure.
- Intrafiber mass transfer with fiber delignification at reaction sites in the fiber.

Hsu and Hsieh (1985b) reported that the mass transfer resistance of oxygen in the gas phase is insignificant in comparison with the liquid phase resistance. The liquid phase resistance is high because of the low solubility of oxygen in the liquid phase. Hsu and Hsieh (1985b) also found that the intra-fiber mass resistance was insignificant in comparison to the liquid phase mass transfer rate. Similarly, Agarwal et al. (1999) reported that there was no improvement in the oxygen delignification rate after the pulp had been refined, which suggests that the intra-fiber mass transfer effect does not influence the delignification rate.

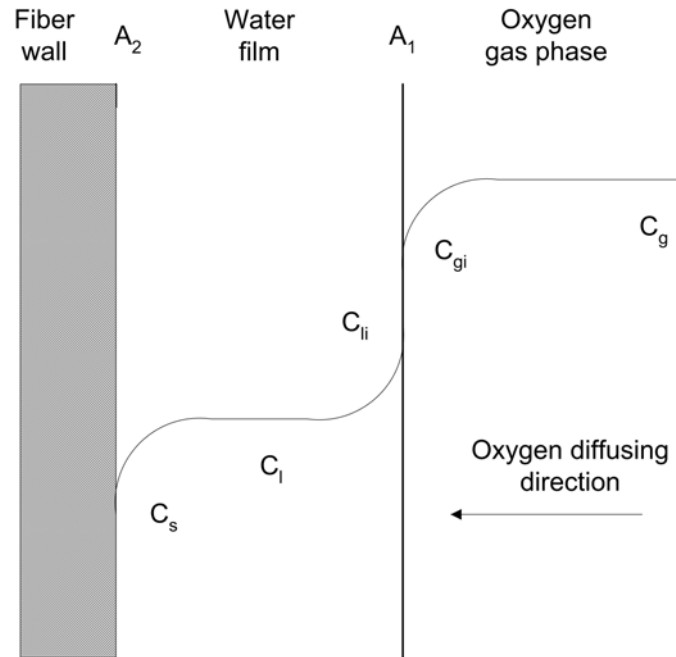


Figure 2.5 Mass transfer of oxygen to fiber wall (Hsu and Hsieh, 1985a)

2.3 The Rate of Oxygen Delignification

Most kinetic models for oxygen delignification are empirical in which the rate of delignification is considered to be proportional to the lignin content expressed as the Kappa number (K), hydroxide ion concentration $[OH^-]$ and oxygen pressure (P_{O_2}) expressed in the form of a power law. This is given by an equation of the form:

$$-r_a = -\frac{dK}{dt} = k [OH^-]^m [P_{O_2}]^n K^q \quad (2.1)$$

The constant m , n and q are determined empirically from experimental data. The reaction rate coefficient k depends on the temperature and is given by the Arrhenius equation:

$$k = A \exp\left(-\frac{E_A}{RT}\right) \quad (2.2)$$

where E_A is the activation energy, R is the gas constant and T is the absolute temperature.

Based on equations 2.1 and 2.2, the rate of oxygen delignification have been described by using one and two region model equations by Olm and Teder (1979), Hsu and Hsieh (1987, 1988), Iribarne and Schroeder (1997) and Agarwal et al. (1999).

Some investigators have treated oxygen delignification by considering that the decrease in Kappa number takes place over two distinct time periods; a rapid initial step followed by a long period during which the change in Kappa number is at a very slow rate. The two different reaction periods are assumed to be related to the various lignin linkages comprising its structure, which have been shown by Johansson and Ljunggren (1994) to have widely different half-lives when exposed to oxygen in alkaline medium.

The most widely accepted kinetic model of two regions is that of Olm and Teder (1979) who assumed pseudo, first order kinetic equations in terms of the Kappa number. They defined the initial Kappa number (K_0) as the sum of quickly (K_{01}) and slowly (K_{02}) eliminated lignin.

$$K_0 = K_{01} + K_{02} \quad (2.3)$$

Equation 2.3 was applied to the two regions in the form of two first order kinetic expressions. The corresponding two-region delignification equation for softwood proposed by Olm and Teder (1979) is,

$$-\frac{dK}{dt} = k_1 [\text{OH}^-]^{0.1} [\text{PO}_2]^{0.1} K_1 + k_2 [\text{OH}^-]^{0.3} [\text{PO}_2]^{0.2} K_2 \quad (2.4)$$

where k_1 and k_2 are the rate constant in the initial and final phases respectively and K_1 and K_2 are the fast and slow eliminated lignin. As an alternative to the two-region representation, the same data can be represented by the one-region model. Kovasin et al. (1987) applied the one region model to Olm and Teder (1979) data and obtained the equation,

$$-\frac{dK}{dt} = k [\text{OH}^-]^{0.6} [\text{P}_{\text{O}_2}]^{0.5} K^{3.2} \quad (2.5)$$

Kovasin et al. (1987) used Equation 2.5 and developed an algorithm for sizing medium-consistency oxygen delignification towers.

Hsu and Hsieh (1987, 1988) carried out delignification experiments in an agitated reactor at ultra-low consistency (0.4%) to eliminate the effect of alkali concentration change and also to eliminate liquid phase mass transfer restriction during the oxygen delignification process. Hsu and Hsieh (1987) studied the effect of alkali concentration, temperature, and oxygen pressure on delignification as well as on carbohydrate degradation. Based on their experiments carried out at 0.4% consistency, a single stage kinetic model was proposed and given in Equation 2.6.

$$-\frac{dK}{dt} = 0.24 \exp\left(-\frac{8.3 \times 10^7}{RT}\right) [\text{OH}^-]^{1.0} [\text{P}_{\text{O}_2}]^{0.89} K^{6.27} \quad (2.6)$$

Also the data was fitted to the two-stage model as Equation 2.7. It was found that the two-stage model fit the data better than the single-region model.

$$\begin{aligned} -\frac{dK}{dt} = & 2.46 \exp\left(-\frac{3.6 \cdot 10^7}{RT}\right) [\text{OH}^-]^{0.78} [\text{P}_{\text{O}_2}]^{0.35} K^{3.07} [u(t) - u(t-2)] \\ & + 143.449 \exp\left(-\frac{7.1 \cdot 10^7}{RT}\right) [\text{OH}^-]^{0.7} [\text{P}_{\text{O}_2}]^{0.74} K^{3.07} u(t-2) \end{aligned} \quad (2.7)$$

In Equation 2.7, $u(t)$ is the unity function which was used to imply that in the first 2 min of reaction time, the kinetic equation was described by the first term and during the rest of the reaction time was described by the second term. Also it was found that decreasing the consistency from 0.4 to 0.3 and 0.2% did not affect the Kappa number reduction, which shows that the effect of fiber entanglement on the overall delignification rate was eliminated in this low range of consistency.

Iribarne and Schroeder (1997) extended the range of oxygen concentration in their experiments through the application of high oxygen pressure in the gas phase. The previous oxygen delignification studies have covered a range of

oxygen pressures up to 1.5 MPa, which implies a maximum possible concentration of 0.012 mole O₂/L in the aqueous media. With increasing the oxygen pressure, it was aimed to increase the delignification rates.

The high pressure delignification data were used to calculate the parameters in two models: a single equation on lignin and two parallel equations on lignin. The single equation model is given in Equation 2.8.

$$-\frac{dK}{dt} = 3 \cdot 10^6 \exp\left(-\frac{51}{RT}\right) [\text{OH}^-]^{0.7} [\text{O}_2]^{0.7} K^2 \quad (2.8)$$

In the two parallel equations model, Equation 2.9, the lignin reaction is modeled as fast reacting (initial phase) and slow reacting lignin (final phase).

$$\begin{aligned} -\frac{dK_i}{dt} &= 6.11 \cdot 10^{11} \exp\left(-\frac{67 \times 10^3}{RT}\right) [\text{OH}^-]^{1.2} [\text{O}_2]^{1.3} K \\ -\frac{dK_f}{dt} &= 6 \cdot 10^4 \exp\left(-\frac{40 \times 10^3}{RT}\right) [\text{OH}^-]^{0.3} [\text{O}_2]^{0.2} K \end{aligned} \quad (2.9)$$

In these equations, t is expressed in min, K in mL/g, [OH⁻] and [O₂] in mole/L, R in J/mole·K and T in K.

Agarwal and co-workers (1999) performed a detailed investigation of the kinetics oxygen delignification for mixed southern hardwoods using mill-cooked pulp. The Kappa number versus time was fitted to a power law rate equation of apparent order q by following the method suggested by Schoon (1982).

$$-r_a = -\frac{dK}{dt} = kK^q \quad (2.10)$$

The reaction rate constant (k) was correlated to the initial alkali concentration [OH⁻, g/L], temperature (T, K), activation energy (E_a, kJ/mole) and oxygen partial pressure (P_{O₂}, psig) by the equation

$$k = 6.59 \cdot 10^6 \exp\left(-\frac{107.2}{RT}\right) [\text{OH}^-]^{0.92} [\text{P}_{\text{O}_2}]^{0.53} \quad (2.11)$$

The three primary process variables affecting the Kappa number decrease are, in decreasing order of importance; the temperature, the alkali concentration and the oxygen pressure. An attractive feature of the power law model, Equations 2.10 and 2.11, is that it can be integrated simply to give an expression that can be used readily for estimating the Kappa number drop with time under various reaction conditions.

$$K = \left[\frac{1}{K_0^{q-1}} + (q-1)kt \right]^{\frac{1}{q-1}}, q \neq 1 \quad (2.12)$$

Agarwal and coworkers (1999) found that the reaction order q for mixed southern hardwoods was 7.7. This extremely high rate order suggests that the delignification process is hindered in the second reaction period. This hindrance could be due to a number of factors; solid state mass transfer of oxygen and caustic into the cell wall, by lignin condensation reactions, or by the presence of carbohydrates such as xylans that are bound to lignin groups and are resistant to delignification under alkaline conditions.

High apparent reaction orders have been observed with respect to the lignin content in kinetic studies of various bleaching processes. Schoon (1982) has shown that a power law equation results when polymer degradation occurs via an infinite number of first-order reactions proceeding in parallel with various moieties in the structure of the polymer. Refractory lignin groups would have low first-order reaction rate coefficients and could account for the slow second-rate period.

Schoon also defined a frequency function $f(k)$ of the rate constant, with $f(k)$ as the fraction of the rate constants having values between k and $k+dk$. This frequency function was defined by equation,

$$\int_0^{\infty} f(k)dk = 1 \quad (2.13)$$

The distribution function $F(a,b)$ is defined as the fraction of the rate constants with the values between $k = a$ and $k = b$ and is given by,

$$F(a,b) = \int_a^b f(k)dk \quad (2.14)$$

Schoon defined a reaction of the α^{th} order which is the net effect of a large number of parallel first order reactions. This is given by Equation 2.15, which has the same form as the power law equation that was used by previous workers to define the kinetics of oxygen delignification. The effects of temperature, alkali concentration, and pressure are incorporated into single rate constant k_α .

$$-\frac{dL}{dt} = k_\alpha L^\alpha \quad (2.15)$$

where L is the total lignin content. The reaction order α , and the rate constant k_α are both determined experimentally.

Based upon Equation 2.15, Schoon derived an expression for the function $f(k)$, which explains the observed rate order α . Schoon's function is given in Equation 2.16.

$$f(k) = \frac{q^{\frac{1}{\alpha-1}} k^{\frac{2-\alpha}{\alpha-1}}}{\Gamma\left(\frac{1}{\alpha-1}\right)} \cdot \exp(-qk) \quad (2.16)$$

In the analysis carried out by Schoon the value of q depends on α , k_α and L_0 , the lignin content at the start of the reaction, and is given by Equation 2.17.

$$q = \left[(\alpha-1)k_\alpha \cdot L_0^{\alpha-1} \right]^{-1} \quad (2.17)$$

The assumption of a large number of parallel first order reactions with different rate constants, given by a distribution function, can adequately explain the observed delignification response. The lignin fractions having high and low values for the rate constant contribute, respectively, to the rapid initial phase, and to the slow second phase of the reaction.

2.4 The Kinetic Analysis of Carbohydrate Degradation

Two competing reactions, delignification and carbohydrate degradation, occur simultaneously during oxygen bleaching, and any kinetic study of oxygen bleaching must include the study of both delignification and carbohydrate degradation. The carbohydrate degradation is monitored by measuring the intrinsic pulp viscosity (ASTM standard D1795). The rate of carbohydrate degradation can also be described in a similar way as that of the rate of delignification. The general kinetic equation for carbohydrate degradation is

$$\frac{dM_n}{dt} = A e^{-\frac{E_A}{R T}} [\text{OH}^-]^o [\text{P}_{\text{O}_2}]^p M_n^r \quad (2.18)$$

where M_n is the moles of cellulose chains per metric ton of pulp. In order to handle Equation 2.18 the measured viscosity should be converted into number of cellulose chains per metric ton of pulp by Equation 2.19 (Olm and Teder, 1979).

$$\log M_n = 4.35 - 1.25 \log \eta \quad (2.19)$$

where M_n is moles of cellulose chains per ton of pulp and η is the intrinsic viscosity, dm^3/kg .

In the literature, there are a limited number of studies on carbohydrate degradation kinetics, and that of Olm and Teder (1979) and Iribarne and Schroeder (1997) are the major ones.

Olm and Teder (1979) used two zero order reactions to express the carbohydrate degradation kinetics during oxygen delignification. The expression is,

$$\frac{dM_n}{dt} = k_3 [\text{OH}^-]^{0.2} \text{P}_{\text{O}_2}^{0.8} + k_4 [\text{OH}^-]^{0.6} \text{P}_{\text{O}_2}^{0.1} \quad (2.20)$$

where M_n is number average molecular weight and k_3 and k_4 are the rate constants for the first and second rate periods.

Iribarne and Schroeder (1997) suggested that due to the different methods of evaluating the molecular weight (M_n) or to a relatively low resolution in their experiment, it was not necessary to use two parallel equations to obtain the apparent zero-order kinetics as proposed by Olm and Teder (1979). Rather, Iribarne and Schroeder (1997) described carbohydrate degradation kinetics during the oxygen delignification stage by a single zero-order equation,

$$\frac{dm_n}{dt} = 7 \cdot 10^{10} \cdot \exp\left(-\frac{78}{RT}\right) [\text{OH}^-]^{0.3} P_{\text{O}_2}^{0.4} \quad (2.21)$$

Oxygen delignification and carbohydrate degradation kinetics have been studied previously by various authors for different pulp types. In this study, the kinetics of oxygen delignification of Turkish Eucalyptus hardwood Kraft pulp is investigated. The objective of the current work is to gain insight into the possible reaction pathways and methods for improving the degree of delignification. The kinetic rate data can be used for design and optimization of oxygen reactor planning to be installed in Mopak Dalaman pulp and paper mill.

CHAPTER 3

EXPERIMENTAL PROCEDURE

3.1 Pulp Preparation and Experimental Setup

Kraft pulp from eucalyptus is obtained from Mopak Dalaman pulp and paper mill located in the southern part of Turkey. The pulp, as received, has a Kappa number of 17.5 and an intrinsic viscosity of 8.5 dl/g. The pulp was thoroughly washed, pressed to about 30 % consistency, and was fluffed by hand. Pulp consistency was determined from an average of three samples. The rest of the pulp was put into well-tied plastic bags and is refrigerated for future use.

The experimental setup is shown in Figure 3.1. The apparatus is a 1 L pressurized reactor produced by Parr Company which is equipped with a stirrer. On the top of the reactor one outlet flow valve was used to regulate the pressure. In addition, one gas inlet and one liquid sampling valve are present on the top of the reactor. In the experiments, the liquid sampling port was also used for the NaOH inlet port. For this purpose, a high-pressure 300 mL feeding tube was purchased from the Parr Company. The temperature was measured by a thermocouple immersed inside the fluid and was controlled by a PID controller. The pressure of the reactor was monitored by the pressure gauge. The reactor is equipped with a turbine type impeller with a six-blade style which produces an excellent mixing action over the range of stirring speeds. The dimensions of the reactor are also given in Figure 3.1.

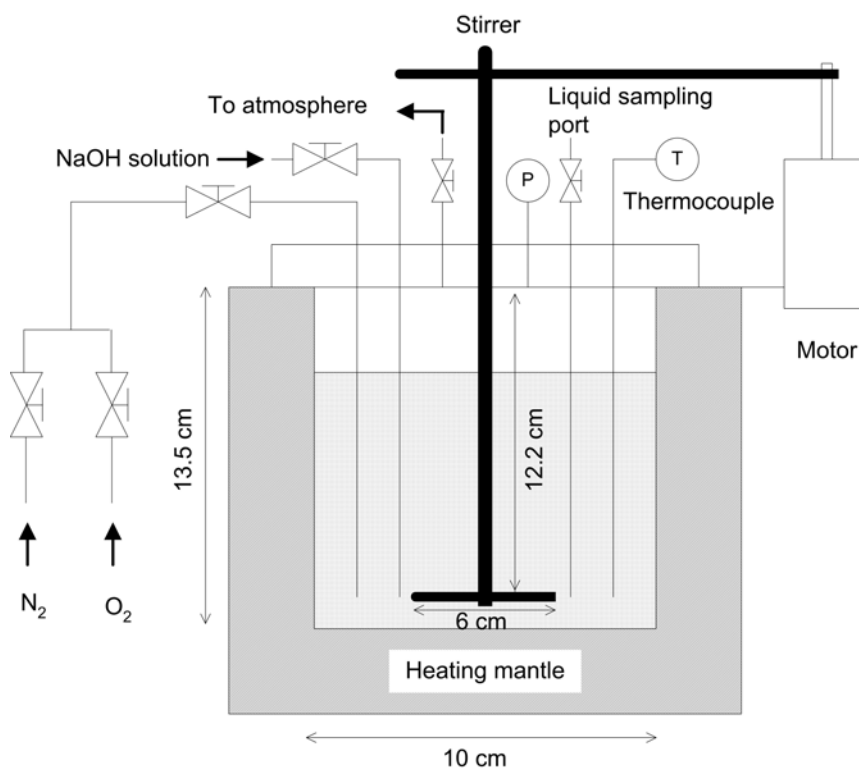


Figure 3.1 The experimental setup for ultra low consistency oxygen bleaching

3.2 Experimental Conditions

The range of process variables used in the oxygen delignification experiments are summarized in Table 3.1. In all experiments 3.5 g of oven dry pulp with a consistency of 0.5% was used. Each run was performed at the predetermined values of temperature, NaOH concentration, oxygen pressure and repeated for the reaction times 5 and 60 minutes.

Table 3.1 Range of process variables

Variable	Range
Temperature	90, 100, 110 °C
Amount of NaOH used	1, 3, 5 % on oven dry pulp used
Oxygen pressure	0.5, 3.5, 6.5 bar
Reaction time	0, 5, 10, 30 and 60 minute
Amount of MgSO ₄ .7H ₂ O used	10 % on oven dry pulp used

3.3 Experimental Procedure

At the start of the experiment, the specified amount of unbleached pulp and 0.35 g of $\text{MgSO}_4 \cdot 7\text{H}_2\text{O}$ were first put into reactor. The magnesium ion concentration (10%) in the liquid phase is equivalent to the typical reported values in the literature. About 670 mL of boiling distilled water is transferred to the reactor from a beaker heated by a hot plate.

The reactor is closed and is set into the heating vessel. Solution inside the reactor is agitated by a stirrer. Nitrogen gas is bubbled through the solution in the reactor for 5 min to purge the whole system. The reactor is heated to the reaction temperature under 2.5 barg nitrogen atmosphere.

It was determined through control runs that the range of Kappa number reduction is within a two Kappa number unit during heat up period without addition of alkali. However, if alkali solution is added before heating, a reduction of 5 Kappa number units was observed for the run at 100 °C and 0.15 g/L of NaOH. Therefore, the NaOH solution was added after the system reached the reaction temperature.

During the heating period, the prepared NaOH solution is placed inside a feeding tube. The feeding tube is connected between the nitrogen gas tank and the reactor. When the temperature reached the set point, the pressure inside the reactor is reduced to 0.5 barg. The valve adjusting the nitrogen flow rate from the gas tank and the valve connecting the feeding tube to the reactor are opened simultaneously. High-pressure nitrogen forces the NaOH solution into the reactor.

A stainless steel tube is connected between the inlet of the valve and the inside of the reactor to prevent any accumulation of NaOH solution in the dead space. The feeding of NaOH solution usually took place several seconds. After feeding the NaOH solution, oxygen is injected and bubbled through the solution quickly to reach the desired oxygen pressure above the solution. At this moment, time is started. This procedure took only a few seconds to complete. The oxygen gas flow rate is then regulated to normal operating conditions. The oxygen pressure is continuously kept at a constant value by an outlet flow valve located on top of the reactor. This outlet valve contained a fine screen to prevent fiber clogging.

At the end of the experiment, oxygen injection is terminated, and pressure inside the reactor is released to the atmosphere by completely opening the outlet flow valve. The reactor is opened quickly, and some of the liquid solution is taken for the tests and the rest of it is poured into cold water. The pulp slurry is filtered through a funnel and washed completely. The washed pulp is air dried for one day and stored for the tests.

3.4 Pulp and Liquor Analyses

The air-dried pulp is first analyzed for Kappa number following the Tappi Standard T-236. The intrinsic viscosity $[\eta]$ is estimated according to ASTM standard D1795. The residual alkali in the liquor from the oxygen delignification experiment is measured following Tappi Standard T-625. The detailed description of the standards is given in Appendix.

CHAPTER 4

RESULTS AND DISCUSSION

4.1 The Analysis of Mass Transfer

In the first part of the study, the effect of inter-fiber mass transfer effect is examined by carrying out experiments at different consistency values. Figure 4.1 shows the change in Kappa number as a function of time at 0.5, 1 and 8% consistency values for oxygen delignification using the mill southern hardwood pulp sample.

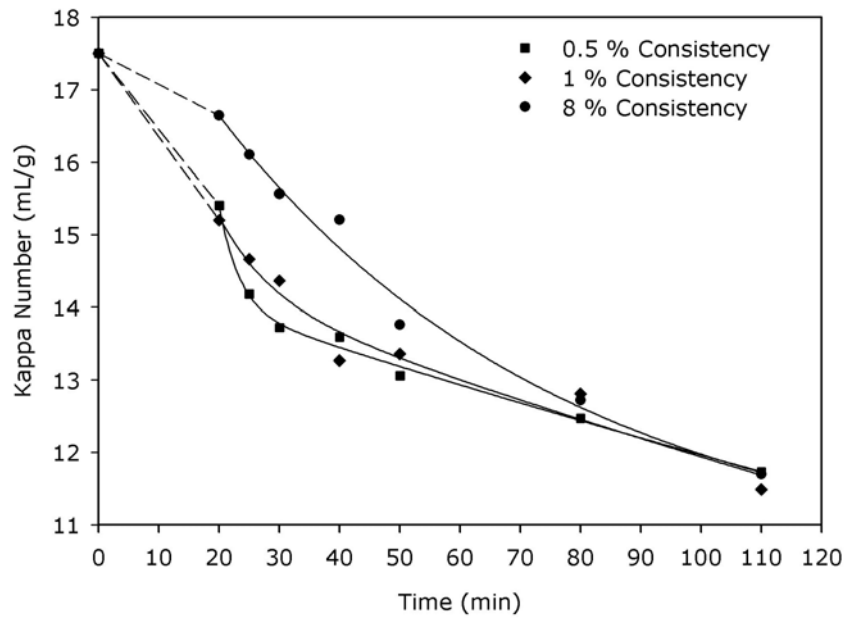


Figure 4.1 The effect of consistency on the change of Kappa number (T = 100 °C, oxygen partial pressure = 6.5 bar and 600 rpm)

In these experiments, there was an initial heat-up period of about 20 minutes (shown with dashed lines), which resulted in an initial decrease in the Kappa number of around 1-2 units. It was seen from the figure that up to 20 minutes the Kappa number of the pulp at 8% consistency is higher than that of the 0.5 and 1% consistency values. There is a significant resistance for the transfer of oxygen in the experiments performed at 8% consistency. However, after 20 minutes the gap between the two lines is decreasing. The oxygen starts to penetrate between the fibers and the inter-fiber mass transfer effects are decreasing. Finally at 90 minutes, they reach the same Kappa number. It was concluded from the figure that, in order to decrease the inter-fiber mass transfer limitations, the experiments should be done in lower consistencies. Therefore, the oxygen delignification and carbohydrate degradation kinetic experiments were performed at 0.5% consistency. Another way of decreasing the inter-fiber mass transfer is changing the mixing rate of the pulp. If the content of the reactor is mixed more rapidly and well, it would be possible to minimize the liquid phase mass transfer restrictions. In Figure 4.2, three set of experiments with different mixing rates (500, 600 and 700 rpm) were performed in order to see the effect of mixing on the oxygen delignification. It was seen from the figure that, different mixing speeds did not have an appreciable effect on the delignification curves. Therefore, all the experiments were performed at 600 rpm mixing rate.

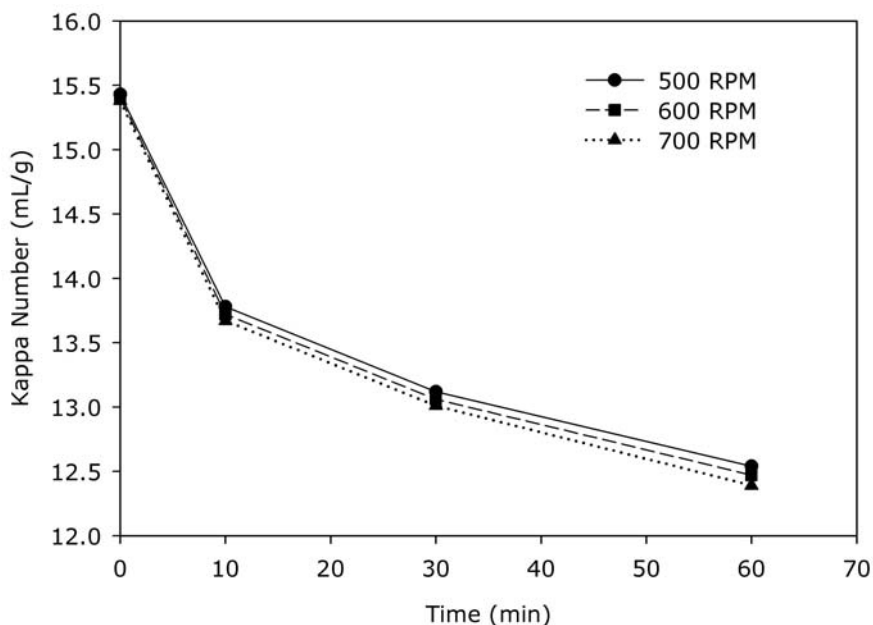


Figure 4.2 The effect of mixing rate on the change of Kappa number (T = 100 °C, partial oxygen pressure = 6.5 bar)

In order to derive the kinetic rate expression of oxygen delignification, NaOH concentration in the experiments should be kept constant. In Figure 4.3 the effect of consistency on NaOH concentration was examined. It was seen from the figure that, at 0.5 and 1% consistency values the NaOH concentration was constant, however at 8% consistency NaOH concentration is decreasing with an increase in the reaction time. It was concluded from the figure that, lower consistencies gives better control of NaOH concentration.

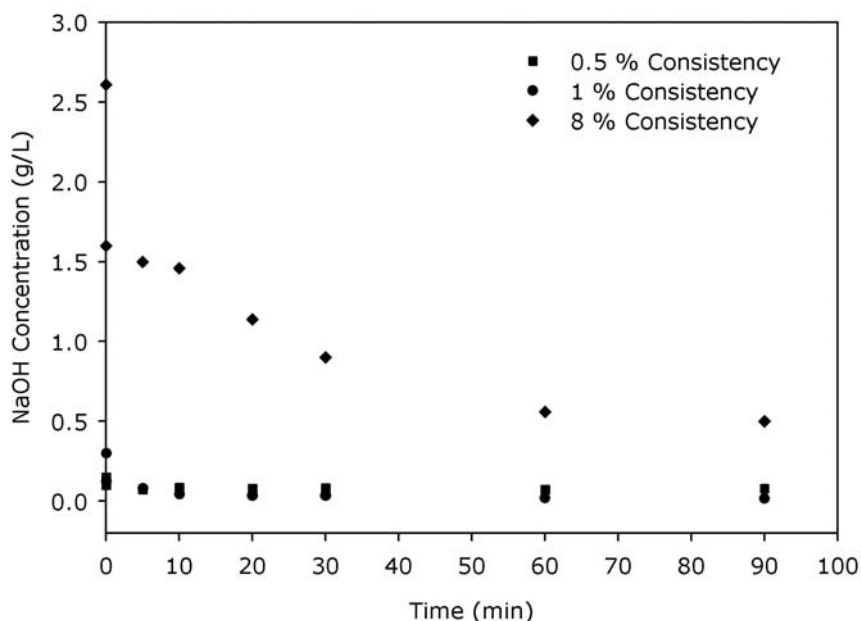


Figure 4.3 The change in residual alkali concentration with respect to time ($T = 100\text{ }^{\circ}\text{C}$ and oxygen partial pressure = 6.5 bar)

In order to investigate the intrafibre mass transfer during oxygen delignification, the refined pulp from the Mopak pulp and paper mill was also used for a set of experiments. Refining shortens, hydrates and fibrillates the pulp, thus increasing the surface area of the fiber tremendously. If the intra-fiber mass transfer is significant, then prerefining the pulp should give higher levels of delignification because of the increased surface area. In Figure 4.4, the effect of refining on the oxygen delignification was shown. It was seen from the figure that, there was no significant effect of refining on the rate of delignification. Therefore, it was concluded that the intrafibre mass transfer resistance was not significant under the conditions studied.

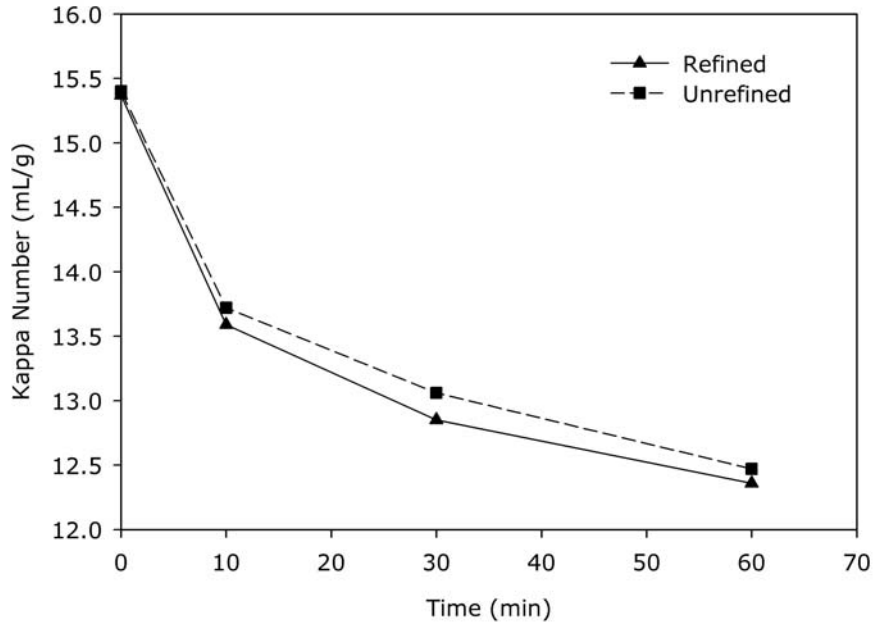


Figure 4.4 The effect of refining on the change of Kappa number (T = 100 °C and oxygen partial pressure = 6.5 bar)

4.2 The results of Oxygen Delignification Experiments

Based on the results summarized in the previous section, the delignification experiments were performed at 0.5 % consistency, thus eliminating inter-fiber mass transfer limitations and the effect of the change in alkali concentration. The data collected were correlated using the general kinetic model given by Equation 4.1.

$$-r_a = -\frac{dK}{dt} = kK^q \quad (4.1)$$

The dependency of temperature, oxygen partial pressure and initial sodium hydroxide concentration can be incorporated into the rate coefficient (k) as shown in the Equation 4.2.

$$k = A \exp\left[\frac{-E_A}{RT}\right] [\text{OH}^-]^m [\text{P}_{\text{O}_2}]^n \quad (4.2)$$

The units used in the correlation are K, Kappa number; $[\text{OH}^-]$, sodium hydroxide concentration (g/L); P_{O_2} , oxygen partial pressure (bar); t, time (min).

Integration of Equation 4.1 under conditions of constant oxygen partial pressure and initial alkali concentration gives the equation for the Kappa number as a function of time.

$$K^{1-q} - K_0^{1-q} = (q-1)kt, \quad q \neq 1 \quad (4.3)$$

The Equation 4.3 may be rewritten as

$$K = \left[\frac{1}{K_0^{q-1}} + (q-1)kt \right]^{\frac{1}{(q-1)}}, \quad q \neq 1 \quad (4.4)$$

The parameter q which denotes the rate order with respect to the Kappa number cannot be found explicitly from Equation 4.4, so a trial and error solution was used following the integral method of analysis. The other parameters were determined by linear regression of the experimental data. The details of the calculation procedure are presented in Appendix B. The value of q was found to be 7.9. The delignification rate equation was found to be

$$-\frac{dK}{dt} = 0.3 \exp\left[\frac{-64504}{RT}\right] [\text{OH}^-]^{0.74} [\text{PO}_2]^{0.32} K^{7.9} \quad (4.5)$$

In Figure 4.5, 4.6 and 4.7, the Kappa number change with respect to time is presented. The solid line represents the delignification rate model equation found as Equation 4.5.

It was seen from the figures that the kinetic model that was estimated by the power law model represents the experimental data well. This model can be used for sizing oxygen delignification reactors and simulation of the bleaching plants.

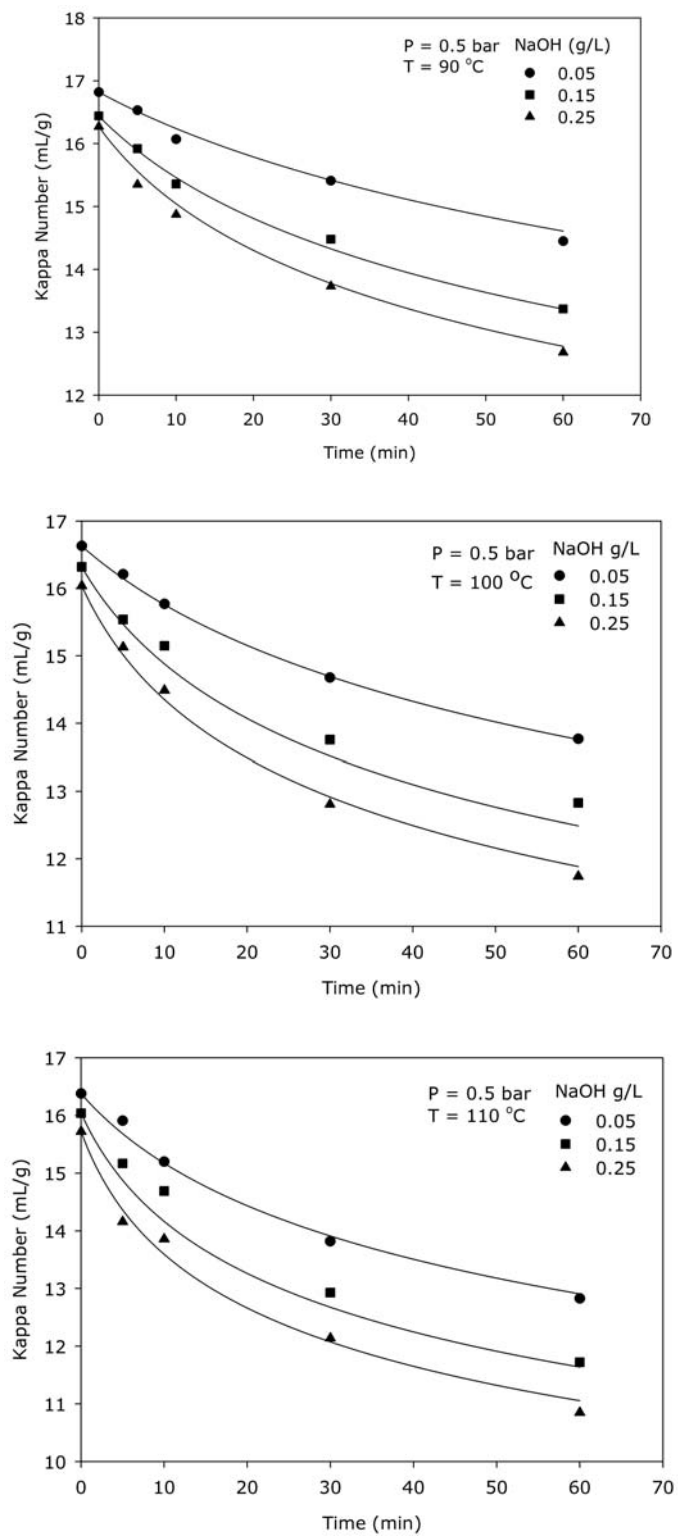


Figure 4.5 The change in Kappa number with respect to time (T = 90, 100, 110 °C, oxygen partial pressure = 0.5 bar, NaOH concentration = 0.05, 0.15, 0.25 g/L)

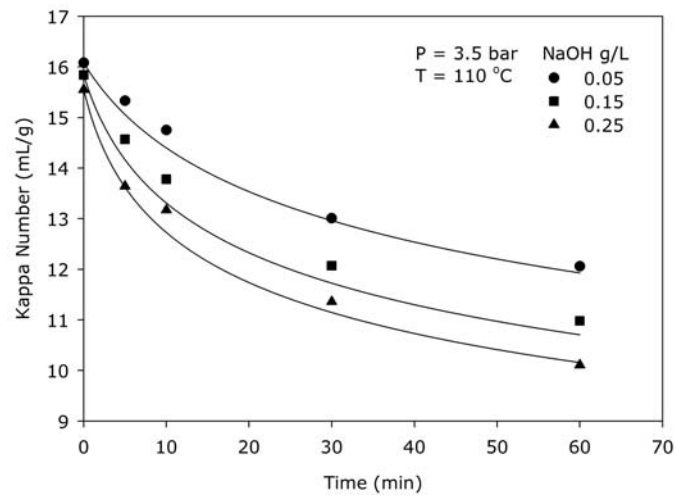
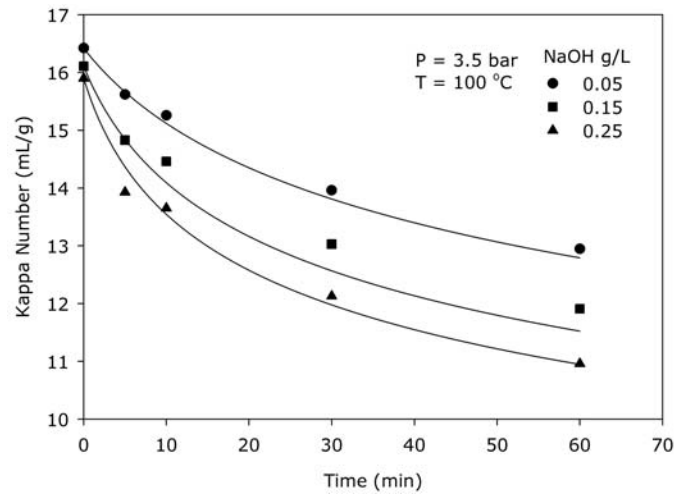
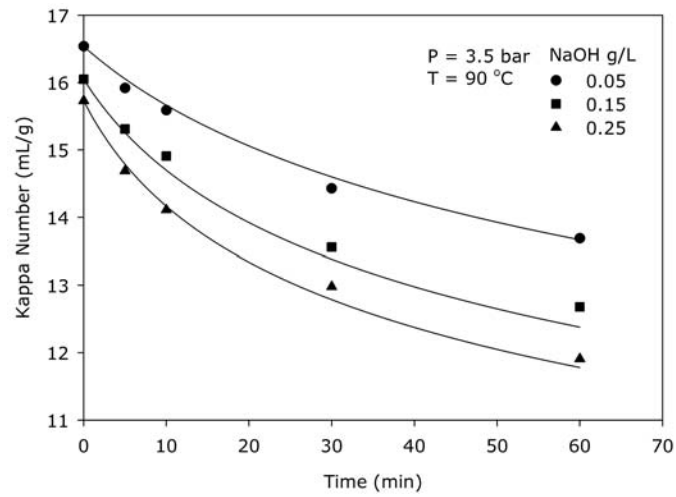


Figure 4.6 The change in Kappa number with respect to time (T = 90, 100, 110 °C, oxygen partial pressure = 3.5 bar, NaOH concentration = 0.05, 0.15, 0.25 g/L)

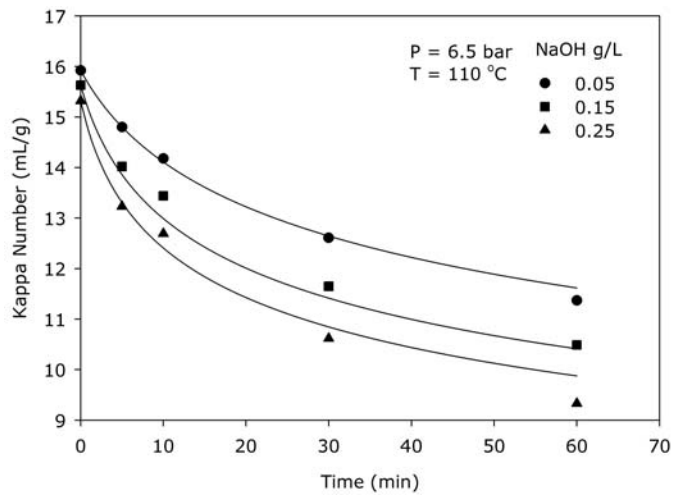
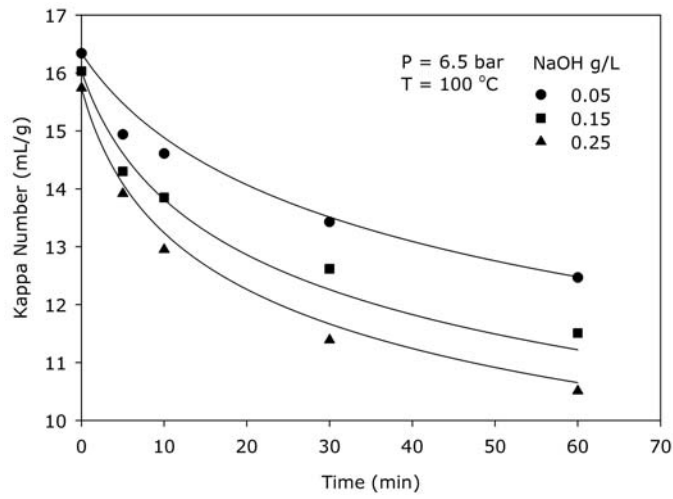
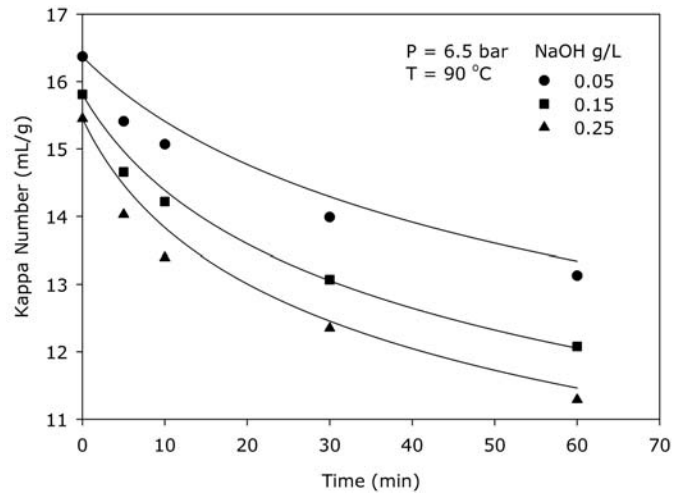


Figure 4.7 The change in Kappa number with respect to time (T = 90, 100, 110 °C, oxygen partial pressure = 6.5 bar, NaOH concentration = 0.05, 0.15, 0.25 g/L)

In order to see the effect of temperature and partial pressure of oxygen on Kappa number, Figure 4.8 and Figure 4.9 are drawn by using the data presented above. In Figure 4.8 the change in Kappa number with respect to time is presented for the temperature interval of 90 to 110 °C at 0.15 g/L alkali charge and 6.5 bar oxygen partial pressure. It was seen from the figure that the greatest reduction in Kappa number, as a measure of the amount of delignification achieved, occurs at the highest level of temperature (110 °C) studied when the alkali concentration and the oxygen partial pressure are kept constant.

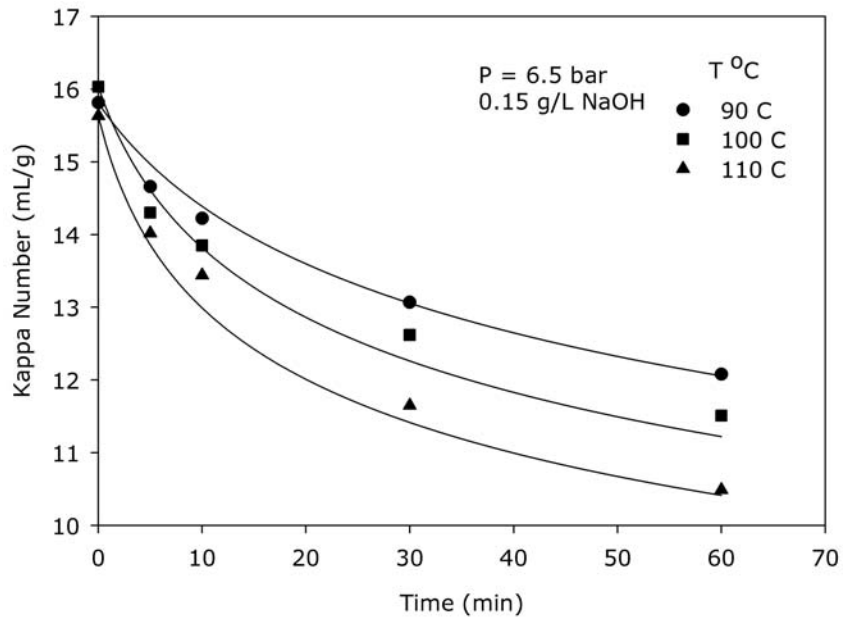


Figure 4.8 The effect of temperature on the change of Kappa number (NaOH concentration = 0.15 g/L and oxygen partial pressure = 6.5)

Figure 4.9 shows the effect of partial pressure of oxygen on the delignification. As can be seen from the Figure 4.9, the highest reduction in Kappa number is obtained at the highest oxygen partial pressure (6.5 bar). This expected result indicates that increasing the partial pressure of oxygen increases the amount of delignification achieved at a fixed time interval, however the installation and operational costs in the plant will also increase likewise.

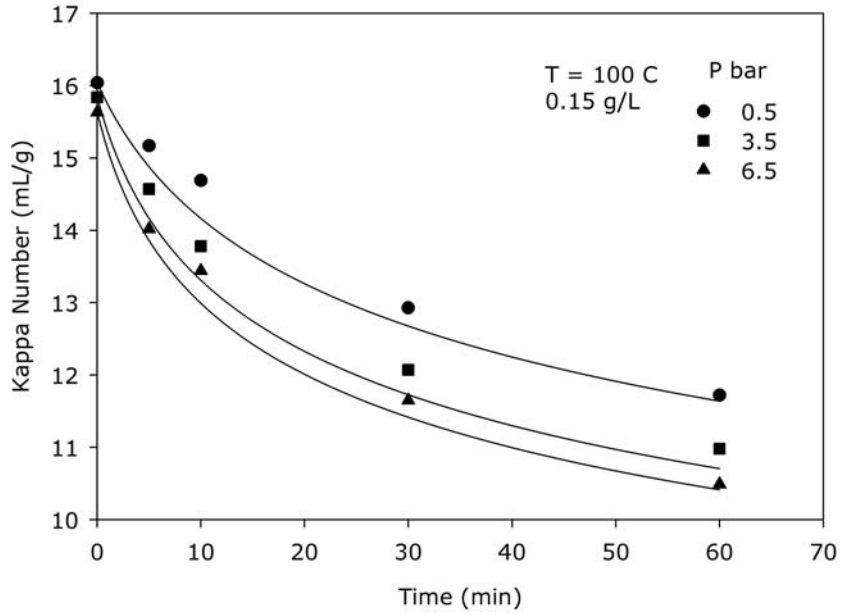


Figure 4.9 The effect of oxygen partial pressure on the change of Kappa number (T = 100 °C and NaOH concentration = 0.15 g/L)

4.3 The Kinetic Analysis of Carbohydrate Degradation

The carbohydrate degradation was monitored by measuring the intrinsic pulp viscosity η (ASTM standard D1795). The rate of carbohydrate degradation can also be analyzed in a similar way as that of delignification. The general rate equation for carbohydrate degradation in terms of viscosity is

$$-\frac{d\eta}{dt} = k\eta^r \quad (4.6)$$

where

$$k = A \exp\left[\frac{-EA}{RT}\right] [\text{OH}^-]^0 [\text{P}_{\text{O}_2}]^p \quad (4.7)$$

The units used in the correlation are η , intrinsic viscosity (dl/g); $[\text{OH}^-]$, sodium hydroxide concentration (g/L); P_{O_2} , oxygen partial pressure (bar); t, time (min).

Integration of Equation 4.6 under conditions of constant oxygen partial pressure and initial alkali concentration gives the equation for the η as a function of time.

$$\eta^{1-r} - \eta_0^{1-r} = (r-1)kt, \quad r \neq 1 \quad (4.8)$$

The Equation 4.8 may be rewritten as

$$\eta = \left[\frac{1}{\eta_0^{r-1}} + (r-1)kt \right]^{\frac{1}{(r-1)}}, \quad r \neq 1 \quad (4.9)$$

The parameter r which denotes the rate order with respect to η cannot be found explicitly from Equation 4.9, so a trial and error solution was used following the integral method of analysis. The other parameters were determined by linear regression of the experimental data. The value of r was found to be 11. The rate expression for carbohydrate degradation was found to be

$$-\frac{d\eta}{dt} = 8.75 \times 10^{-8} \exp\left[\frac{-30231}{RT}\right] [\text{OH}^-]^{0.43} [\text{PO}_2]^{0.35} \eta^{11} \quad (4.10)$$

The results are shown in Figure 4.10, 4.11 and 4.12. The solid lines represent the predictions of the model equation.

The above analysis, based on one stage power law model, represented the experimental data quite well for most cases but some deviations from experimental data were also observed. A sharp decrease encountered for certain range of experimental data is in a way the result of high reaction order on the intrinsic viscosity. Therefore, it was concluded that a two stage zero order power law model may represent the data better than one power law model.

The general equation for the two stage zero order power model for the rate of carbohydrate degradation using viscosity as the dependent variable is

$$-\frac{d\eta}{dt} = A_1 \exp\left[\frac{-E_{A1}}{RT}\right] [\text{OH}^-]^a [\text{PO}_2]^b (u(t) - u(t-10)) + A_2 \exp\left[\frac{-E_{A2}}{RT}\right] [\text{OH}^-]^c [\text{PO}_2]^d u(t-10) \quad (4.11)$$

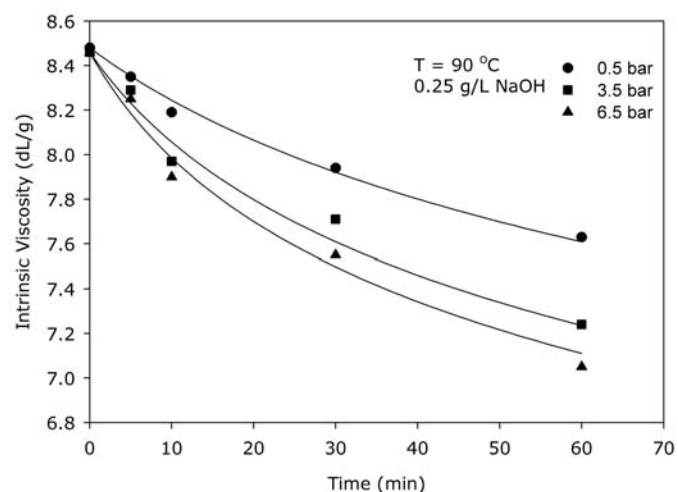
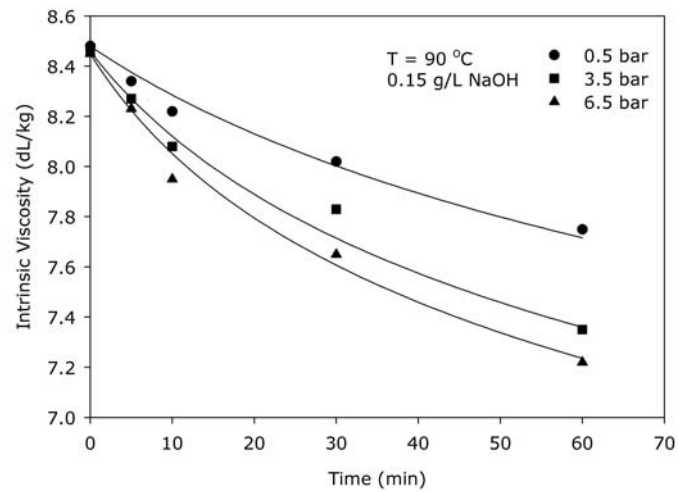
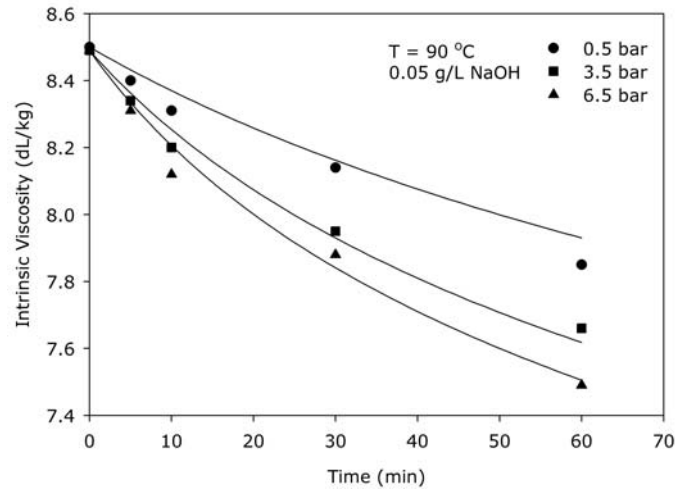


Figure 4.10 Intrinsic viscosity with respect to time ($T = 90\text{ }^{\circ}\text{C}$, oxygen partial pressure = 0.5, 3.5, 6.5 bar and NaOH concentration = 0.05, 0.15, 0.25 g/L)

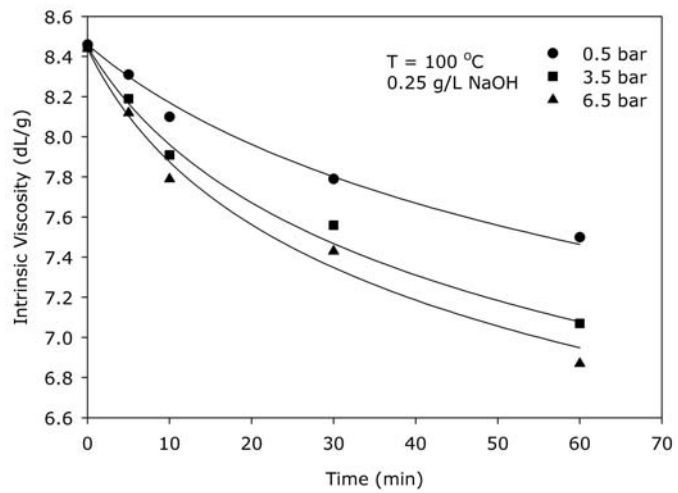
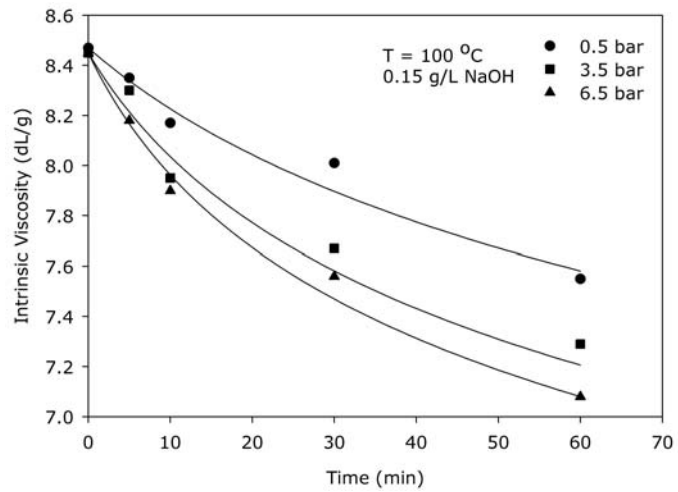
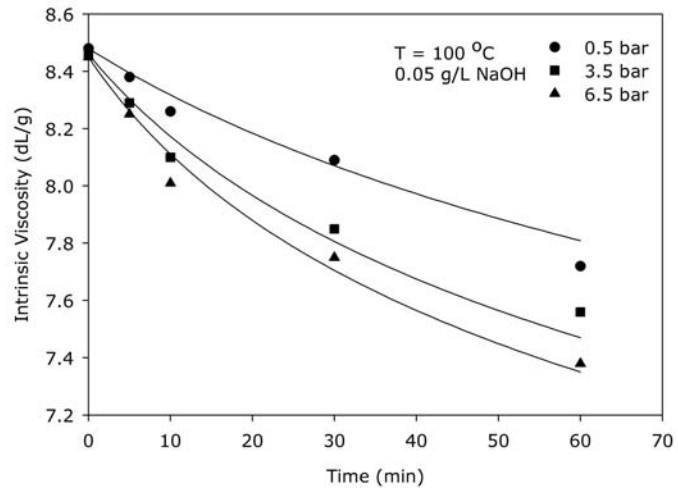


Figure 4.11 Intrinsic viscosity with respect to time ($T = 100\text{ }^{\circ}\text{C}$, oxygen partial pressure = 0.5, 3.5, 6.5 bar and NaOH concentration = 0.05, 0.15, 0.25 g/L)

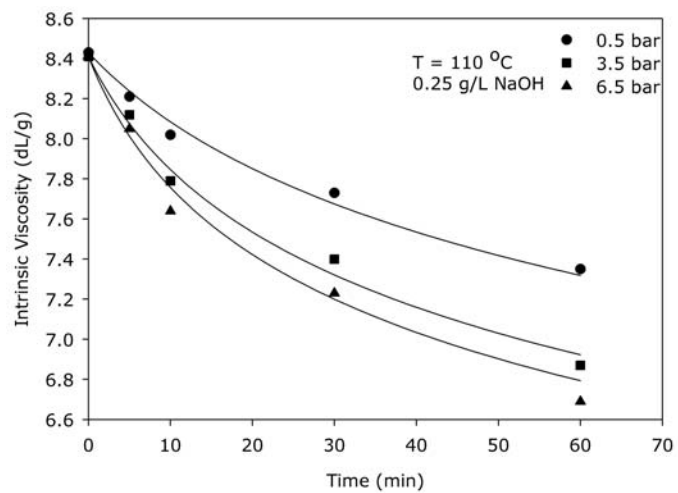
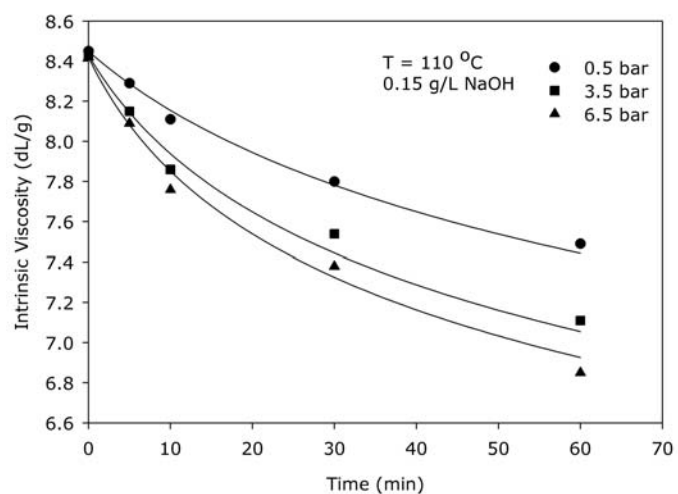
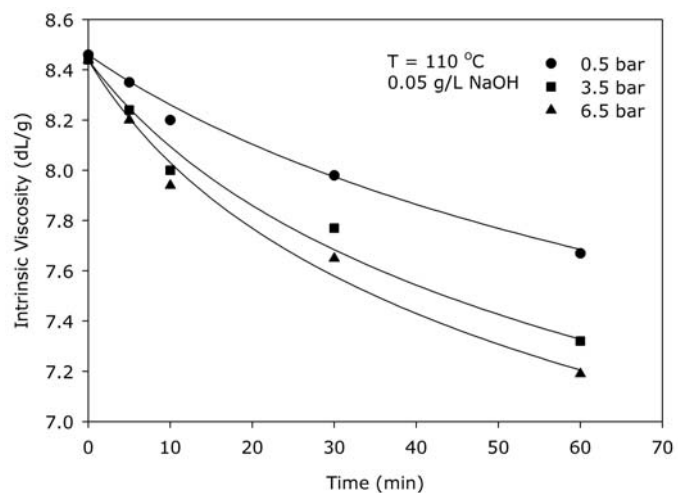


Figure 4.12 Intrinsic viscosity with respect to time ($T = 110\text{ }^{\circ}\text{C}$, oxygen partial pressure = 0.5, 3.5, 6.5 bar and NaOH concentration 0.05, 0.15, 0.25 g/L)

where $u(t)$ is the unity function which was used to imply that in the first 10 min of reaction time, the kinetic equation was described by the first term and for larger reaction time values was described by the second term.

The parameters a , b , c , d were determined by linear regression of the experimental data. The details of the calculation procedure are presented in Appendix C. The rate equation of carbohydrate degradation rate equation based on the two stage zero order power law model was found as

$$-\frac{d\eta}{dt} = 24.77 \exp\left[\frac{-18828}{RT}\right] [\text{OH}^-]^{0.26} [\text{PO}_2]^{0.25} (u(t) - u(t-10)) + 0.542 \exp\left[\frac{-10592}{RT}\right] [\text{OH}^-]^{0.18} [\text{PO}_2]^{0.13} u(t-10) \quad (4.12)$$

The comparison of the previously shown experimental data with the model predictions of the two stage power model are given in Figures 4.13, 4.14 and 4.15. As it can be seen, better agreement between the model predictions represented by the solid lines and the experimental data points were obtained.

Figure 4.16 indicates the effect of temperature on the carbohydrate degradation. It was concluded that increasing temperature during oxygen delignification increases carbohydrate degradation in both of the phases defined as the initial and the final phases. Therefore, the oxygen delignification units should not be operated at high temperatures above 100 °C.

The carbohydrate degradation achieved during oxygen delignification increased with increasing alkali concentration as well as with increasing oxygen partial pressure. Figure 4.17 shows the effect of alkali charge (0.05, 0.15, 0.25 g/L NaOH) on carbohydrate degradation, which indicates that the highest reduction in intrinsic viscosity is obtained at the highest level of the alkali concentration (0.25 g/L NaOH).

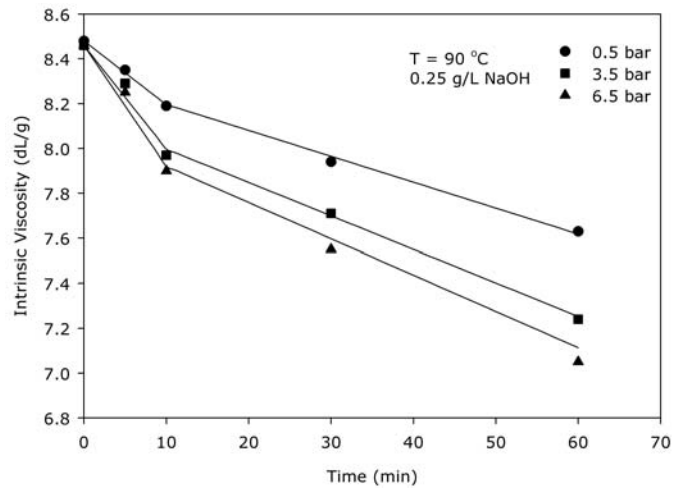
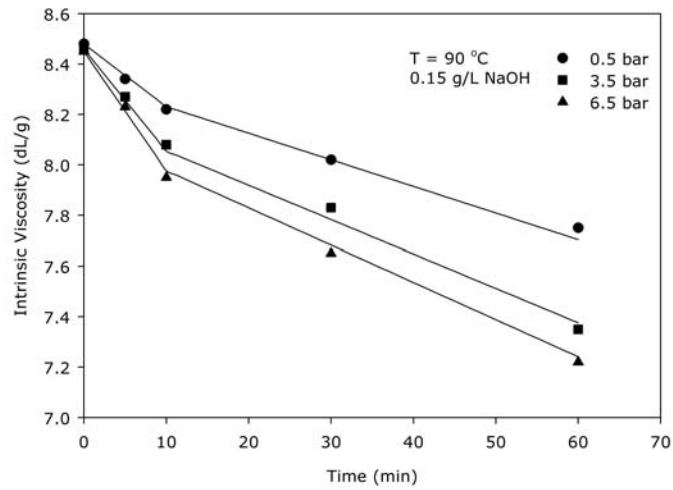
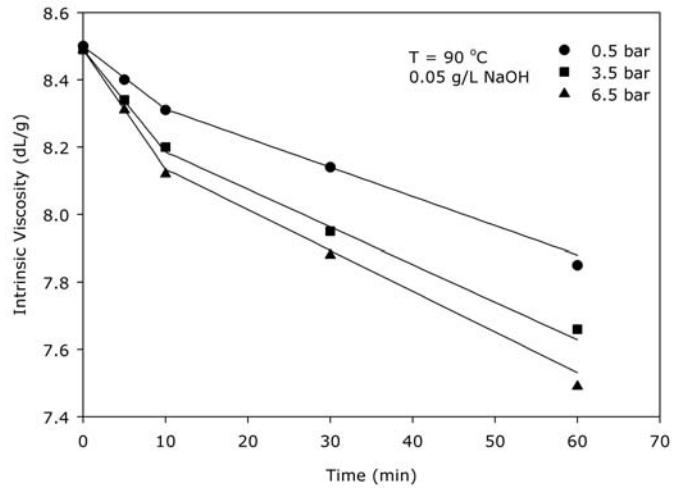


Figure 4.13 The two stage zero order power law model for intrinsic viscosity ($T = 90\text{ }^{\circ}\text{C}$, oxygen partial pressure = 0.5, 3.5, 6.5 bar and NaOH concentration = 0.05, 0.15, 0.25 g/L)

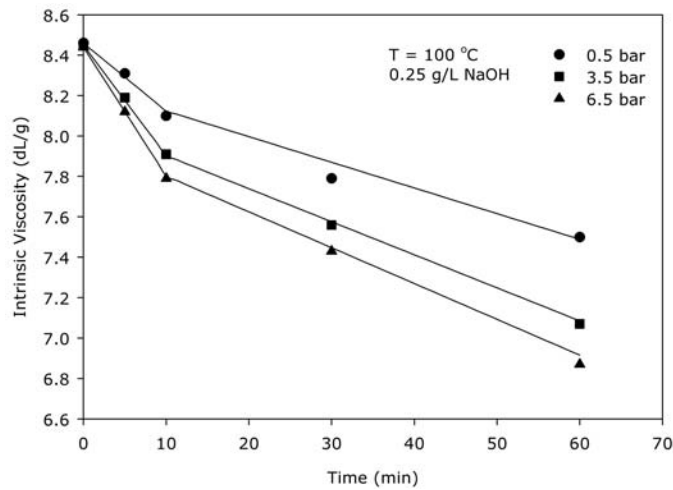
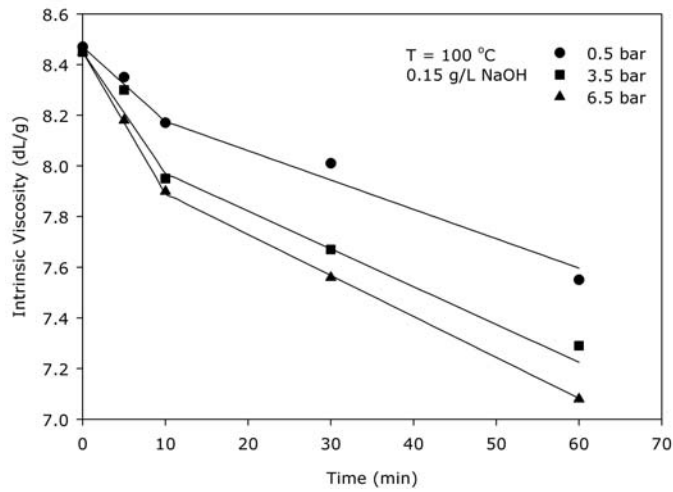
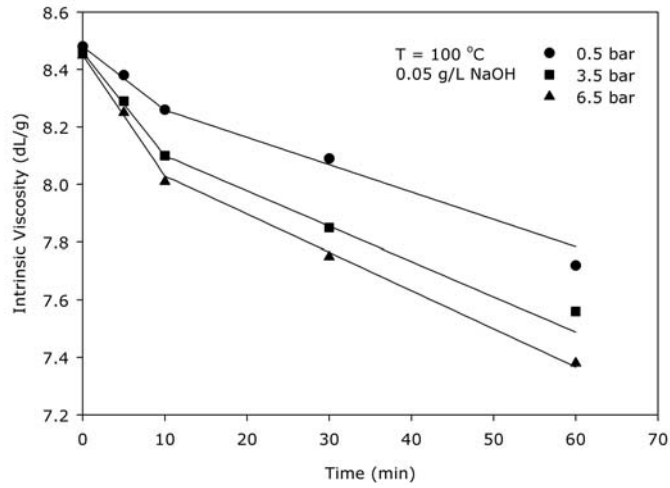


Figure 4.14 The two stage zero order power law model for intrinsic viscosity ($T = 100\text{ }^{\circ}\text{C}$, oxygen partial pressure = 0.5, 3.5, 6.5 bar and NaOH concentration 0.05, 0.15, 0.25 g/L)

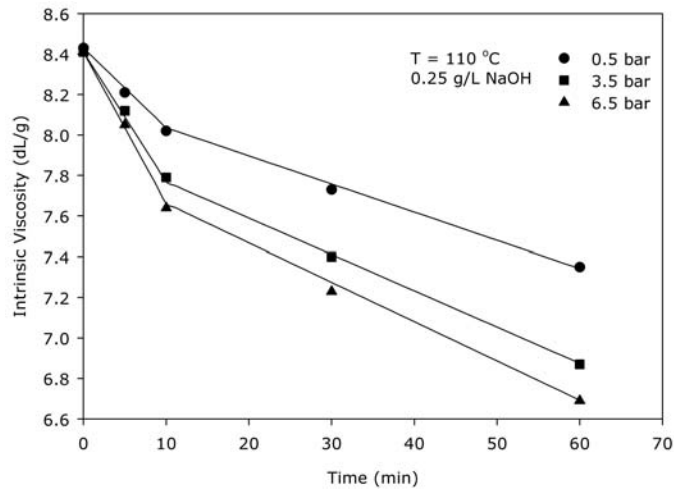
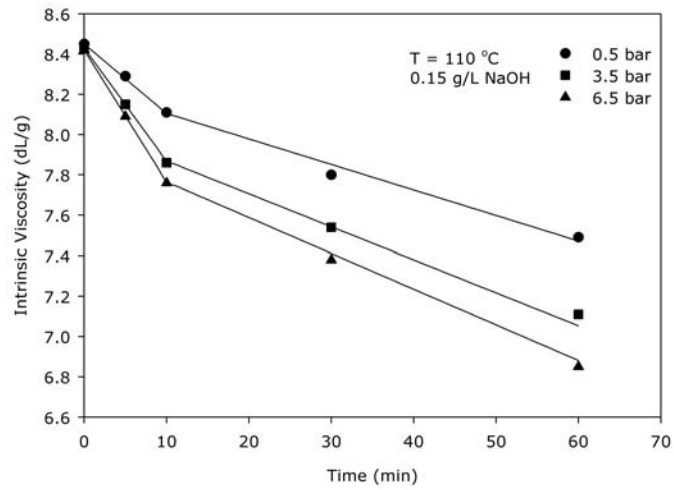
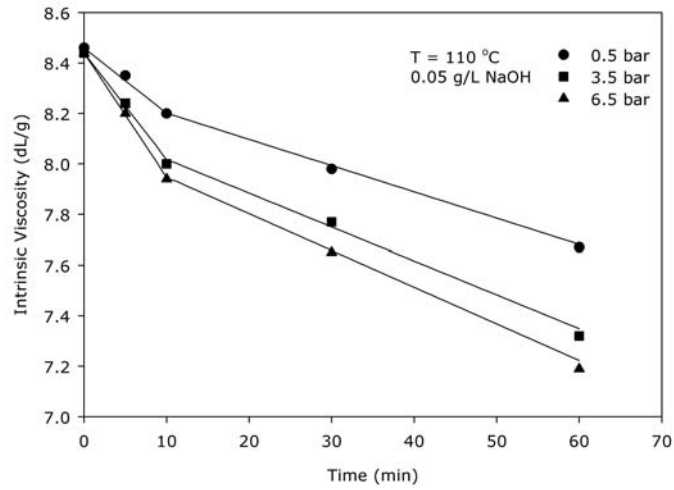


Figure 4.15 The two stage zero order power law model for intrinsic viscosity ($T = 110\text{ }^{\circ}\text{C}$, oxygen partial pressure = 0.5, 3.5, 6.5 bar and NaOH concentration = 0.05, 0.15, 0.25 g/L)

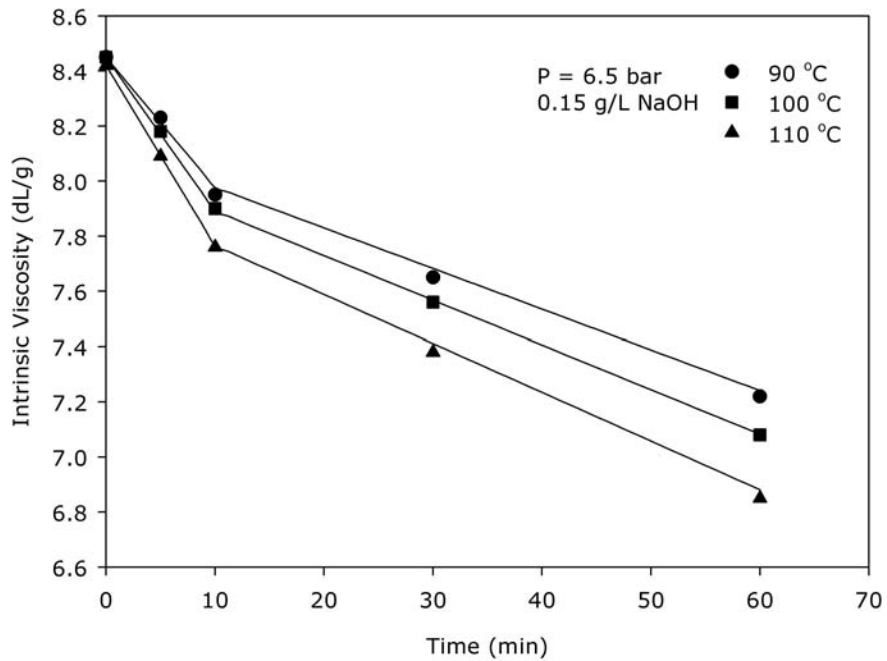


Figure 4.16 The effect of temperature on the carbohydrate degradation (NaOH concentration = 0.15 g/L and oxygen partial pressure = 6.5 bar)

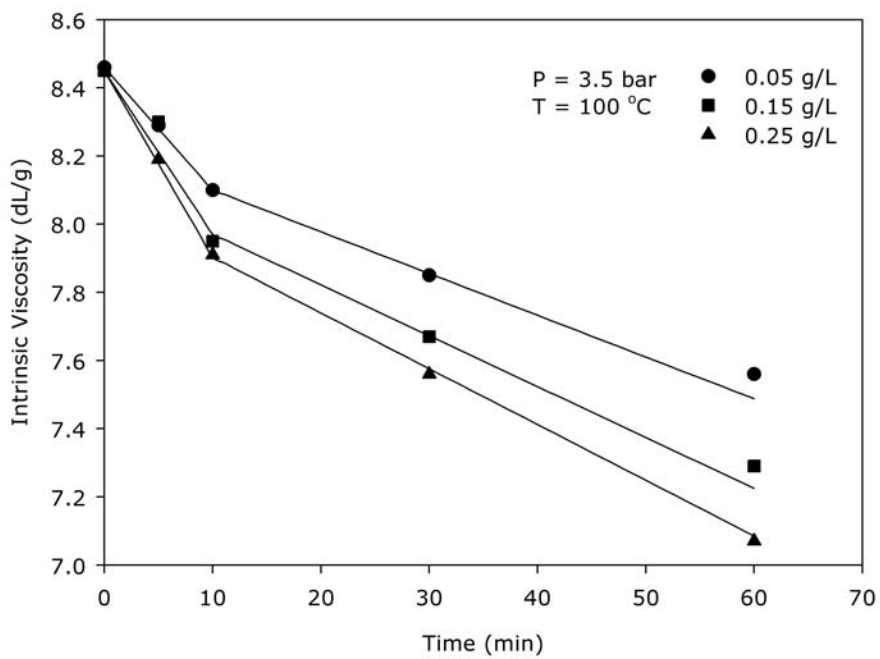


Figure 4.17 The effect of sodium hydroxide concentration on the carbohydrate degradation (T= 100 °C and oxygen partial pressure = 3.5 bar)

Moreover, the kinetic analysis of carbohydrate degradation kinetics can be based on the moles of cellulose chains per ton of pulp, M_n . The intrinsic viscosity was converted into the moles of cellulose chains per ton of pulp (Olm and Teder, 1979) as

$$\log M_n = 4.35 - 1.25 \log \eta \quad (4.13)$$

where M_n , moles of cellulose chains per ton of pulp; η , intrinsic viscosity, dL/g. The use of M_n can be more suitable in kinetic studies than viscosity because in kinetics both the reactants and the reaction products should be expressed in chemical units. Previously, this equation was used in two studies (Olm and Teder, 1979; Iribarne and Schroeder, 1997). However, the validity of the Equation 4.13 is not proved.

In order to compare the results obtained in this study with the previous ones, the intrinsic viscosity is converted into moles of cellulose chains per ton of pulp and the kinetic rate expression was derived for two stage zero order power law model as

$$\begin{aligned} \frac{dM_n}{dt} = & 33.70 \exp\left[\frac{-20502}{RT}\right] [\text{OH}^-]^{0.28} [\text{PO}_2]^{0.26} (u(t) - u(t-10)) + \\ & 1.93 \exp\left[\frac{-14641}{RT}\right] [\text{OH}^-]^{0.23} [\text{PO}_2]^{0.17} u(t-10) \end{aligned} \quad (4.14)$$

The method used was the same as in the previous calculations. The carbohydrate degradation during oxygen delignification with respect to M_n (moles of cellulose chains per ton of pulp) is presented in Figures 4.10, 4.11 and 4.12. The solid line in the figures represents model predictions.

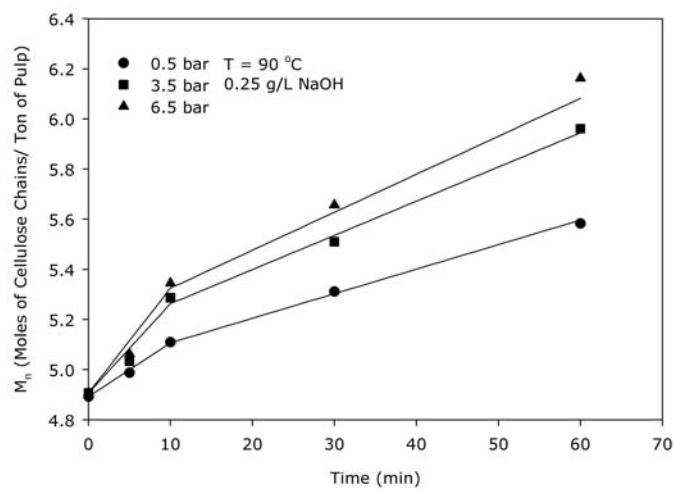
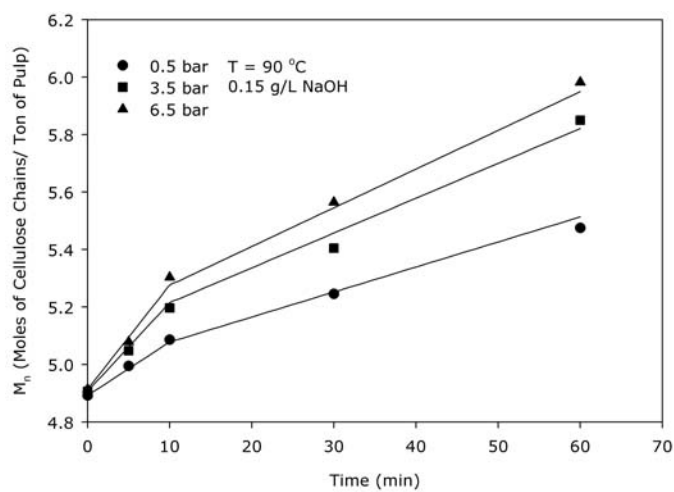
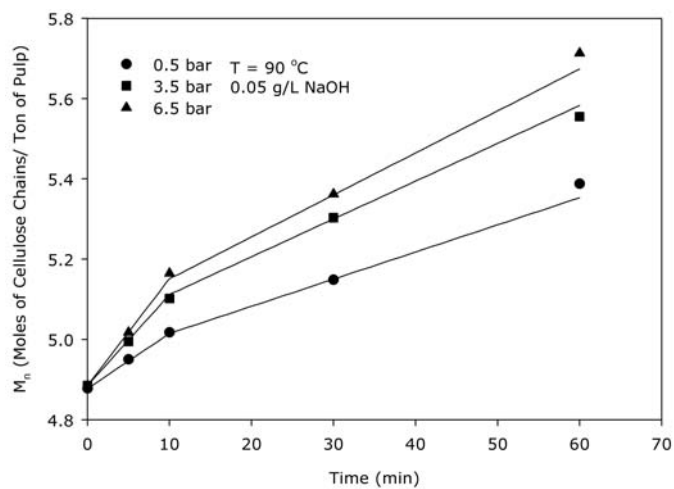


Figure 4.18 The moles of cellulose chains per ton of pulp with respect to time ($T = 90\text{ }^{\circ}\text{C}$, oxygen partial pressure = 0.5, 3.5, 6.5 bar and NaOH concentration = 0.05, 0.15, 0.25 g/L)

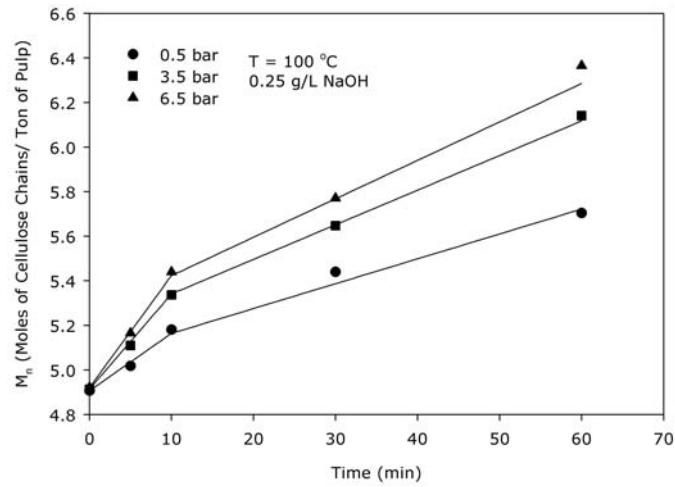
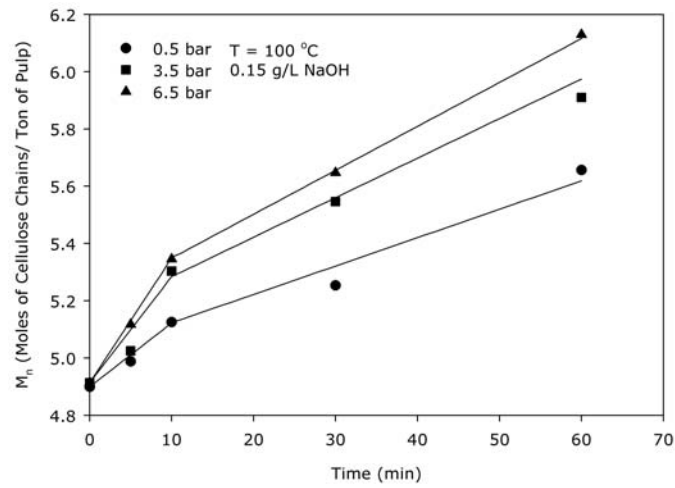
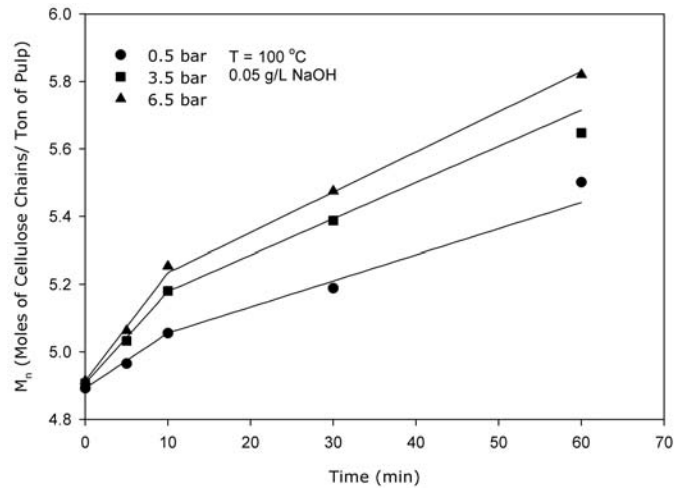


Figure 4.19 The moles of cellulose chains per ton of pulp with respect to time ($T = 100\text{ }^{\circ}\text{C}$, oxygen partial pressure = 0.5, 3.5, 6.5 bar and NaOH concentration = 0.05, 0.15, 0.25 g/L)

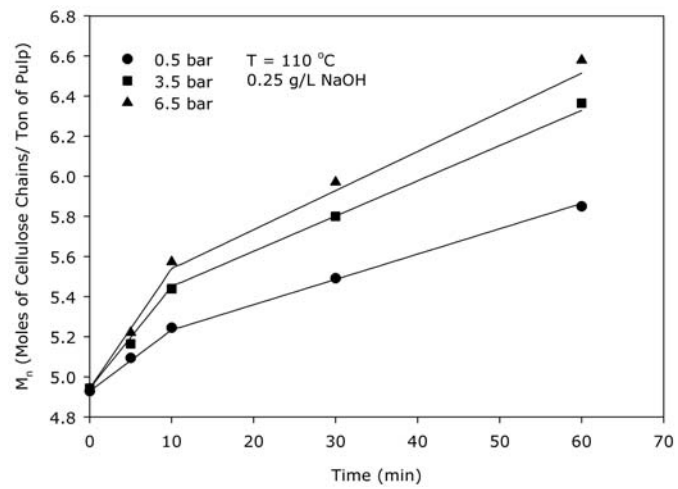
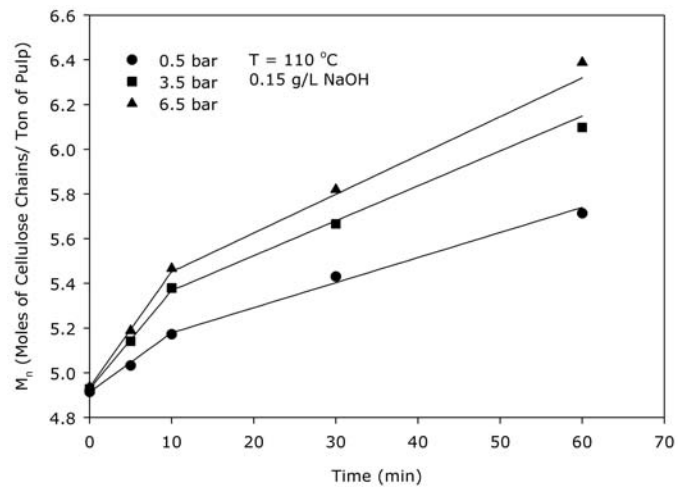
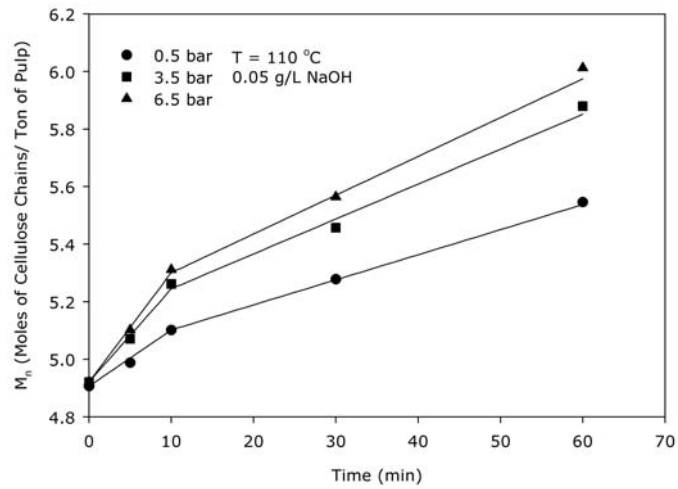


Figure 4.20 The moles of cellulose chains per ton of pulp with respect to time (T = 110 °C, oxygen partial pressure = 0.5, 3.5, 6.5 bar and NaOH concentration = 0.05, 0.15, 0.25 g/L)

4.4 Comparison with Literature Data

As it was mentioned previously, there are a number of studies in the literature (Hartler et al. (1970), Olm and Teder (1979), Hsu and Hsieh (1987, 1988), Iribarne and Schroeder (1997) and Agarwal et al. (1999)) related with the kinetic analysis of oxygen delignification. However, there is a wide variation in terms of the type of pulp, the conditions of Kraft pulping prior to oxygen delignification, consistencies and experimental conditions that were used. In Figure 4.21, the change in Kappa number with respect to time was presented based on the results of the previous studies mentioned above and the comparison with the present study is also given.

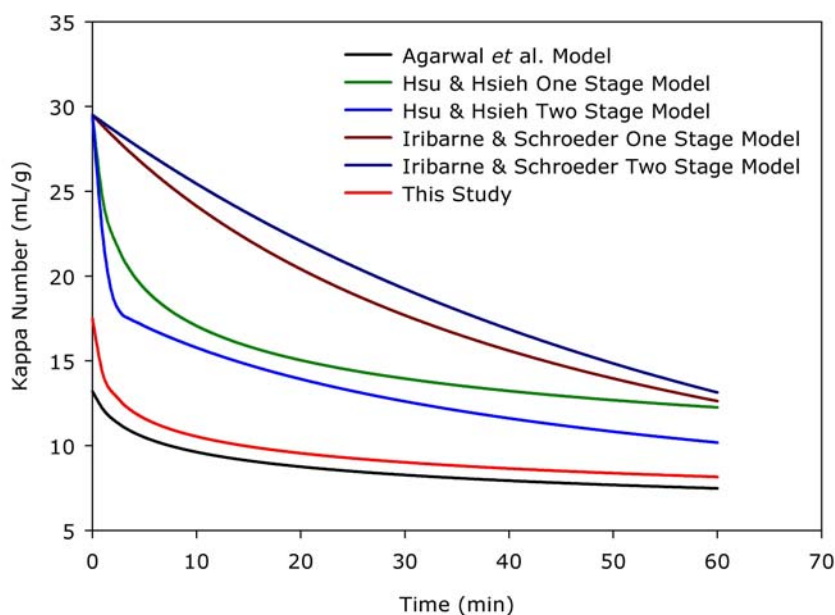


Figure 4.21 The oxygen delignification kinetics for this study and the previous studies (oxygen partial pressure = 414 kPa, T = 100 °C, NaOH concentration = 4 g/L)

It is seen from Figure 4.21 that different results were obtained due to the differences in the experimental variables mentioned above. The initial Kappa number and the change in the absolute value of the Kappa number with respect to time is also different in each study.

The studies on carbohydrate degradation are much more limited in literature (Olm and Teder, 1979; Iribarne and Schroeder, 1997) compared to the studies related with kinetic analysis of oxygen delignification. In Figure 4.22, the results

of this study is compared with the study done by Iribarne and Schroeder (1997) at 414 kPa oxygen partial pressure, 100 °C reaction temperature and 4 g/L sodium hydroxide concentration. It was not possible to present the data by Olm and Teder (1979) on this figure because of the missing data in terms of the Arrhenius constants, E_a and A . Since pulping conditions prior to oxygen delignification and the wood species are different, the initial mole of cellulose chains per ton of pulp is also different.

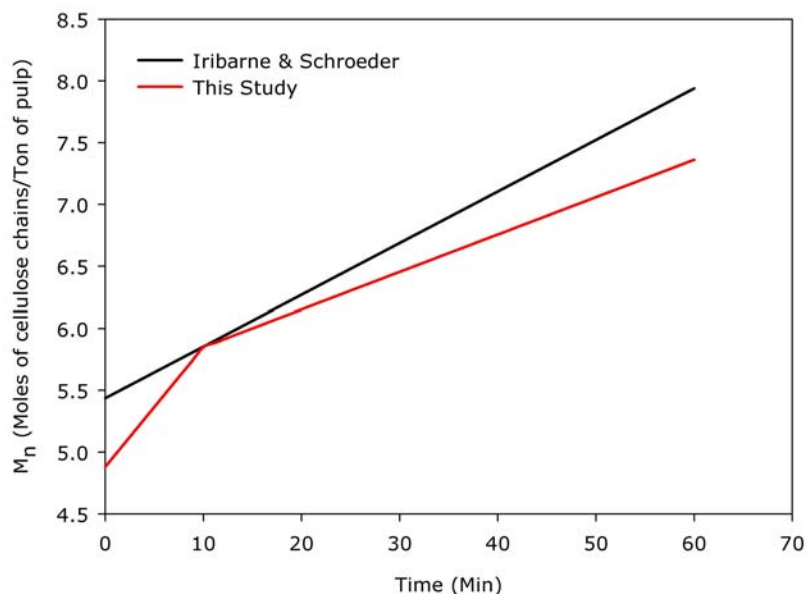


Figure 4.22 The carbohydrate degradation kinetics for this study and previous study (1997) (oxygen partial pressure = 414 kPa, $T = 100$ °C, NaOH concentration = 4 g/L)

4.5 The Method of Dimensionless Parameters

Based on the variables indicated in the previous section, the literature values during oxygen delignification in terms of the initial value of the Kappa number and the change in the absolute value with respect to time is different.

Therefore, in order to generalize both the results obtained in this study and also the literature values, dimensionless variables were defined in terms of the Kappa number and the reaction time. The Kappa number was converted to the extent of delignification defined as in Equation 4.15.

$$\mathbf{K} = \frac{K_0 - K}{K_0} \quad (4.15)$$

where K_0 is the initial Kappa number and K is the point value of the Kappa number at any time.

The maximum amount of delignification achieved in this study is different for each set of experimental conditions. Also literature values show a wide variation. In order to define a dimensionless time value the relationship given in Equation 4.16 was used based on the half time concept of the maximum value achieved.

$$\boldsymbol{\tau} = \frac{t}{t_{(\max/2)}} \quad (4.16)$$

The results obtained in this study in terms of dimensionless variables are shown in Figure 4.23. The dimensionless Kappa number was fitted to a nonlinear equation with a regression coefficient equal to 0.9857 as shown in Equation 4.17. This equation can also be used in the control of the oxygen delignification towers, because it relates the Kappa number change in the tower with respect to reaction time with a simple equation.

$$\mathbf{K} = 0.31408(1 - e^{-0.6761\tau}) \quad (4.17)$$

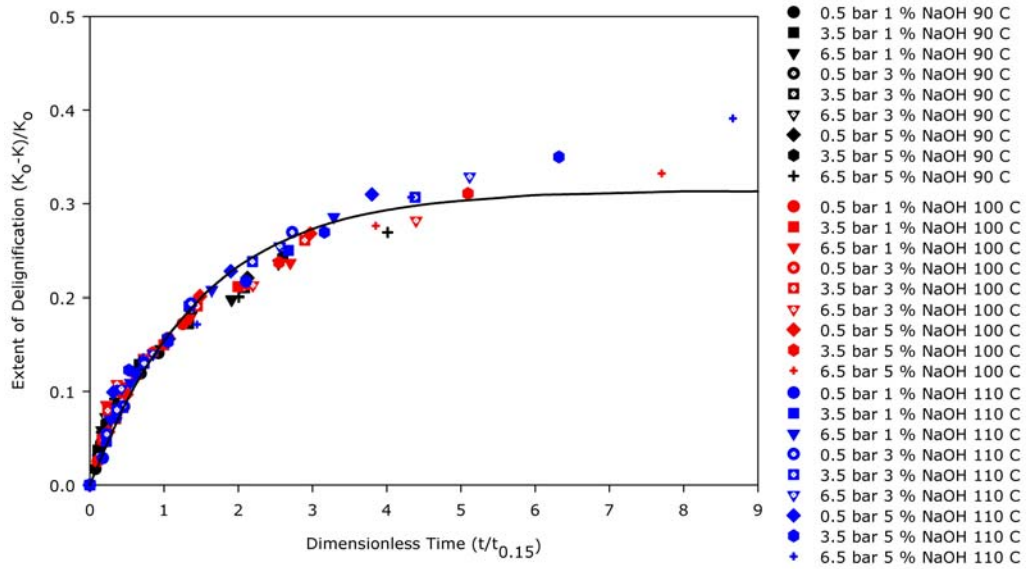


Figure 4.23 The extent of delignification versus dimensionless time ($\tau=t/t_{0.15}$) for this study

The same approach was also tested using the data of Agarwal et al (1999). In that study the maximum extent of delignification achieved was 0.4. Thus, the dimensionless time was calculated using the time value corresponding to the fractional delignification of 0.20 ($\tau=t/t_{0.20}$). Also in this study, the same trend in the dimensionless parameters was seen, however at higher dimensionless time values there is some deviation from the data. From Figures 4.23 and 4.24, it was concluded that, although the experimental conditions were different in each study, the data sets can be represented by a simple equation. The dimensionless parameters were fitted to a nonlinear equation with a regression coefficient of 0.9874 as Equation 4.18. The fitted equation was drawn with a solid line in Figure 4.24.

$$K = 0.3724(1 - e^{-0.7980\tau}) \quad (4.18)$$

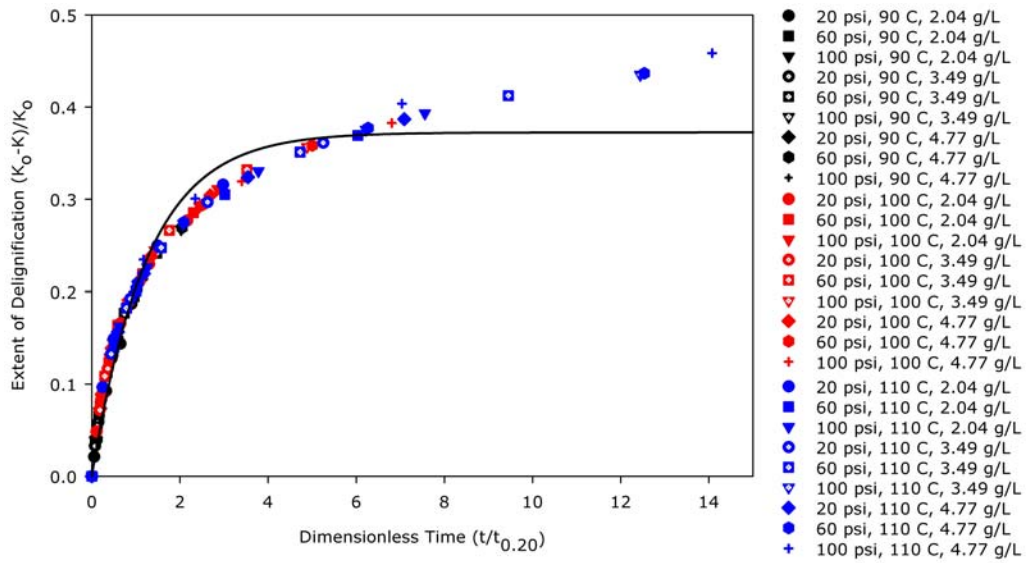


Figure 4.24 Extent of delignification versus dimensionless time ($\tau=t/t_{0.20}$) for Agarwal et al. (1999)

In Figure 4.25 the same dimensionless parameter method is applied to Hsu and Hsieh (1988) data. In the first approach, in the definition of τ a common time value corresponding to fractional delignification of 0.25 was used. It is seen from the figure that the data is scattered for the experiments performed at 100 and 125 °C experiments. The corresponding maximum delignification values are much higher for these temperatures. As a second approach, times corresponding to fractional delignification 0.4 and 0.55 were used respectively for the experiments performed at 100°C and 125°C. In Figure 4.26, the same data is replotted and three different sets of equation were obtained as shown in Equations 4.19, 4.20 and 4.21.

$$K = 0.39506(1 - e^{-1.1547\tau}), \quad T = 75 \text{ } ^\circ\text{C} \quad (4.19)$$

$$K = 0.6102(1 - e^{-1.2409\tau}), \quad T = 100 \text{ } ^\circ\text{C} \quad (4.20)$$

$$K = 0.7559(1 - e^{-1.5096\tau}), \quad T = 125 \text{ } ^\circ\text{C} \quad (4.21)$$

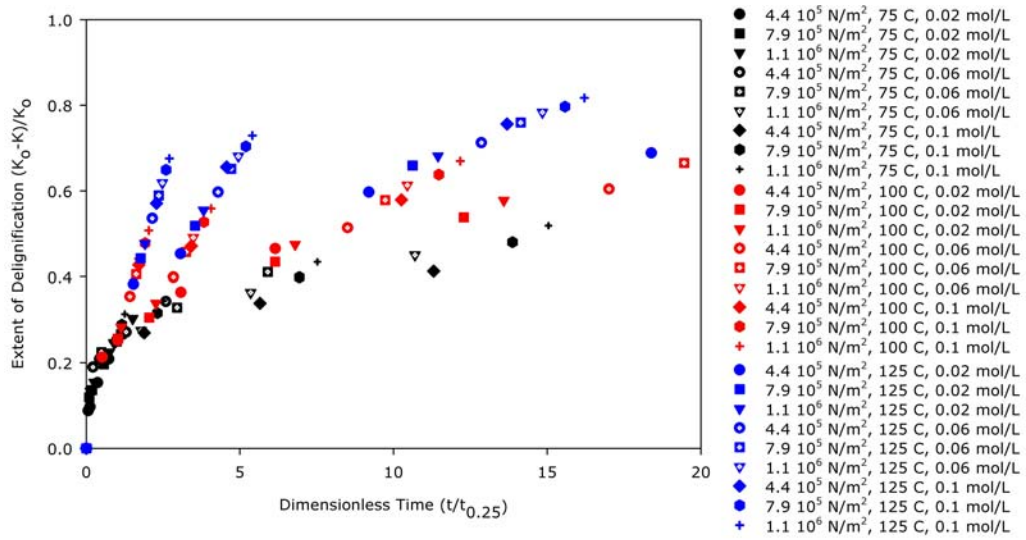


Figure 4.25 Extent of delignification versus dimensionless time ($\tau=t/t_{0.25}$) for Hsu & Hsieh (1988)

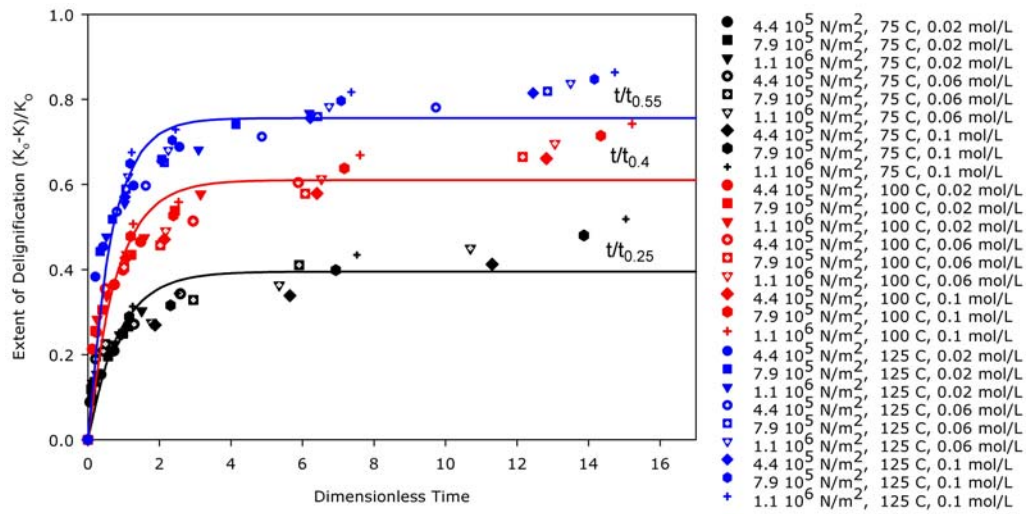


Figure 4.26 Extent of delignification versus dimensionless time for Hsu & Hsieh (1988) with different τ

The same dimensionless parameter approach was also tested using the carbohydrate degradation data in terms of viscosity. The dimensionless carbohydrate degradation M and the dimensionless time τ are defined as given in Equations 4.22 and 4.23.

$$M = \frac{\eta_0 - \eta}{\eta_0} \quad (4.22)$$

$$\tau = \frac{t}{t_{\max/2}} \quad (4.23)$$

where η_0 is the initial intrinsic viscosity of the pulp. τ was the fraction of absolute time to the time at which half of the maximum extent of carbohydrate degradation ($t_{(\max/2)}$) occurred. For the carbohydrate degradation data the maximum extent of degradation occurs at around 0.2.

In Figure 4.27 the extent of carbohydrate degradation data versus dimensionless time ($\tau=t/t_{0.1}$) is presented. The data fit to a nonlinear equation as given in Equation 4.24 with regression coefficient 0.9871 and is drawn with a solid line in Figure 4.27.

$$M = 0.1902(1 - e^{-0.8245\tau}) \quad (4.24)$$

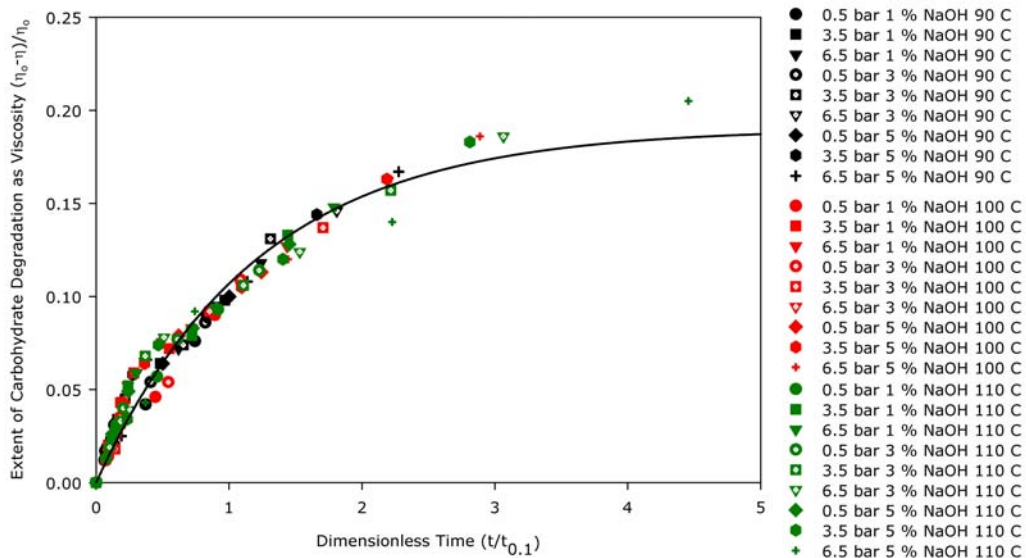


Figure 4.27 Extent of carbohydrate degradation as viscosity versus dimensionless time ($\tau=t/t_{0.1}$) for this study

4.6 Simulation of CEHDED Bleach Plant with Oxygen Delignification Tower

Mopak Dalamam pulp and paper mill is in the process of installing an oxygen delignification unit in front of its traditional bleaching unit (chlorination, sodium hydroxide extraction, hypochlorite, chlorine dioxide, sodium hydroxide

extraction, chlorine dioxide; CEHDED). The CEHDED bleaching unit was previously modeled by (Dogan and Gürüz, 2004; Dogan, 2000) at steady state. The flowsheet of Mopak Dalaman pulp and paper mill CEHDED bleaching plant is shown in Figure 4.28. Each stage is composed of three unit operations as mixer, retention tower and washer.

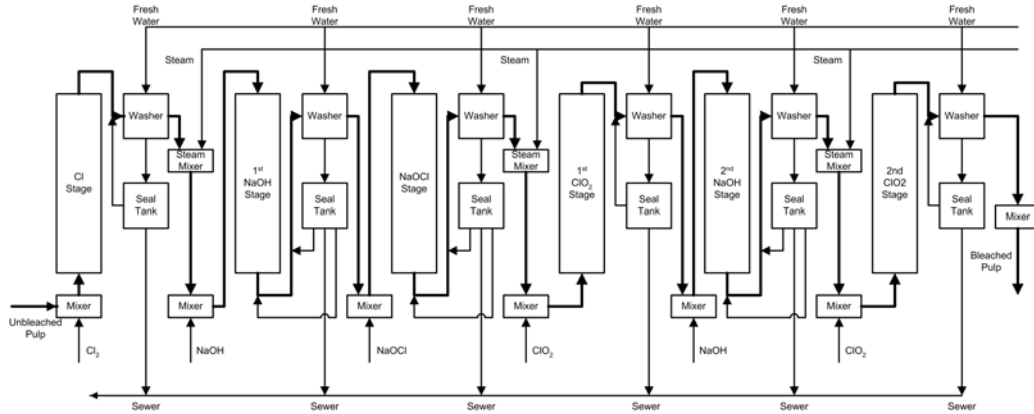


Figure 4.28 Process flow diagram of CEHDED bleach plant

4.6.1 Mathematical Models of the Unit Operations

In a bleaching stage mixers are used to mix the fiber suspensions with bleaching chemicals, steam or recycle streams. The mass balance equations in the mixer for the liquor, fibers, chromophores, chemicals and dissolved solids are presented in Table 4.1 based on the assumption of perfect mixing and quasi-steady state.

Table 4.1 The mathematical models used to simulate the mixer in bleach plant

	Model Equations
Liquors	$L_o = L_i + V_i$ (4.25)
Fibers	$L_o \frac{C_{mo}}{1 - C_{mo}} = L_i \frac{C_{mi}}{1 - C_{mi}}$ (4.26)
Chromophores	$K_o = K_i$ (4.27)
Chemicals & DS	$L_o X_{j,o} = L_i X_{j,i} + V_i Y_{j,i}$ (4.28)

In the retention tower, the reaction between the bleaching chemicals and the fibers takes place. Wang (1993) examined different models in order to represent the retention tower. Among the models that are tested, it was found that the sequence of CSTRs-PFR-CSTRs gives the best agreement with the experimental retention time distributions. Moreover in this study, the percentage of the residence time taken by plug flow was found to vary from 79 to 85% for C tower and 82-90% for E and D towers. Therefore, in the modeling of the retention tower, the ratio of the residence time of the plug flow to overall residence time is taken as 0.8 for C tower and 0.9 for the other towers. In order to represent the mixing in the inlet and outlet of the retention tower the number of CSTRs is taken as 1 for the C tower, and 2 for the other towers for the inlet and 1 for the outlet. By assuming constant density of the pulp fluid, the steady-state model equations for CSTR and PFR are obtained and are given in Table 4.2.

Table 4.2 The CSTR and PFR model equations to represent the retention tower

	Model Equations	
	CSTR	PFR
Liquors	$L_o = L_i$ (4.29)	$L_o = L_i$ (4.30)
Fibers	$C_{mo} = C_{mi}$ (4.31)	$C_{mo} = C_{mi}$ (4.32)
Chromophores	$\frac{K_o - K_i}{t_c} - r = 0$ (4.33)	$\frac{dK}{dt_p} = -r$ (4.34)
Chemicals & DS	$\frac{X_{j,o} - X_{j,i}}{t_c} - \frac{C_{mo}}{1 - C_{mo}} \times \psi_i \times r = 0$ (4.35)	$\frac{dX_i}{dt_p} = -\frac{C_{mo}}{1 - C_{mo}} \times \psi_i \times r$ (4.36)

The modeling of the drum washer is done by dividing it into three parts; as the dilution vat, drum filter and seal tank. In the dilution vat the liquor from the seal tank is mixed with the main pulp stream in order to dilute the pulp to the desired consistency. Therefore it can be modeled as a steady-state mixer. The drum filter is used to remove the dissolved solids and unreacted chemicals from the pulp with wash water. In order to model the drum filter, different models can be used. In this study, Norden efficiency approach (Norden and Pekkanen, 1987; Norden, 1973) was used in order to model the drum filter. In the model, the Norden efficiency factor is taken as 3 for all the washers. In the seal tank the part of the liquor coming from the drum filter is recycled back into the dilution

vat and the rest of it is sent to the sewer, which cause different environmental problems. Thus the seal tank can be modeled as a splitter. The model equations for those unit operations are given in Table 4.3.

Table 4.3 The mathematical model equations for the washer

	Liquors	Chemicals and Dissolved Solids
Dilution Vat	$L_v = L_i + V_r \quad (4.37)$	$X_{DS,v} = \frac{L_i X_{DS,i} + V_r Y_{DS,r}}{L_v} \quad (4.38)$
Drum Filter	$L_1 = L_i \frac{C_{mi}}{1 - C_{mi}} \frac{1 - C_{m1}}{C_{m1}} \quad (4.39)$ $V_d = V_2 + L_v - L_1 \quad (4.40)$	$X_{DS,1} = \begin{cases} Y_{DS,2} + \frac{RW - 1}{RW^{E_N} V_d / L_v - 1} (X_{DS,v} - Y_{DS,2}) & RW \neq 1 \\ Y_{DS,2} + \frac{1}{E_N} (X_{DS,v} - Y_{DS,2}) & RW = 1 \end{cases}$ <p style="text-align: center;">where $RW = \frac{V_2}{L_1} \quad (4.41)$</p> $Y_{DS,d} = \frac{V_2 Y_{DS,2} + L_v X_{DS,v} - L_1 X_{DS,1}}{V_d} \quad (4.42)$
Seal Tank	$V_d = V_1 + V_r \quad (4.43)$	$Y_{DS,d} = Y_{DS,1} \quad (4.44)$

4.6.2 Kinetic Models

In the modeling of the retention tower the most important parameter is the bleaching reaction kinetics. In the literature different kinetic models are proposed for the bleaching steps. The kinetic models that are used in this study are tabulated in Table 4.4.

In the process kinetic models employed, Kappa number is used for the chromophore removal for the delignification stages (C, E₁). However, in the brightening stages (H, D₁, E₂, D₂) light absorption coefficient is used. Therefore, the Kappa number after the first extraction stage (E₁) should be related with the inlet light absorption coefficient of the hypochlorination stage (H). Wang et al. (1995) used a correlation with the light absorption coefficient and the Kappa number of a bleached pulp by fitting the published experimental data. In our study, this correlation was used in order to link the Kappa number after the E₁ stage and the light absorption coefficient entering the H stage as

Table 4.4 The kinetic expressions used in the model

Reference		Rate Expression	ψ
C	Ackert et al. (1975)	$r_f = k_1 [Cl_2] K_{C,f}$ (4.45)	0.208
		$r_s = -\frac{dK_{Cl,s}}{dt} = k_2 [Cl_2] K_{C,s}$ (4.46)	
		$k_1 = 1123 \exp\left(\frac{-250}{T}\right)$ (4.47)	
		$k_2 = 22.47 \exp\left(\frac{-250}{T}\right)$	
		$K_{Cl,fi} = 0.4K_i$ $K_{Cl,si} = 0.3K_i$ (4.48)	
E	Axegard (1979)	$r_f = k_1 [OH^-]^{0.2} K_{E_1,f}$ (4.49)	
		$r_s = k_2 [OH^-]^{0.05} K_{E_1,s}$	
		$k_1 = 1.96 \times 10^6 \exp\left(\frac{-4691}{T}\right)$ (4.50)	
		$k_2 = 0.0103 \exp\left(\frac{-241}{T}\right)$	
		$\frac{K_{E_1,fi}}{K_{E_1,si}} = 1.75 \times 10^5 \exp\left(\frac{-3368}{T}\right) [OH^-]^{0.25f}$ (4.51)	
H	Axegard and Tormund (1985)	$r_H = k [OCl^-]^{0.6} [OH^-]^{-0.1} K_H^{3.5}$ (4.52)	$\frac{0.688}{K_H^{1.67}}$ (4.54)
		$k = 7.9657 \times 10^{10} \exp\left(\frac{-9622}{T}\right)$ (4.53)	
D	Teder and Tormund (1980)	$r_{D_1} = k [ClO_2]^{0.5} [H^+]^{-0.3} (K_{D_1} - 0.1)^3$ (4.55)	$\frac{0.059}{K_{D_1}^{1.15}}$ (4.57)
		$k = 0.096 \times 10^9 \left(\frac{1}{K_{D_1,i}^2} + 0.023 \right) \exp\left(\frac{-7096}{T}\right)$ (4.56)	
E,D	Teder and Tormund (1980)	$r_{D_2} = k [ClO_2]^{0.5} [H^+]^{-0.3} (K_{D_2} - 0.1)^3$ (4.58)	$\frac{0.078 K_{D_2,i}}{K_{D_2}^{2.3}}$ (4.60)
		$k = 0.117 \times 10^9 \left(\frac{1}{K_{D_2,i}^2} + 0.01 \right) \exp\left(\frac{-7096}{T}\right)$ (4.59)	

$$K_{H,i} = 4.69K_{E_1} + 0.01 \quad (4.61)$$

After the extraction stage, the light absorption coefficient should be converted to brightness, because the full mills are using brightness for the quality of the bleached pulp. In order to convert the light absorption coefficient to brightness, the Kubelka-Munk (1931) equation was used

$$\frac{K}{S} = \frac{(1-R_\infty)^2}{2 \times R_\infty} \quad (4.62)$$

where R_∞ denotes the brightness, and S is the light scattering coefficient. The value of the scattering coefficient is used as $50 \text{ m}^2/\text{kg}$ (Wang et al., 1995). K is the light absorption coefficient of the pulp.

4.6.3 Oxygen Delignification Unit Simulation and Case Studies Performed

In this part of the study, the oxygen delignification unit was simulated by incorporated into the simulated CEHDDED bleaching plant (Dogan, 2004). A range of different operational variables were tested in the oxygen delignification unit with the aim of decreasing the amount of dissolved solids coming out from the six washers.

In the simulation of the oxygen delignification unit the kinetic model that is proposed in this study is used as Equation 4.63. Mopak Dalaman pulp and paper mill management has decided to run the oxygen delignification tower at 8% consistency, with 1% NaOH (on oven dry pulp), at a temperature of $100 \text{ }^\circ\text{C}$ and 1 bar oxygen partial pressure. Although the experiments performed in this study were done at 0.5%, the simulation results will give us an idea about the results of the whole bleach plant. In the simulation in order to represent the oxygen delignification tower, a PFR is used. The residence time of the oxygen delignification tower is planned to be 60 min, thus in the simulation 60 minutes is used for the residence time of the oxygen delignification tower. The model equations for the PFR are given in Table 4.4. The washer in the oxygen delignification unit will use $5000 \text{ kg}/\text{min}$ water in order to effectively clean the outlet pulp. Since the consistency in the chlorination stage is 3%, the outlet consistency of the washer in the oxygen delignification unit should be 3%.

$$-\frac{dK}{dt} = 0.3 \exp\left[\frac{-64504}{RT}\right] [\text{OH}^-]^{0.74} [\text{PO}_2]^{0.32} K^{7.9} \quad (4.63)$$

The input data that is used in the simulation are tabulated in Table 4.5. The steady state Kappa number or brightness and the dissolved solids content of the filtrate from the washer for each stage with and without oxygen delignification unit are calculated and presented in Table 4.6.

Table 4.5 The input data for simulation of CEHDED bleach plant

	C	E	H	D	E	D
Mill Data						
Cl₂						
Flow Rate, Kg/min	10	-	-	-	-	-
Concentration, %	100	-	-	-	-	-
NaOH						
Flow Rate, Kg/min	-	80	15	-	40	-
Concentration, %	-	8	8	-	8	-
NaOCl						
Flow Rate, Kg/min	-	-	110	-	-	-
Concentration, %	-	-	4	-	-	-
ClO₂						
Flow Rate, Kg/min	-	-	-	225	-	40
Concentration, %	-	-	-	4.5	-	4.5
Steam, Kg/min	-	55	-	150	-	50
Tower						
Temperature, °C	25	65	45	75	65	75
Residence Time, t _r , min	70	90	190	240	90	240
Washer						
Wash Liquor, Kg/min	7075	2150	2150	2300	2150	2150
Outlet Consistency, %	13.3	13.0	14.6	12.7	11.7	13.3
Unbleached Pulp						
Pulp Flow Rate = 2042 kg/min			Consistency = 8.1%			
Kappa Number = 17.5			Dissolved Solids = 0.001%			

Table 4.6 The simulation results with and without oxygen delignification

Stage	Kappa Number		Dissolved Solids (%)	
	Without O ₂ Bleaching	With O ₂ Bleaching	Without O ₂ Bleaching	With O ₂ Bleaching
O	-	9.65	-	0.0444
C	5.25	1.93	0.0370	0.0307
E	1.94	0.71	0.1571	0.1343
	Brightness (% ISO)		Dissolved Solids (%)	
H	82.0	82.38	0.1135	0.1061
D	91.73	91.80	0.0126	0.0121
D	92.94	92.95	0.0036	0.0034

It was seen from Table 4.6 that, the addition of an oxygen delignification step resulted in a sharp decrease in the Kappa numbers in the first three stages of the bleaching unit. Also, a decrease in the amount of the dissolved solids coming out from the washers was observed. The total amount of dissolved solids coming out from the six washers decreased from 10.86 kg/min to 9.44 kg/min with the addition of the oxygen delignification unit operating with a reaction time of 60 min, at a temperature of 100 °C, 1 bar oxygen partial pressure and 1% NaOH (% on oven dry pulp) concentration. There is a 13.07% decrease in the total amount of dissolved solids, indicating the same amount of decrease in the total pollutants coming out from the bleach plant.

In addition to the operational variables used above in the oxygen delignification unit, these variables can further be optimized in order to decrease the amount of dissolved solids. The oxygen delignification tower can be simulated at 60 min reaction time, at a temperature of 110 °C, 6.5 bar oxygen partial pressure and 5% NaOH (% on oven dry pulp) concentration. The total amount of dissolved solids content is dropped to 8.91 kg/min. Thus, when the oxygen delignification tower is fully optimized, there is a 17.96% decrease in the total amount of pollutants with output brightness of 92.95.

After the optimization of the oxygen delignification tower, the optimization of the CEHDED bleach plant was performed in order to decrease the amount of total dissolved solids coming out from the six washers of the bleach plant. The retention tower reaction temperature, residence time, the flow rate of the

bleaching liquor, inlet consistency of the pulp and the wash liquor flow rate in the washer for each stage is decreased in order to see the effect on the total dissolved solids content. All the operational variables in the bleaching plant are decreased because when the oxygen delignification unit is added to the mill, at the inlet of the bleaching plant the Kappa number of the pulp is decreased. Thus, lower values of the operational variables are sufficient to bleach the pulp to a desired brightness.

The wash water flow rate in the washer is one of the most important parameter because the volume and the amount of dissolved solids in the filtrate are highly affected by the wash water flow rate. Furthermore, the amount of chemicals used in the bleaching stage can be reduced effectively by adding an oxygen delignification tower. The range of process parameters used in this study is given in Table 4.7. The bold numbers represents the steady state values of the process parameters.

Table 4.7 The range of the process parameters studied in process parameter optimization

Parameter	C	E	H	D	D
Temperature °C	15 - 25	55 - 65	35 - 45	65 - 75	65 - 75
Res. Time Min	40 - 70	50 - 90	100 - 190	120 - 240	120 - 240
Bleaching Liq. kg/min	2 - 10	40 - 80	60 - 110	120 - 225	20 - 40
Consistency %	2.5 - 3	11.5 - 12	11.5 - 12	10.5 - 11	10.5 - 11
Wash Liq. ton/min	5 - 7	1.9 - 2.1	1.9 - 2.1	2.1 - 2.3	1.9 - 2.1

4.6.3.1 Bleaching Chemicals

As the fiber moves through the bleach plant, different reactive chemicals are added in proportion to the pulp mass flow rate and Kappa number. When an oxygen stage is installed in front of a CEHDED bleach plant, the chemicals used in each stage can be reduced up to 50% because most of the lignin removal is achieved in the oxygen delignification stage. In order to see the effect of oxygen

delignification stage on the bleaching chemicals used in the CEHDED bleach plant, different simulation runs of the system is done and presented in Table 4.8. As it was mentioned in the previous section, with the addition of the oxygen delignification unit the total amount of dissolved solids coming out from the washers was calculated as 8.91 kg/min indicating a 17.96% decrease in the amount of pollutants in the CEHDED bleach plant. It was seen from Table 4.8 that the maximum amount of decrease in the amount of dissolved solids is achieved in the first three stages of the sequence by decreasing the bleaching chemicals in each stage. As it can be seen from Table 4.7, in the chlorination stage, the amount of chlorine is reduced by 80% and in the rest of the stages, the amount of chemicals used can be reduced up to 50%. When the optimized values of the bleaching chemicals are simulated for each stage, a 22% decrease in the total amount of dissolved solids coming out from the washers is achieved.

Table 4.8 The optimization of the bleaching chemicals for each stage

	Total Dissolved Solids (Kg/min)	Brightness (%)	Percent Decrease (%)
C	8.62	92.97	20.6
E	8.64	92.97	20.4
H	8.60	92.91	20.8
D ₁	8.68	92.84	20.1
D ₂	8.83	92.77	18.7
Overall Optimization	8.47	92.38	22.0

4.6.3.2 Retention Tower Reaction Temperature

The temperature in the retention tower is an important parameter because it affects the reaction rate and selectivity. Therefore, it has a direct effect on the total amount of pollutants. In Table 4.9, the optimization of retention tower temperature for each stage is presented. The most effective stage is the hypochlorination stage, because when the temperature of the hypochlorination stage decreases there is a 19.5% decrease in the amount of wastes coming out from the six washers. When the optimized values for each stage is simulated, a 21.2% overall decrease in the total amount of dissolved solids is obtained.

Table 4.9 The optimization of the reaction temperature for each stage

	Total Dissolved Solids (Kg/min)	Brightness (%)	Percent Decrease (%)
C	8.85	92.97	18.5
E	8.86	92.96	18.4
H	8.74	92.83	19.5
D ₁	8.85	92.72	18.5
D ₂	8.83	92.76	18.7
Overall Optimization	8.56	92.17	21.2

4.6.3.3 Retention Time in the Tower

The retention time in the bleaching stage determines the contact time of the bleaching chemicals with the pulp. The amount of dissolved solids can be minimized by adjusting the retention time in the tower. In Table 4.10, the optimization of the retention times for each stage is presented. The highest reduction in the total amount of dissolved solids is obtained in the hypochlorination stage. In the first two stages the effect of retention time is smaller than the hypochlorination stage because when the retention time is decreased in the first two stages, the undissolved lignin found in the pulp is reacted in the hypochlorination stage. Therefore, the total amount of dissolved solids at the end of the sixth stage is not changed.

Table 4.10 The optimization of the retention time for each stage

	Total Dissolved Solids (Kg/min)	Brightness (%)	Percent Decrease (%)
C	8.68	92.97	20.1
E	8.69	92.96	20.0
H	8.60	92.88	20.8
D ₁	8.68	92.67	20.1
D ₂	8.84	92.9	18.6
Overall Optimization	8.62	92.49	20.6

4.6.3.4 Consistency in the Tower

The consistency in the retention tower determines the amount of water available for the gas dissolution and affects the concentration of chemical in the solution. Traditionally, bleach plants have operated the bleaching stages at around 12% consistency because this consistency was produced by the rotary drum washer in the previous stage. The exception was chlorination stage which was run at 3% consistency to provide enough water for complete dissolution of the chlorine gas. In Table 4.11, the highest reduction in the amount of total dissolved solids is achieved in the chlorination stage. In the other stages the effect of retention tower consistency is not significant. When the consistency is optimized in all of the stages, there is a 20.8% decrease in the amount of dissolved solids.

Table 4.11 The optimization of the consistency for each stage

	Total Dissolved Solids (Kg/min)	Brightness (%)	Percent Decrease (%)
C	8.65	93.04	20.3
E	8.85	92.99	18.5
H	8.85	92.98	18.5
D ₁	8.84	92.98	18.6
D ₂	8.84	92.97	18.6
Overall Optimization	8.6	93.06	20.8

4.6.3.5 Wash Water Flow Rate in the Washer

Washing removes the dissolved solids from the pulp after the bleaching reaction. The washing step is important because residual materials carried through one stage to another may interfere with the efficiency of the later stages. The amount of wash water flow rates in the CEHDED bleach plant can be reduced by the installation of the oxygen delignification tower. Since the amount of lignin is decreased by the addition of oxygen delignification tower, the amount of dissolved solids coming out in the bleach plant washers are reduced. Therefore, less amount of water is sufficient to clean the pulp. In Table 4.12, the optimized values for each bleaching stage are presented. It can be seen from the table that the highest reduction in the amount of dissolved solids is obtained in the sodium hydroxide extraction stage.

Table 4.12 The optimization of the wash water flow rates in the washers

	Total Dissolved Solids (Kg/min)	Brightness (%)	Percent Decrease (%)
C	8.84	92.97	18.6
E	8.68	92.97	20.1
H	8.73	92.97	19.6
D ₁	8.84	92.97	18.6
D ₂	8.85	92.97	18.5
Overall Optimization	8.55	92.97	21.3

4.6.3.6 Overall Optimization

Among the case studies investigated, with the optimization of the bleaching chemicals used in the bleach plant, the highest reduction in the total amount of dissolved solids (22.0%) is achieved. In addition to the reduction in the amount of dissolved solids, the amount of chemicals used in the bleaching plant is decreased up to 50% as can be seen from Table 4.7. Thus, the cost of the chemicals that is used in the bleach plant can be reduced. Another important reduction in the wastes (21.3%) is achieved by the optimization of wash water flow rate in the washers. Moreover, the amount of water used in the washers is reduced up to 20% as it can be seen from Table 4.7. In the other case studies performed which are temperature, residence time and consistency in the retention tower, there is up to a 21.2% decrease in the total amount of dissolved solids content. With the optimization of these variables, there can be a reduction in the energy cost of the bleaching plant.

After completing the optimization of the process variables used in the bleaching plant, OCEHDED bleach plant was simulated with the optimized values of the process variables. At the end of the simulation, it was seen that there is a 25.97% decrease in the total amount of dissolved solids coming out from the six washers with output brightness of 89.5 which is an acceptable value for commercial paper.

CHAPTER 5

CONCLUSIONS AND RECOMMENDATIONS

5.1 Conclusions

In this work, the kinetics of oxygen delignification of Turkish southern Kraft pulp was studied. The study is separated into different stages. In the first stage of the work, the mass transfer effects were examined. In oxygen delignification, there are two main mass transfer resistances which are inter-fiber and intra-fiber mass transfer of oxygen into the pulp. The effect of inter-fiber mass transfer was investigated by performing experiments at 0.5, 1 and 8% consistency values. From the experiments it was concluded that the inter-fiber mass transfer resistance was insignificant in lower consistencies. Therefore, the oxygen delignification experiments were performed at 0.5% consistency. To investigate the significance of intra-fiber diffusion during oxygen delignification, the pulp was refined before being subjected to oxygen delignification in Mopak Dalaman pulp and paper mill. It was concluded from the experiments that, there was no significant effect of refining on the delignification rate. Therefore, the intra-fibre mass transfer resistance was not significant under the conditions studied.

In the following stage of the study, the oxygen delignification experiments were completed at industrially significant conditions of temperature (90, 100 and 110 °C), alkali charge (1, 3, 5% on oven dry pulp), and oxygen pressure (0.5, 3.5, 6.5 bar). The rate of oxygen delignification equation was derived by integral method of analysis. The kinetic model was well represented the experimental data. The oxygen delignification kinetics of Turkish southern Kraft pulp was not studied previously by any author. Therefore, the oxygen delignification rate equation that was derived in this study can form a basis for the oxygen

delignification tower that is planning to be built in Mopak Dalaman pulp and paper mill.

Another important factor in oxygen delignification is the carbohydrate degradation kinetics. The rate of carbohydrate degradation was derived by measuring the intrinsic viscosity of the pulp obtained in the second part of the study. The integral method of analysis was used in the derivation of the kinetic rate equation. The two stage zero order power law model was derived for the carbohydrate degradation data. This model represents the experimental data very well. There are a few studies on carbohydrate degradation kinetics in the literature. Therefore, the data obtained in this study give information on the carbohydrate degradation of hardwood Eucalyptus Kraft pulp. Moreover, the carbohydrate degradation rate expression can be used in the design of the oxygen delignification tower that is built in Dalaman.

As it was mentioned in the literature survey, there are several oxygen delignification kinetics studies in the literature. However, these studies were performed with different pulp types, Kraft pulping conditions prior to oxygen delignification, consistencies and experimental conditions. The initial Kappa number and the absolute value of the Kappa number with respect to time is changing for different work. In this stage of the study the Kappa numbers and the reaction times for this study and the other studies are converted into dimensionless numbers. For this study, by applying the dimensionless parameters method all the experimental data sets were fitted to a nonlinear equation. Also, for the studies done by Agarwal et al. (1999) and Hsu and Hsieh (1988) the dimensionless parameters method was applied satisfactorily. Although, there are a few studies on carbohydrate degradation kinetics, the same dimensionless parameters method was applied to the carbohydrate degradation data with respect to intrinsic viscosity. With the help of these dimensionless parameters, the data was fitted to a nonlinear equation. The dimensionless parameters method was firstly applied to oxygen delignification kinetics in this study and it seems to be very effective in order to represent the rate data in a simple equation.

Finally, the oxygen delignification unit was simulated by incorporated into the simulated CEHDED bleaching plant (Doğan, 2000) in order to see affect on the amount of total dissolved solids. By adding oxygen delignification unit to the plant, the amount of total dissolved solids coming out from the six washers was

dropped 17.96%, without affecting the output brightness 92.95. By addition of an oxygen delignification unit, the operational variables in the CEHDED bleach plant can be reduced. The retention tower reaction temperature, residence time, the flow rate of the bleaching liquor, inlet consistency of the pulp and the wash liquor flow rate in the washer for each stage is decreased in order to see the effect on the total amount of dissolved solids content. Among the parameters investigated, the highest reduction in the total amount of dissolved solids was achieved in the bleaching chemicals optimization with a 22.0% decrease. After completing the optimization of the process variables used in the bleaching plant, OCEHDED bleach plant was simulated with the optimized process variables and a 25.97% decrease in the total amount of dissolved solids is achieved.

5.2 Recommendations

This current work suggests several other that can be conducted to investigate the oxygen delignification and kinetics study. In this study, the oxygen delignification experiments are conducted at ultra-low consistency 0.5%, however in the industrial scale the consistency is ranging between 8-12%. As a future work, the oxygen delignification kinetics can be studied with 8% consistency with better mixing equipments.

In this study, in the experiments hardwood Eucalyptus Kraft pulp is used. This work can be extended to softwood pulps. The delignification and carbohydrate degradation rate equation for softwood pulp will be different since softwood contains less hemicelluloses and higher residual lignin than hardwood.

The oxygen delignification is greatly affected by pretreatment and removal of metal ions. Oxygen delignification can be improved by hydrogen peroxide reinforcement, pretreatment with DTPA to remove and sequester metal ions and addition of Mg^{+2} during hydrogen peroxide reinforcement. Further work can be done to investigate oxygen pre-treatments and lignin activation.

As it was mentioned in the conclusion, the pulping conditions prior to oxygen bleaching have a great effect on the oxygen delignification kinetics. The effect of effective alkali level, cooking temperature in the digester and pulp yield on the performance of an oxygen delignification stage can be studied for different pulp types.

REFERENCES

- Ackert, J.E., Koch, D.D., Edwards, L.L., (1975), " Displacement Chlorination of Kraft Pulps – An Experimental Study and Comparison of Models", *Tappi J.*, Vol. 58, Iss. 10, pp. 141-145
- Agarwal, S.B., Genco, J.M., Cole, B.J.W., Miller, W., (1999), "Kinetics of Oxygen Delignification", *Journal of Pulp and Paper Science*, Vol. 25, Iss. 10, pp. 361-366
- Argyropoulos, D.S., (2001), *Oxidative Delignification Chemistry Fundamentals and Catalysis*, American Chemical Society, Washington DC
- Axegard, P., (1979), "Kinetics of Alkaline Bleaching for the Kraft CE Sequence", *Svensk Papperstiding*, Vol. 81, Iss. 12, pp. 361-367
- Dence, C.W., Reeve, D.W., (1996), *Pulp Bleaching Principles and Practice*, Tappi Press, Atlanta, Georgia
- Doğan, İ., Gürüz, A.G., (2004), Waste Minimization in a Bleach Plant, *Advances in Environmental Research*, Vol. 8, Iss. 3-4, pp. 359-369
- Doğan, İ., (2000), *Flow Sheet Optimization by the Concept of Sustainable Development in Pulp and Paper Industry*, Masters Thesis, Middle East Technical University
- Gierer, J., Imsgrad, F., (1977), "Reactions of Lignins With Oxygen and Hydrogen-Peroxide in Alkaline Media", *Svensk Papperstiding*, Vol. 80, Iss. 16, pp. 510-518
- Gierer, J., (1986), "Chemistry Of Delignification .2. Reactions of Lignins During Bleaching", *Wood Science and Technology*, Vol. 20, Iss. 1, pp. 1-33
- Gilbert, A.F., Pavlovova, E., Rapson, W.H., (1973), "Mechanism of Magnesium Retardation of Cellulose Degradation During Oxygen Bleaching", *Tappi J.*, Vol. 56, Iss. 6, pp. 95-99
- Gratzl, J.S., (1992), "The Chemical Principles of Pulp Bleaching with Oxygen, Hydrogen-Peroxide and Ozone - A Short Review", *Papier*, Vol. 46, Iss. 10A, pp. V1-V8

- Gratzl, J.S., (1990), "Reactions of Polysaccharides and Lignins in Bleaching with Oxygen and Related Species", 1990 Tappi Oxygen Delignification Symposium Notes, Tappi Press, Atlanta, pp. 1
- Gratzl, J.S., (1987), "Degradation Reactions of Carbohydrates and Lignine by Non-Chlorine Bleaching Agents - Mechanisms as well as Potential for Stabilization", Vol. 41, Iss. 3, pp. 120-130
- Hartler, N., Norrstrom, H., Rydin, S., (1970), "Oxygen-Alkali Bleaching of Sulphate Pulp", Svensk Papperstidning, Vol. 73, Iss. 21, pp. 696
- Hsu, C.L., Hsieh, J.S., (1985a), "Fundamentals of Oxygen Bleaching: Measurement of Oxygen Diffusion Rates in Medium and High Consistency Pulp", Tappi Journal, Vol. 68, Iss.6, pp. 92-95
- Hsu, C.L., Hsieh, J.S., (1985b), "Effects of Mass transfer on Medium Consistency Oxygen Bleaching Kinetics", Tappi Journal, Vol. 68, Iss.11, pp. 126-130
- Hsu, C.L., Hsieh, J.S., (1987), "Oxygen Bleaching Kinetics at Ultra-low Consistency", Tappi Journal, Vol. 70, Iss.12, pp. 107-11
- Hsu, C., Hsieh, J.S., (1988), "Reaction Kinetics in Oxygen Bleaching", AIChE J., Vol. 34, Iss. 11, pp. 116-122
- Iribarne, J., Schroeder, L.R., (1997), " High-Pressure Oxygen Delignification of Kraft Pulps 1. Kinetics", Tappi J., Vol. 80, Iss. 10, pp. 241-250
- Johanson, E., Ljunggren, S., (1994), "The Kinetics of Lignin Reaction During Oxygen Delignification, Part 4. The Reactivates of Different Lignin Model Compounds and the Influence on Metal Ions on the Rate of Degredation", Journal of Wood Chemistry and Technology, Vol. 14, Iss. 4, pp. 507
- Kovasin, K., Malmsten, E., (1987), "Experience from Hydrostatic Medium-Consistency Oxygen Delignification at Rauma Pulp-Mill", Pulp and Paper Canada, Vol. 88, Iss. 8, pp. 36-39
- Kubelka, P., Munk, F., (1931), Z. Tech. Physik, Vol. 12, pp. 593
- Norden, H.V., (1973), "Statistical Analysis of Pulp Washer on an Industrial Rotary Drum", Pulp Paper Mag. Can., Vol. 74, Iss. 10, pp. 83-90
- Norden, H.V., Pekkanen, M., (1987), "General Calculation Method for Stagewise Models of Pulp Washing and Other Mass and Heat Transfer", Symp. Pulp Washing, CPPA, Marieham, Finland, pp. 237
- Olm, L., Teder, A., (1979), "The Kinetics of Oxygen Bleaching", Tappi Journal, Vol. 62, Iss. 12, pp. 43-46

- Qushsho'o, M.H., (1997), "Improvements of the Bleaching Process of Dalaman Pulp and paper Plant to Reduce the Environmental Impacts", Master's Thesis, METU, Ankara
- Schoon, N.H., (1982), "Interpretation of Rate Equations from Kinetic Studies of Wood Pulping and Bleaching", *Svensk Papperstidning*, R185-R193
- Singh, A., (1987), "Phenoxy- and Oxy- Radicals and Their Role in Oxygen Delignification", 1987 Tappi International Oxygen Delignification Conference Proceedings, Tappi Press, Atlanta, pp. 111
- Singh, R.P., (1979), *The bleaching of Pulp*, Tappi, 3rd ed.
- Sjöström, E., (1981), "The Chemistry of Oxygen Delignification", *Paperi Ja Puu-Paper and Timber*, Vol. 63, Iss. 6-7, pp. 438-442
- Sjöström, E., (1980), *Chemistry of Delignification with Oxygen, Ozone and Peroxides*, University of Tokyo, Tokyo, pp. 61
- Smook, G.A., (2002), *Handbook for Pulp & Paper Technologists*, Angus Wilde Publications Inc., 3rd ed., Vancouver, Canada
- Teder, A., Tormund, D., (1977), "Kinetics of Chlorine Dioxide Bleaching", *Trans. Tech. Sect. CPPA*, Vol. 3, Iss. 2, pp. 41-46
- Teder, A., Tormund, D., (1980), "Mathematical Model for Chlorine Dioxide Bleaching and its Applications", *AIChE Symp. Ser.*, Vol. 76, pp. 133-142
- Theander, O., (1980), *Chemistry of Delignification with Oxygen, Ozone and Peroxides*, University of Tokyo, Tokyo, pp. 43
- Valchev, I., Valcheva, E., Christova, E., (1999), "Kinetics of Oxygen Delignification of Hardwood Kraft Pulp", *Cellulose Chemistry and Technology*, Vol. 33, Iss. 3-4, pp. 303-310
- Wang, R.X., Tessier, P.J.C., Bennington, C.P.J., (1995), "Modeling and Dynamic Simulation of a Bleach Plant", *AIChE Journal*, 41 (12), 2603-2613.
- Wang, R.X., (1993), "Dynamic Simulation of Brown Stock Washers and Bleach Plants", Master's Thesis, Univ. of British Columbia, Vancouver, BC
- Yetis, U., Selcuk, A., Gokcay, C.F., (1996), "Reducing Chlorinated organics, AOX, in the Bleachery Effluents of a Turkish Pulp and Paper Plant", *Water Science and Technology*, Vol. 34, Iss. 34, pp. 97-104
- Yetis, U., Ataberk, S., Gokcay, C.F., Sahin, S.M., (1997), "Characterization of Effluents from Chlorine Dioxide Substitution Bleaching and Oxygen Reinforced Extraction", *Water Science and Technology*, Vol. 36, Iss 2-3, pp. 353-360

APPENDIX A

STANDARDS

A.1 Kappa number of pulp (Tappi T236)

Weight about 5 g of oven dry test specimen. Disintegrate the test specimen in not more than 500 ml of distilled water until free from the fiber clots and from large fiber bundles. Avoid methods of disintegration, which will involve extensive cutting of the fibers. Transfer the disintegrated test specimen to a 1500 ml reaction beaker and rinse out the disintegrator with sufficient water to bring the total volume to 790 ml.

Place the beaker in the constant temperature bath, adjusted so that the reaction temperature stays at 25 °C during the entire reaction. Adjust the agitator to obtain a vortex approximately 25 mm deep in the solution.

With a pipette, add 100 ml of the potassium permanganate solution (0.02 mol/l) and 100 ml of the sulphuric acid solution (2mol/l) to a 250 ml beaker. Bring this mixture to 25 °C, add it quickly to the disintegrated test specimen and simultaneously start the timing device. Rinse out the 250 ml beaker, using at least 10 ml of distilled water, and add the washings to the reaction mixture. The total volume shall be 100 ml. At the end of exactly 10 min, terminate the reaction by adding 20 ml of the potassium iodide solution (1 mol/l) from a graduated cylinder.

Immediately after mixing but without filtering out the fibers, titrate the free iodine with the sodium thiosulphate solution (2 mol/l). Add a few drops of the starch indicator solution (2 g/l) toward the end of the titration.

Carry out a blank test, using exactly the same procedure as above, but omitting the pulp. The potassium iodide solution may be added immediately after the potassium permanganate and sulphuric acid addition.

Make two determinations, the results of which shall, for Kappa number values above 20, fall within $\pm 1\%$ of the mean Kappa number value. If the difference between duplicate determinations is greater than 2%, include a third determination in the calculation of the mean Kappa value.

The Kappa number X expressed as a numerical value only, is calculated by

$$V_1 = \frac{(V_2 - V_3) \cdot c}{0.02 \times 5} \quad (\text{A.1})$$

$$X = \frac{V_1 \cdot d}{m}$$

where V_1 is the volume of the potassium permanganate solution consumed in the determination, in ml; V_2 is the volume of the sodium thiosulphate solution consumed in the blank test, in ml; V_3 is the volume of the sodium thiosulphate solution consumed in the determination, in ml; c is the concentration of the sodium thiosulphate solution, expressed in mol/l; d is the correction factor to 50% (mass/mass) permanganate consumption; d is dependent on the value of V_1 Table A.1; m is the oven dry mass of the test specimen, in g.

Table A.1 Correction factor d, expressed as a function of V_1

V₁ ml	D									
	0	1	2	3	4	5	6	7	8	9
30	0.958	0.960	0.962	0.964	0.966	0.968	0.970	0.973	0.975	0.977
40	0.979	0.981	0.983	0.985	0.987	0.989	0.991	0.994	0.996	0.998
50	1.000	1.002	1.004	1.006	1.009	1.011	1.013	1.015	1.017	1.019
60	1.022	1.024	1.026	1.028	1.030	1.033	1.035	1.037	1.039	1.042
70	1.044									

A.2 Viscosity of pulp (ASTM D 1795 or Tappi T230)

To avoid undesirable effects from long heating at high temperature, samples should be air-dried and the moisture content determined on a portion that is not used for measurement of viscosity. The mass of air-dried samples is then corrected for moisture to obtain the mass of oven-dried cellulose used to calculate concentration.

The sample size is dependent upon the nature of the material, smaller masses of high-viscosity celluloses and larger masses of low-viscosity celluloses being used in order to keep the viscosity of the solutions within rather narrow limits. The concentration for each sample is chosen according to the rule.

$$[\eta]c = 3.09 \pm 0.5 \quad (\text{A.2})$$

where $[\eta]$ is the intrinsic viscosity, dL/g and c is the cellulose concentration, g/dL.

Alkaline solutions of cellulose are known to be sensitive to oxidation. Hence it is usually necessary to exclude air during solution of the sample; several ways of doing this are described in the literature, but the following is simple and adequate. Weight out the calculated amount of air-dried cellulose (corrected to oven dry mass) and transfer quantitatively to a suitable glass or polyethylene container that can be tightly closed by a stopper or screw cap. Add 25 mL of distilled water from a pipette or burette, insert the stopper or cap, and shake in order to wet out and disperse the sample. Sweep the air from the vessel with a stream of nitrogen and with the nitrogen still flowing, add 25 mL of solvent. Stopper or cap tightly and shake vigorously by hand or in a mechanical shaker until the cellulose is completely dissolved.

Transfer 7 mL of the solution by means of a syringe or pipette to a viscometer previously placed in the bath at 25 °C and flushed with nitrogen. Allow at least 5 min for the solution to reach bath temperature.

By applying either pressure or suction, draw the solution into the lower bulb of the viscometer until the top meniscus is a little above the mark between the two bulbs. Measure the time t required for the meniscus to pass from this mark to

the mark below the lower bulb. Repeat at least twice and average the observations, which should not differ by more than 0.3%.

In the same way, measure the outflow time, t_0 for the solvent. This of course must be determined not for the 1.00 M solvent as prepared or purchased, but for this solvent diluted with an equal volume of water.

Calculate the viscosity, η in centipoises, as follows:

$$\eta = Ctd \quad (A.3)$$

where c is the viscometer constant, t is the outflow time, and d is the density, g/mL.

Calculate the relative viscosity, η_{rel} , as follows:

$$\eta_{rel} = \eta / \eta_0 \quad (A.4)$$

where η_0 is the viscosity of the solvent. Since the densities of solvent and solution are practically the same, they cancel in determining relative viscosity. Hence a little work may be saved by determining the kinematic viscosity, ε , in centistokes, for solution and solvent:

$$\varepsilon = Ct \quad (A.5)$$

and then

$$\eta_{rel} = \varepsilon / \varepsilon_0 \quad (A.6)$$

If both solution and solvent are measured in the same viscometer, relative viscosity may be obtained directly from the ratio of outflow times

$$\eta_{rel} = t/t_0 \quad (A.7)$$

By means of Table 3 in ASTM Standard D 1797-90, determine the product $[\eta]c$ corresponding to the value of the relative viscosity. From this value and the concentration, calculate the intrinsic viscosity in decilitres per gram.

A.3 Determination of Residual Alkali (Tappi T625)

After adding few drops of phenolphthalein indicator to 100mL of extraction stage effluent filtrate, the sample is titrated with 0.1 N HCl until the color disappears. Then the volume of the HCl spent is recorded and the concentration of residual alkaline is calculated as A.8.

$$\text{NaOH, g/L} = \text{mL } 0.1\text{N HCl} \times 0.04 \quad (\text{A.8})$$

APPENDIX B

DELIGNIFICATION KINETICS CALCULATION PROCEDURE

B.1 Estimation of Rate Order q and Rate Constant k

The delignification data were fit to the general model

$$-r_a = -\frac{dK}{dt} = kK^q \quad (\text{B.1})$$

where

$$k = A \exp\left[\frac{-EA}{RT}\right] [\text{OH}^-]^m [\text{PO}_2]^n \quad (\text{B.2})$$

K, Kappa number; $[\text{OH}^-]$, sodium hydroxide concentration (g/L); PO_2 , oxygen partial pressure (bar); t, time (min)

A trial and error method was used to find the reaction order (q), since it can not be obtained explicitly from Equation B.1. The integral method was used to estimate q based on the correlation coefficient (R^2) obtained by plotting the Kappa number versus time data.

B.1 .1 Integral Method

Integration of Equation B.1 gives

$$y = \frac{K^{1-q} - K_o^{1-q}}{(q-1)} = kt, \quad q \neq 1 \quad (\text{B.3})$$

where K_0 is the initial Kappa number and q is the reaction order. Equation B.3 is the equation for a linear line passing through zero with slope k . to evaluate reaction order (q) requires a trial and error solution. In the integral method, the value of q is assumed and left hand side of Equation B.3 evaluated. The value of y is then plotted versus time. The correct value will be obtained when the regression coefficient (R^2) reach a maximum. The calculations are shown in Tables B.1 through B.27. Figures B.1 through B.54 plot the data graphically. Table B.28 summarizes the best values of q for the 27 set of experiments. From these values, the average value for the q was found to be 7.9. After finding the average value for q ($q=7.9$), the rate constants k for each set of experiments were found by the help of equation B.3 for $q=7.9$ and summarized in Table B.29.

Table B.1 Value for q and k estimated from the integral method for 0.5 bar, 0.05 g/L NaOH and 90 °C experiment

Time (min)	Kappa Number	$K^{(1-q)} - K_0^{(1-q)} / (q-1)$
0	16.82	
5	16.53	6.11006E-10
10	16.07	1.7514E-09
30	15.41	3.85343E-09
60	14.45	8.32797E-09

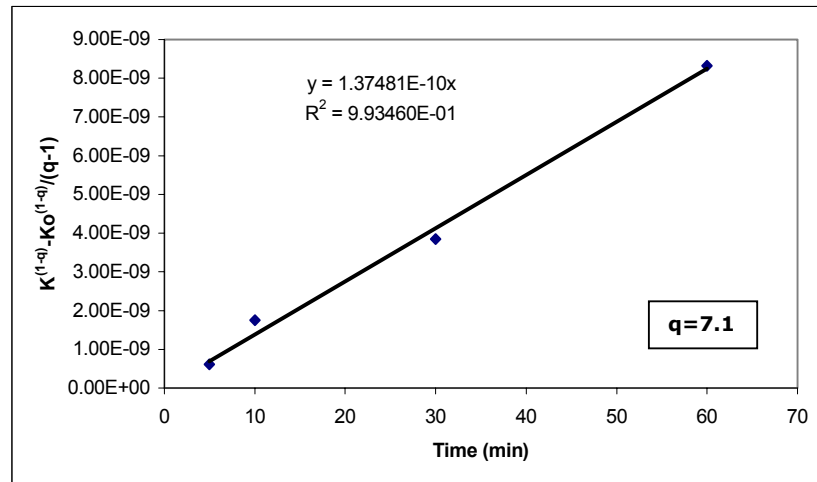


Figure B.1. Estimation of q and k for 0.5 bar, 0.05 g/L NaOH and 90 °C experiment using the integral method

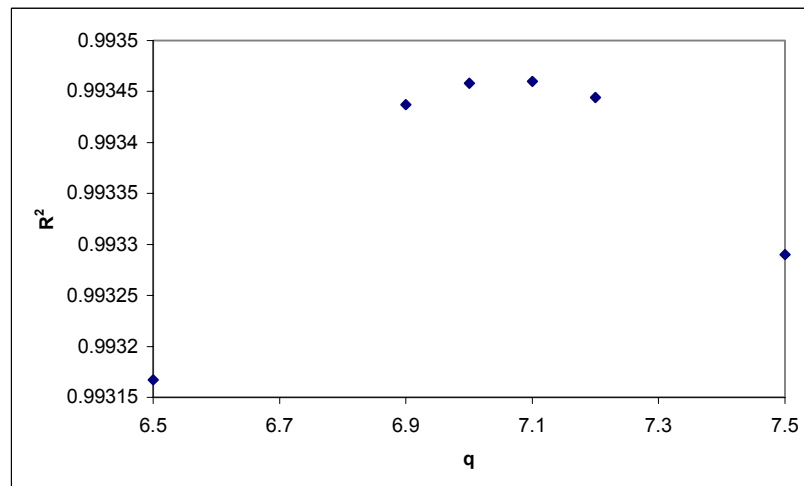


Figure B.2. Value of R^2 plotted versus q for 0.5 bar, 0.05 g/L NaOH and 90 °C

Table B.2 Value for q and k estimated from the integral method for 0.5 bar, 0.15 g/L NaOH and 90 °C experiment

Time (min)	Kappa Number	$K^{(1-q)} - K_0^{(1-q)} / (q-1)$
0	16.44	
5	15.92	1.79556E-09
10	15.36	4.24931E-09
30	14.48	9.63977E-09
60	13.37	2.07365E-08

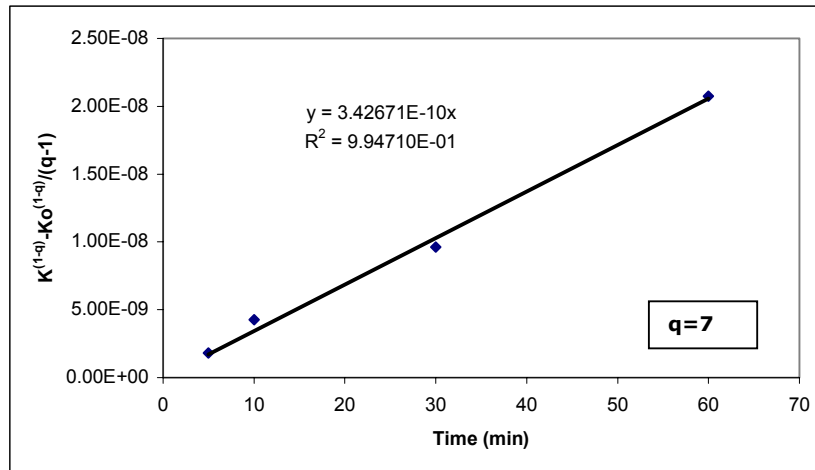


Figure B.3. Estimation of q and k for 0.5 bar, 0.15 g/L NaOH and 90 °C experiment using the integral method

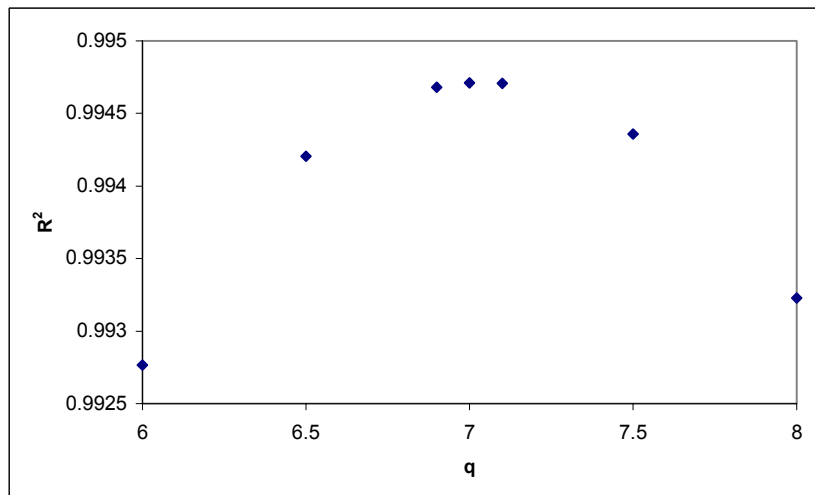


Figure B.4. Value of R^2 plotted versus q for 0.5 bar, 0.15 g/L NaOH and 90 °C

Table B.3 Value for q and k estimated from the integral method for 0.5 bar, 0.25 g/L NaOH and 90 °C experiment

Time (min)	Kappa Number	$K^{(1-q)} - K_0^{(1-q)} / (q-1)$
0	16.27	
5	15.35	1.37141E-10
10	14.87	2.40096E-10
30	13.73	6.30773E-10
60	12.68	1.32222E-09

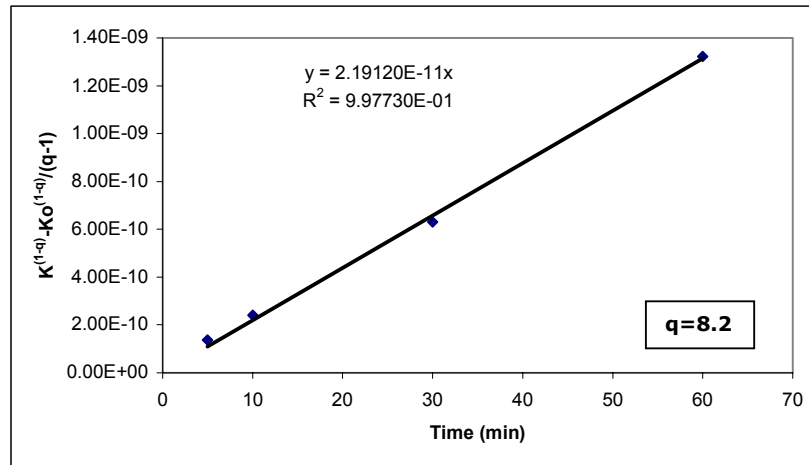


Figure B.5. Estimation of q and k for 0.5 bar, 0.25 g/L NaOH and 90 °C experiment using the integral method

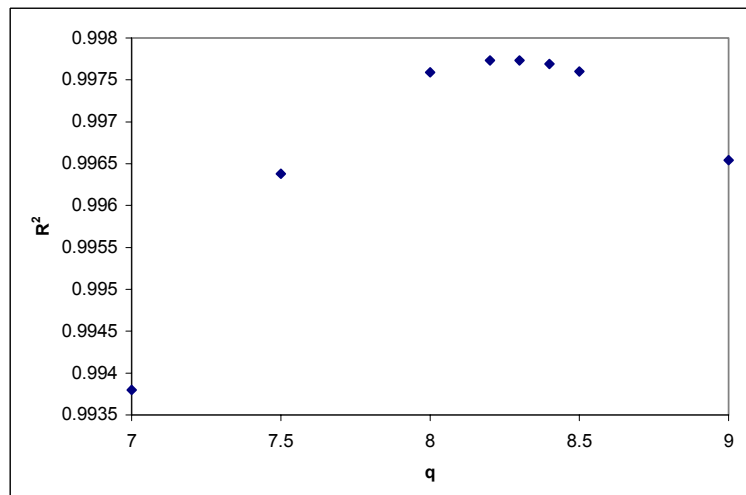


Figure B.6. Value of R^2 plotted versus q for 0.5 bar, 0.25 g/L NaOH and 90 °C

Table B.4 Value for q and k estimated from the integral method for 0.5 bar, 0.05 g/L NaOH and 100 °C experiment

Time (min)	Kappa Number	$K^{(1-q)} - K_0^{(1-q)} / (q-1)$
0	16.63	
5	16.21	7.96373E-11
10	15.77	1.82831E-10
30	14.68	5.66221E-10
60	13.77	1.1157E-09

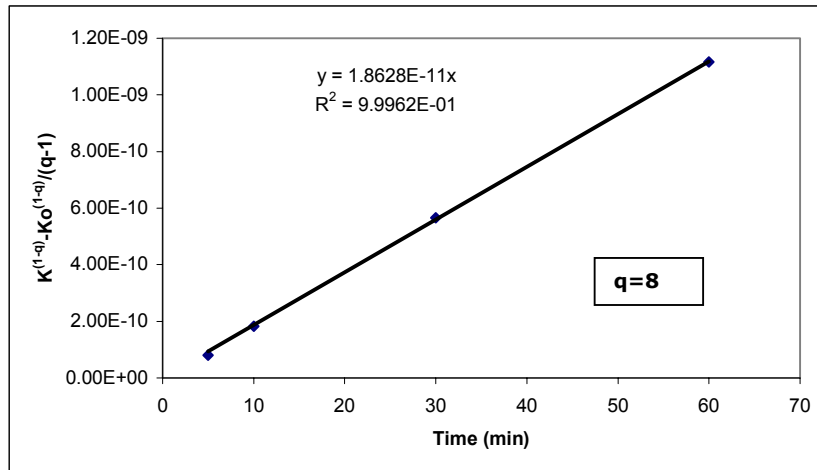


Figure B.7. Estimation of q and k for 0.5 bar, 0.05 g/L NaOH and 100 °C experiment using the integral method

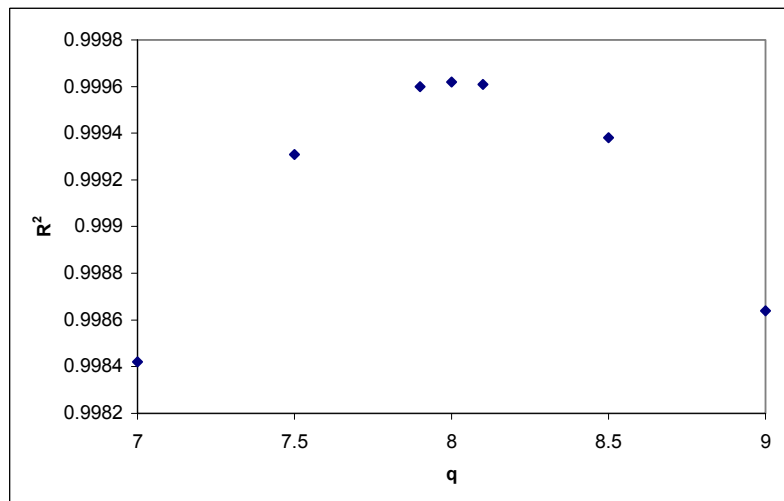


Figure B.8. Value of R^2 plotted versus q for 0.5 bar, 0.05 g/L NaOH and 100 °C

Table B.5 Value for q and k estimated from the integral method for 0.5 bar, 0.15 g/L NaOH and 100 °C experiment

Time (min)	Kappa Number	$K^{(1-q)} - K_0^{(1-q)} / (q-1)$
0	16.32	
5	15.54	4.75075E-11
10	15.15	7.99631E-11
30	13.76	2.7782E-10
60	12.83	5.43449E-10

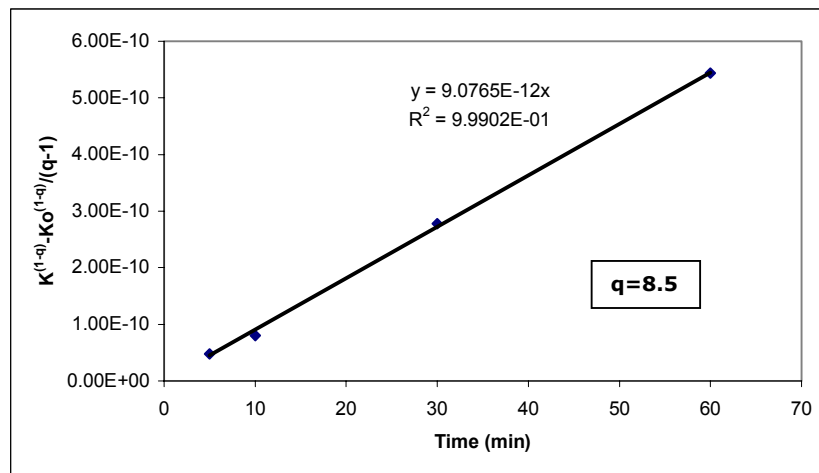


Figure B.9. Estimation of q and k for 0.5 bar, 0.15 g/L NaOH and 100 °C experiment using the integral method

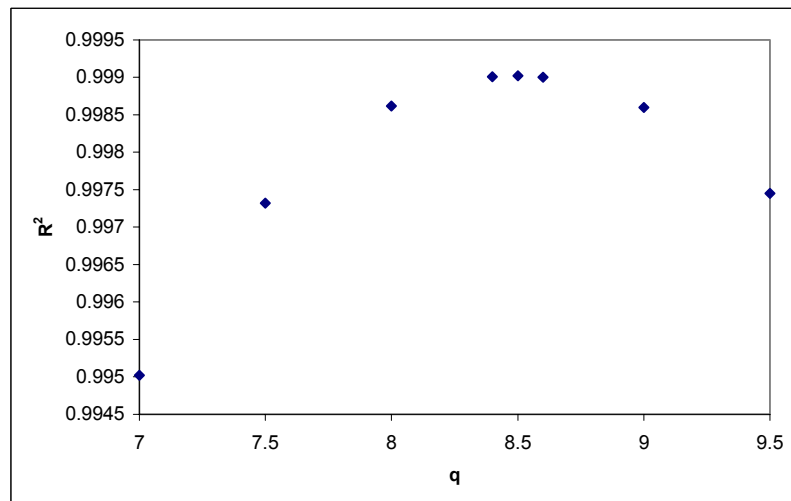


Figure B.10. Value of R^2 plotted versus q for 0.5 bar, 0.15 g/L NaOH and 100 °C

Table B.6 Value for q and k estimated from the integral method for 0.5 bar, 0.25 g/L NaOH and 100 °C experiment

Time (min)	Kappa Number	$K^{(1-q)} - K_0^{(1-q)} / (q-1)$
0	16.04	
5	15.13	3.12155E-09
10	14.49	6.26338E-09
30	12.81	2.14556E-08
60	11.74	4.16502E-08

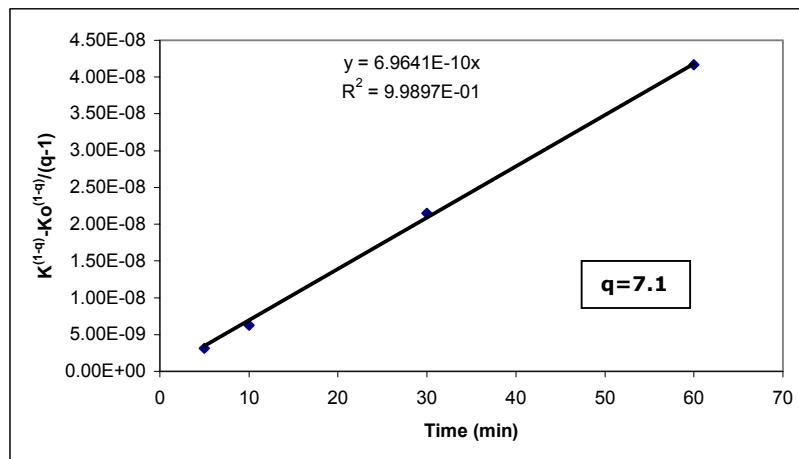


Figure B.11. Estimation of q and k for 0.5 bar, 0.25 g/L NaOH and 100 °C experiment using the integral method

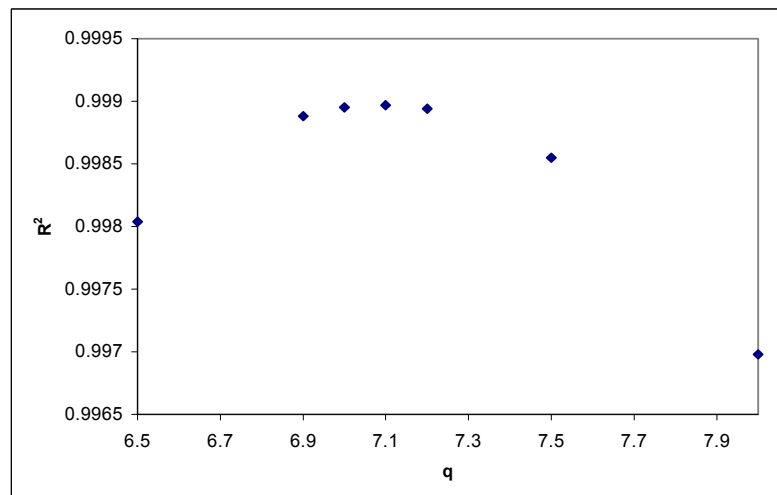


Figure B.12. Value of R^2 plotted versus q for 0.5 bar, 0.25 g/L NaOH and 100 °C

Table B.7 Value for q and k estimated from the integral method for 0.5 bar, 0.05 g/L NaOH and 110 °C experiment

Time (min)	Kappa Number	$K^{(1-q)} - K_0^{(1-q)} / (q-1)$
0	16.38	
5	15.91	3.10464E-10
10	15.2	9.34931E-10
30	13.82	3.03337E-09
60	12.83	5.88235E-09

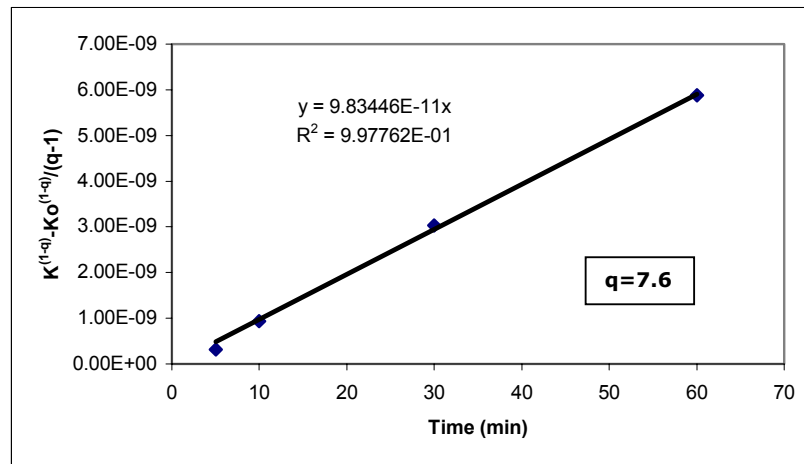


Figure B.13. Estimation of q and k for 0.5 bar, 0.05 g/L NaOH and 110 °C experiment using the integral method

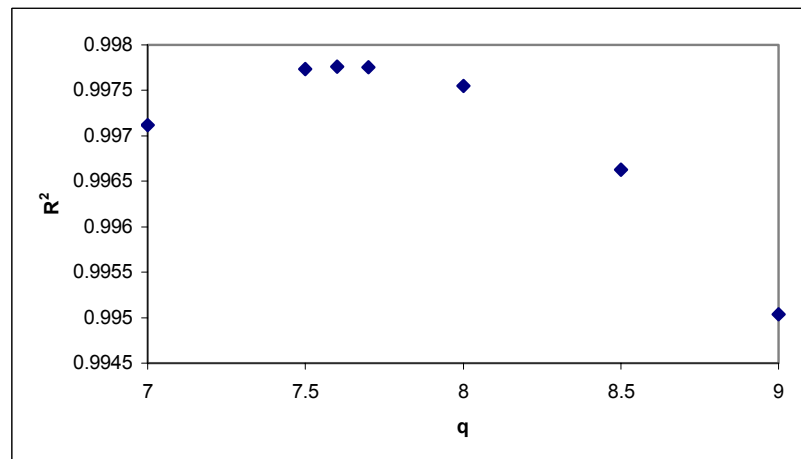


Figure B.14. Value of R^2 plotted versus q for 0.5 bar, 0.05 g/L NaOH and 110 °C

Table B.8 Value for q and k estimated from the integral method for 0.5 bar, 0.15 g/L NaOH and 110 °C experiment

Time (min)	Kappa Number	$K^{(1-q)} - K_o^{(1-q)} / (q-1)$
0	16.04	
5	15.17	7.97174E-08
10	14.69	1.36609E-07
30	12.93	4.7572E-07
60	11.72	9.2679E-07

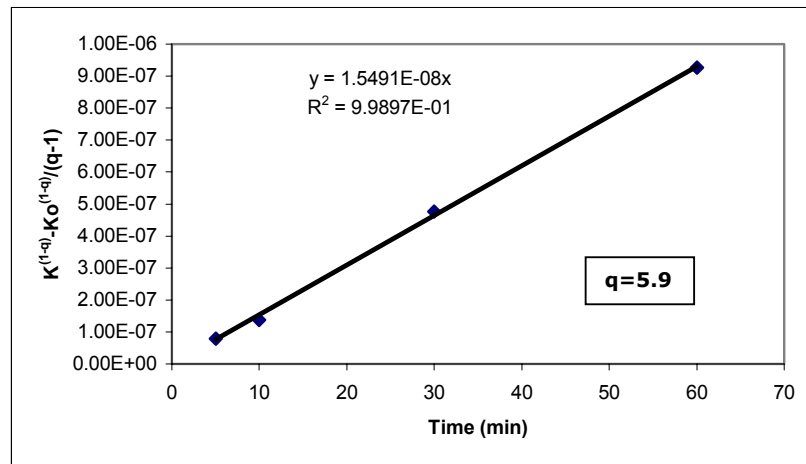


Figure B.15. Estimation of q and k for 0.5 bar, 0.15 g/L NaOH and 110 °C experiment using the integral method

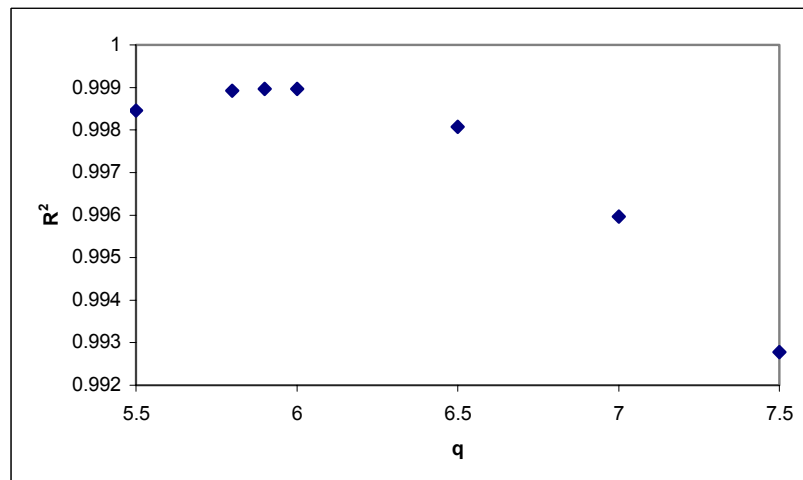


Figure B.16. Value of R^2 plotted versus q for 0.5 bar, 0.15 g/L NaOH and 110 °C

Table B.9 Value for q and k estimated from the integral method for 0.5 bar, 0.25 g/L NaOH and 110 °C experiment

Time (min)	Kappa Number	$K^{(1-q)} - K_0^{(1-q)} / (q-1)$
0	15.72	
5	14.16	6.36488E-08
10	13.86	8.16351E-08
30	12.14	2.52344E-07
60	10.85	5.27681E-07

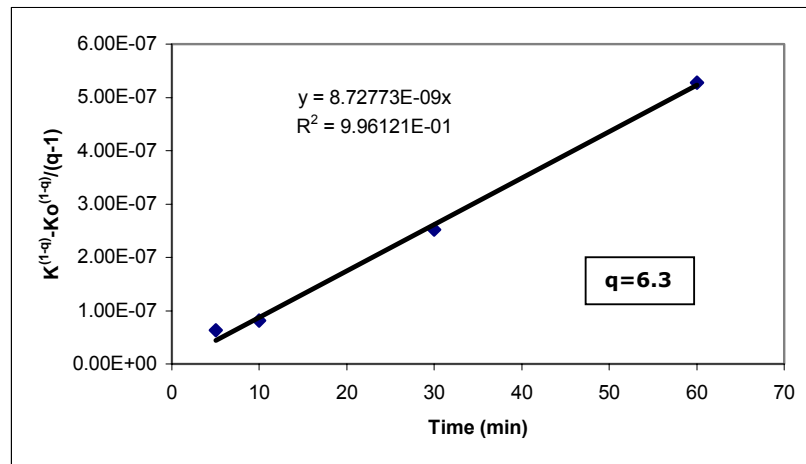


Figure B.17. Estimation of q and k for 0.5 bar, 0.25 g/L NaOH and 110 °C experiment using the integral method

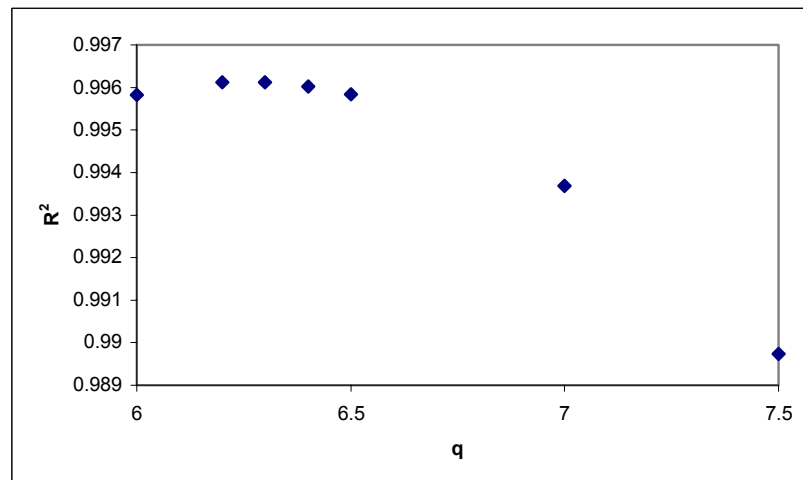


Figure B.18. Value of R^2 plotted versus q for 0.5 bar, 0.25 g/L NaOH and 110 °C

Table B.10 Value for q and k estimated from the integral method for 3.5 bar, 0.05 g/L NaOH and 90 °C experiment

Time (min)	Kappa Number	$K^{(1-q)} - K_o^{(1-q)} / (q-1)$
0	16.54	
5	15.92	3.03649E-14
10	15.59	5.26471E-14
30	14.43	1.90208E-13
60	13.69	3.6722E-13

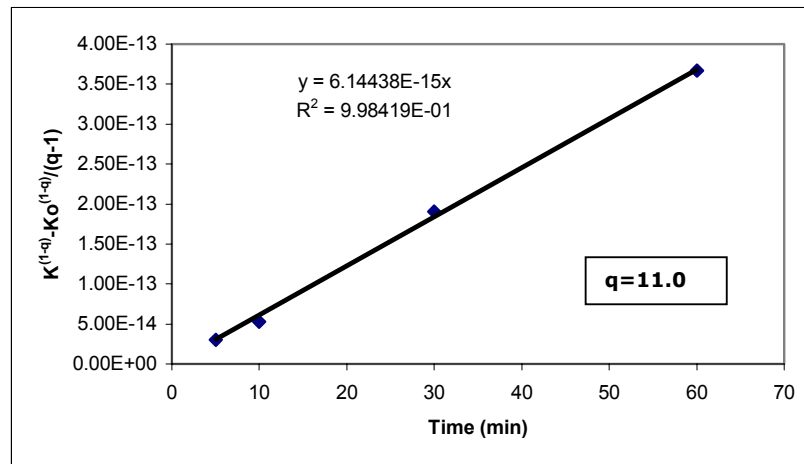


Figure B.19. Estimation of q and k for 3.5 bar, 0.05 g/L NaOH and 90 °C experiment using the integral method

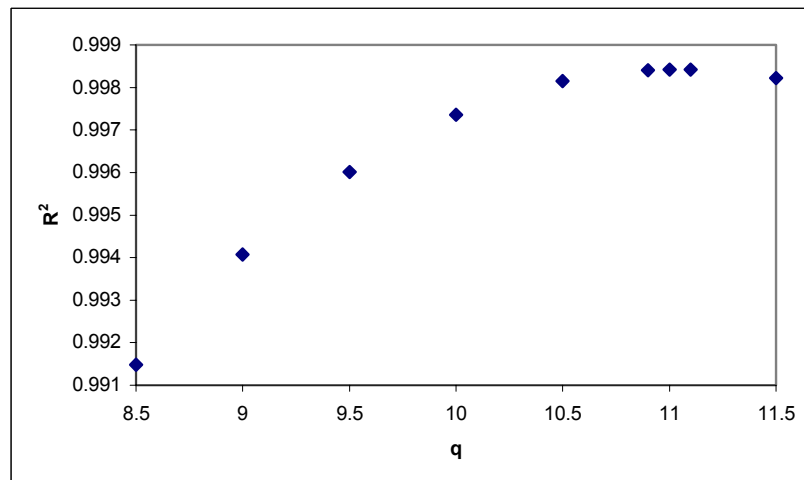


Figure B.20. Value of R² plotted versus q for 3.5 bar, 0.05 g/L NaOH and 90 °C

Table B.11 Value for q and k estimated from the integral method for 3.5 bar, 0.15 g/L NaOH and 90 °C experiment

Time (min)	Kappa Number	$K^{(1-q)} - K_o^{(1-q)} / (q-1)$
0	16.05	
5	15.31	2.25767E-11
10	14.91	3.9389E-11
30	13.56	1.38198E-10
60	12.68	2.68119E-10

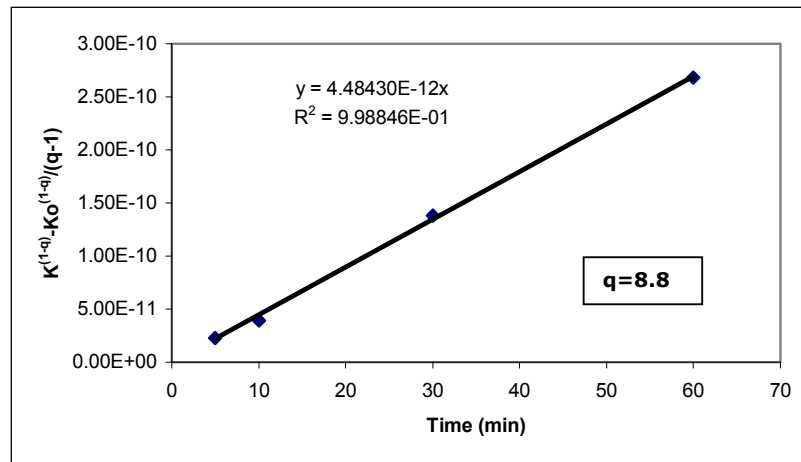


Figure B.21. Estimation of q and k for 3.5 bar, 0.15 g/L NaOH and 90 °C experiment using the integral method

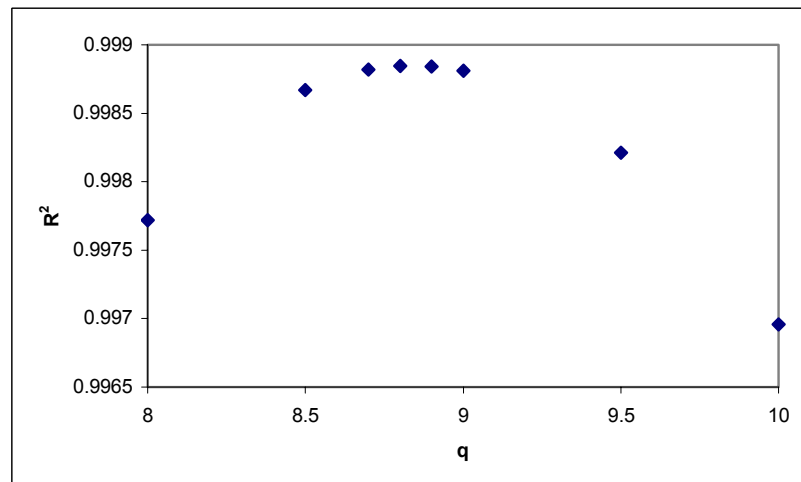


Figure B.22. Value of R^2 plotted versus q for 3.5 bar, 0.15 g/L NaOH and 90 °C

Table B.12 Value for q and k estimated from the integral method for 3.5 bar, 0.25 g/L NaOH and 90 °C experiment

Time (min)	Kappa Number	$K^{(1-q)} - K_o^{(1-q)} / (q-1)$
0	15.73	
5	14.69	2.80556E-10
10	14.11	5.22021E-10
30	12.98	1.30715E-09
60	11.91	2.7855E-09

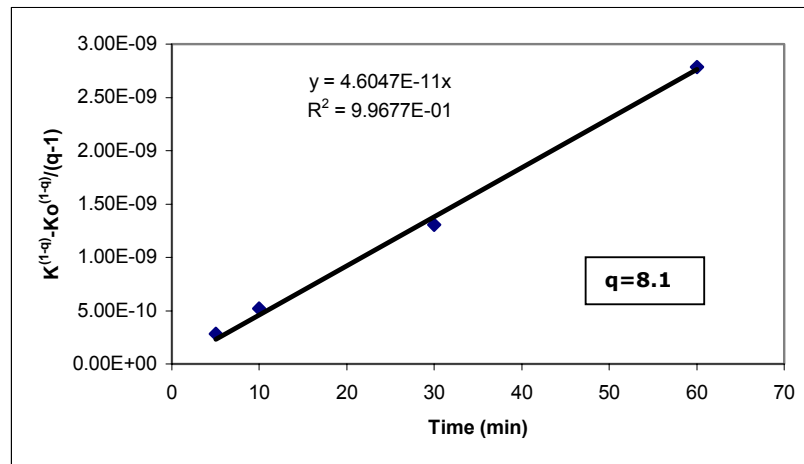


Figure B.23. Estimation of q and k for 3.5 bar, 0.25 g/L NaOH and 90 °C experiment using the integral method

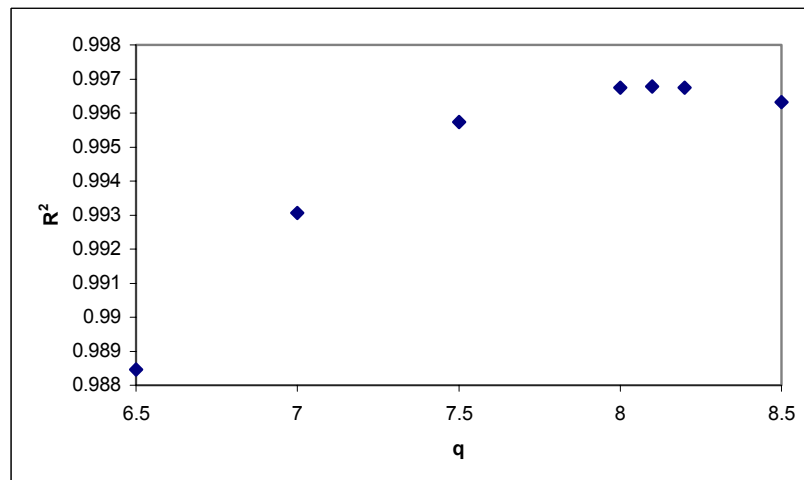


Figure B.24. Value of R^2 plotted versus q for 3.5 bar, 0.25 g/L NaOH and 90 °C

Table B.13 Value for q and k estimated from the integral method for 3.5 bar, 0.05 g/L NaOH and 100 °C experiment

Time (min)	Kappa Number	$K^{(1-q)} - K_0^{(1-q)} / (q-1)$
0	16.42	
5	15.62	2.45148E-10
10	15.26	3.91932E-10
30	13.96	1.22998E-09
60	12.95	2.46965E-09

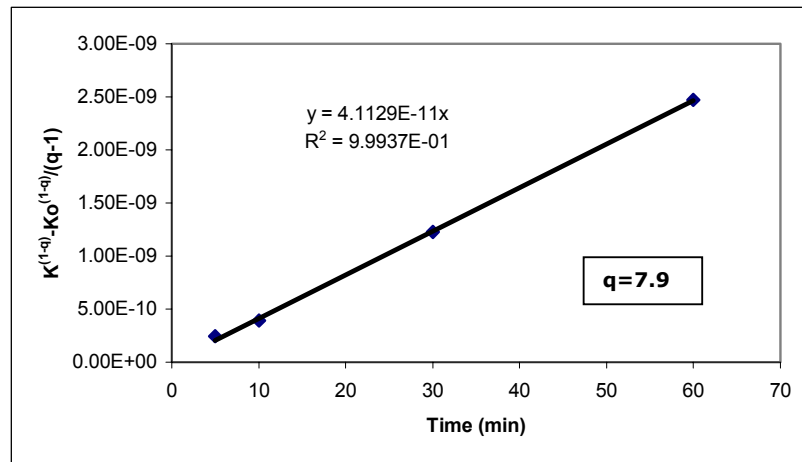


Figure B.25. Estimation of q and k for 3.5 bar, 0.05 g/L NaOH and 100 °C experiment using the integral method

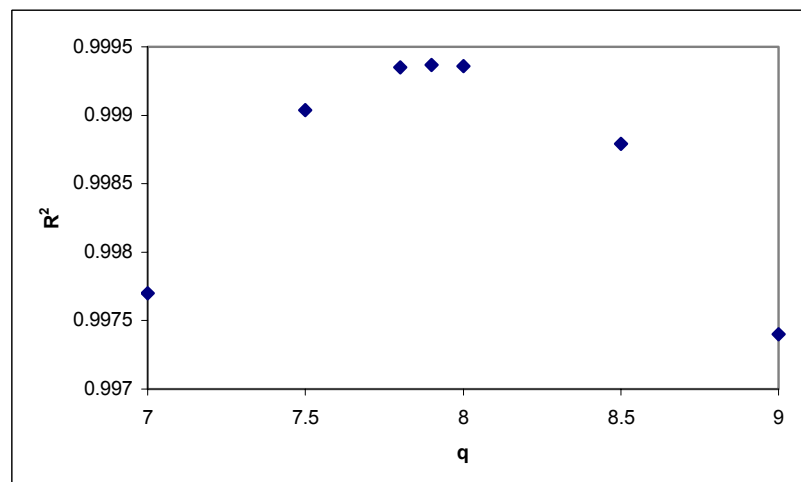


Figure B.26. Value of R^2 plotted versus q for 3.5 bar, 0.05 g/L NaOH and 100 °C

Table B.14 Value for q and k estimated from the integral method for 3.5 bar, 0.15 g/L NaOH and 100 °C experiment

Time (min)	Kappa Number	$K^{(1-q)} - K_0^{(1-q)} / (q-1)$
0	16.11	
5	14.83	9.0454E-10
10	14.46	1.29643E-09
30	13.03	3.83582E-09
60	11.91	8.01237E-09

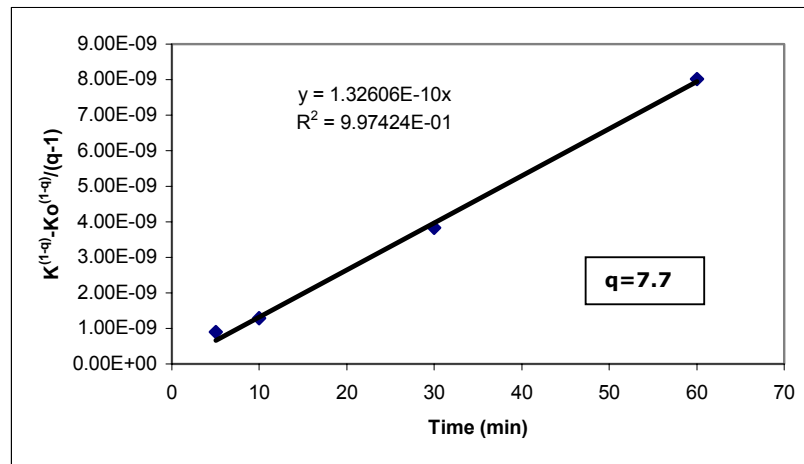


Figure B.27. Estimation of q and k for 3.5 bar, 0.15 g/L NaOH and 100 °C experiment using the integral method

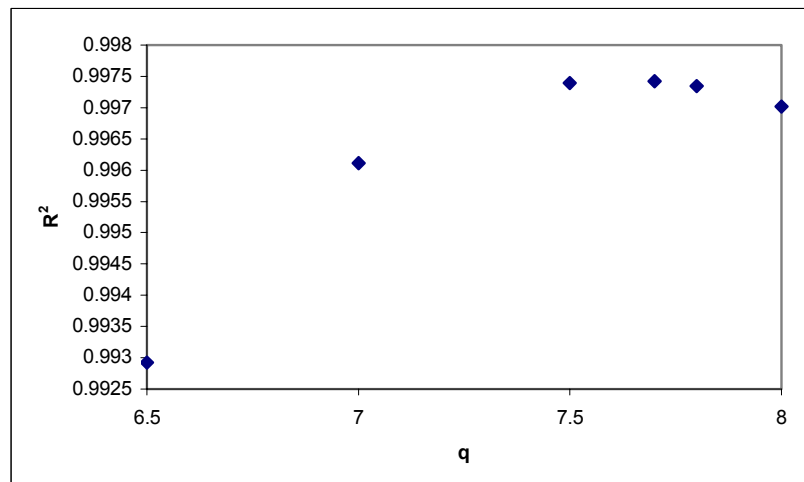


Figure B.28. Value of R^2 plotted versus q for 3.5 bar, 0.15 g/L NaOH and 100 °C

Table B.15 Value for q and k estimated from the integral method for 3.5 bar, 0.25 g/L NaOH and 100 °C experiment

Time (min)	Kappa Number	$K^{(1-q)} - K_0^{(1-q)} / (q-1)$
0	15.9	
5	13.93	2.48617E-09
10	13.65	3.09846E-09
30	12.13	8.85747E-09
60	10.96	1.89996E-08

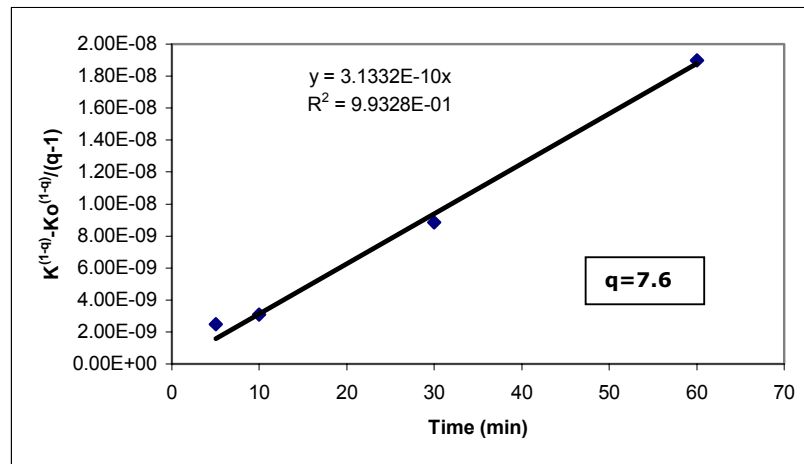


Figure B.29. Estimation of q and k for 3.5 bar, 0.25 g/L NaOH and 100 °C experiment using the integral method

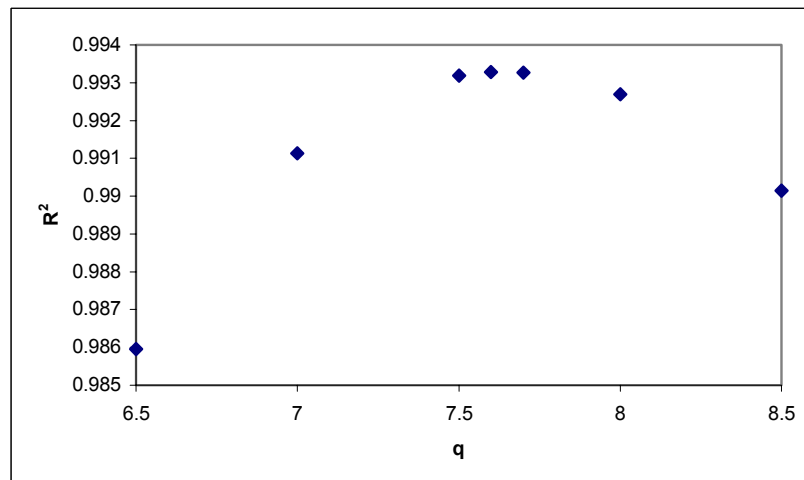


Figure B.30. Value of R^2 plotted versus q for 3.5 bar, 0.25 g/L NaOH and 100 °C

Table B.16 Value for q and k estimated from the integral method for 3.5 bar, 0.05 g/L NaOH and 110 °C experiment

Time (min)	Kappa Number	$K^{(1-q)} - K_o^{(1-q)} / (q-1)$
0	16.08	
5	15.33	3.53832E-10
10	14.75	7.36429E-10
30	13.01	2.97205E-09
60	12.06	5.5992E-09

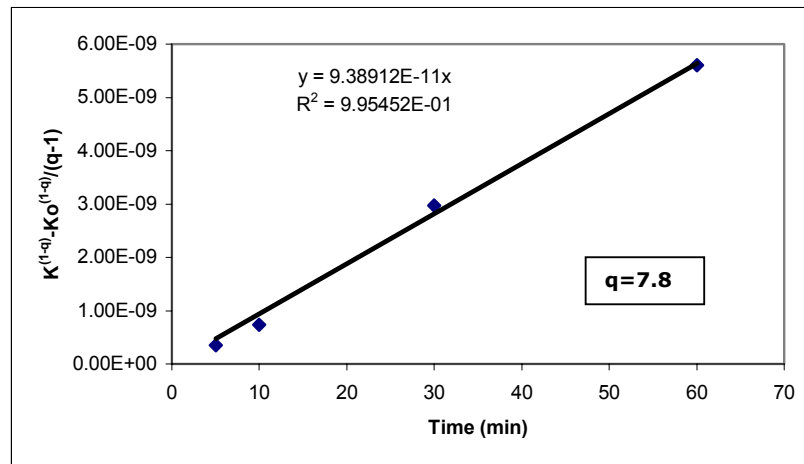


Figure B.31. Estimation of q and k for 3.5 bar, 0.05 g/L NaOH and 110 °C experiment using the integral method

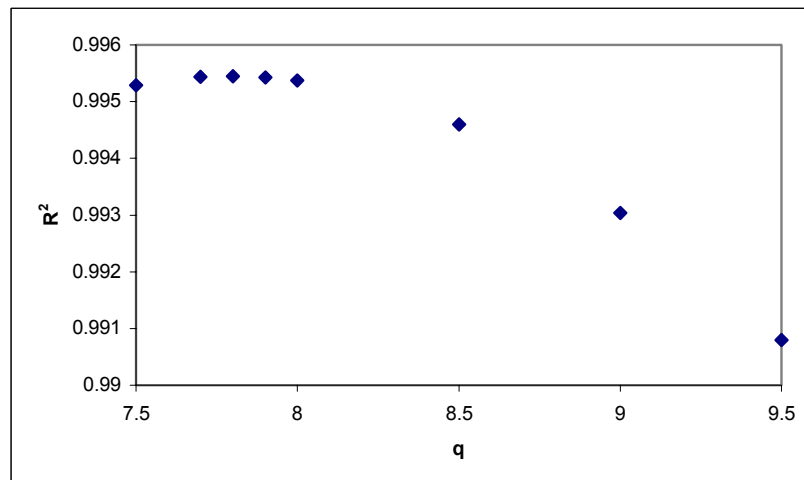


Figure B.32. Value of R^2 plotted versus q for 3.5 bar, 0.05 g/L NaOH and 110 °C

Table B.17 Value for q and k estimated from the integral method for 3.5 bar, 0.15 g/L NaOH and 110 °C experiment

Time (min)	Kappa Number	$K^{(1-q)} - K_o^{(1-q)} / (q-1)$
0	15.84	
5	14.57	5.2355E-09
10	13.78	1.05449E-08
30	12.07	3.34557E-08
60	10.98	6.57466E-08

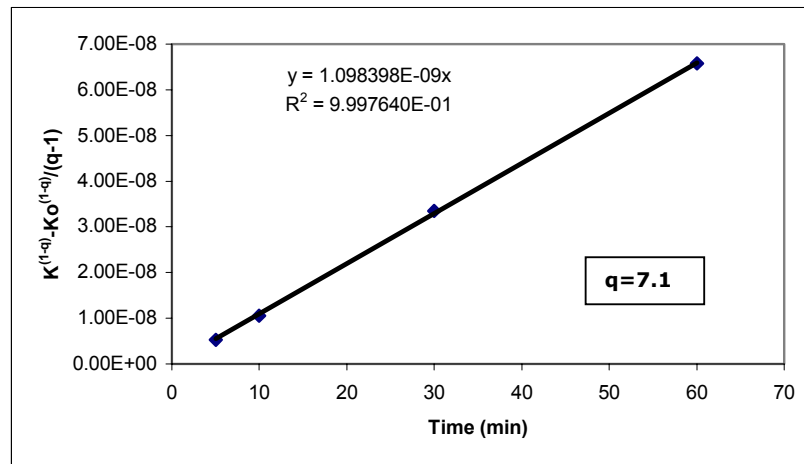


Figure B.33. Estimation of q and k for 3.5 bar, 0.15 g/L NaOH and 110 °C experiment using the integral method

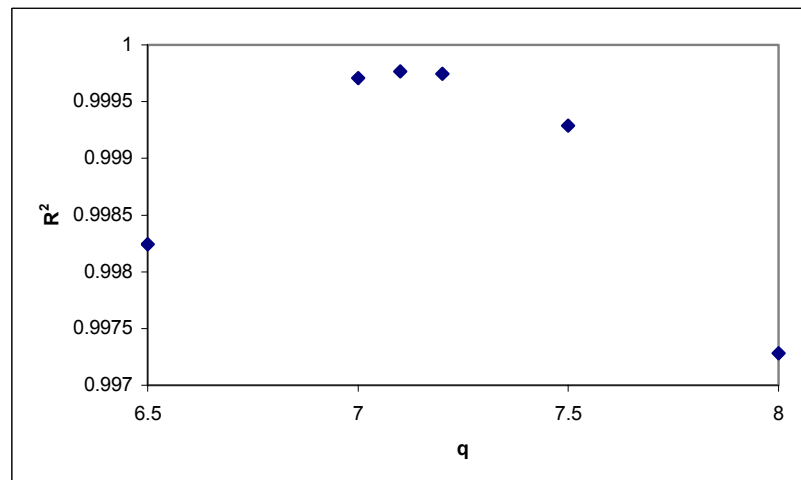


Figure B.34. Value of R^2 plotted versus q for 3.5 bar, 0.15 g/L NaOH and 110 °C

Table B.18 Value for q and k estimated from the integral method for 3.5 bar, 0.25 g/L NaOH and 110 °C experiment

Time (min)	Kappa Number	$K^{(1-q)} - K_o^{(1-q)} / (q-1)$
0	15.55	
5	13.64	9.13697E-08
10	13.17	1.28638E-07
30	11.36	3.89975E-07
60	10.11	8.01259E-07

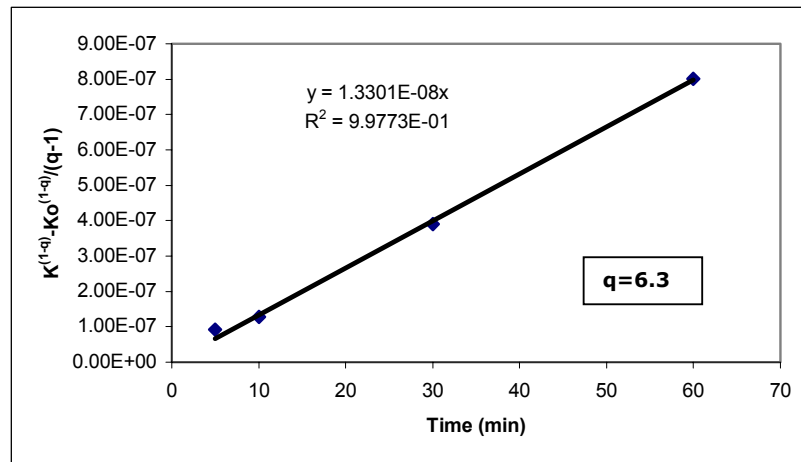


Figure B.35. Estimation of q and k for 3.5 bar, 0.25 g/L NaOH and 110 °C experiment using the integral method

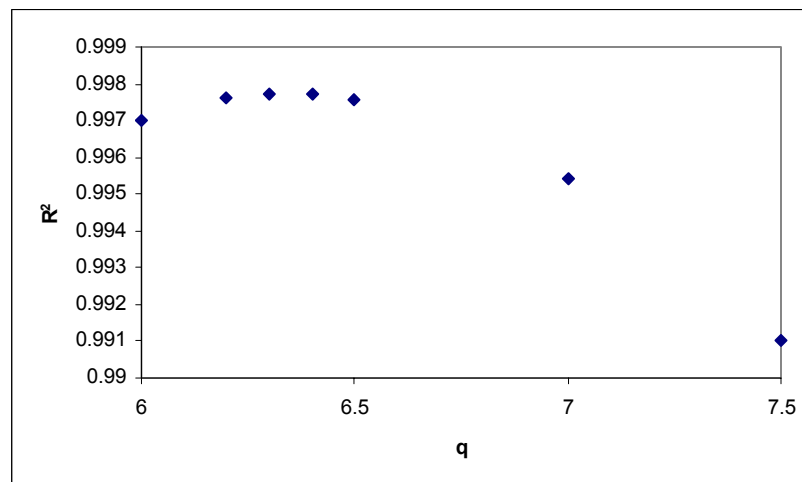


Figure B.36. Value of R^2 plotted versus q for 3.5 bar, 0.25 g/L NaOH and 110 °C

Table B.19 Value for q and k estimated from the integral method for 6.5 bar, 0.05 g/L NaOH and 90 °C experiment

Time (min)	Kappa Number	$K^{(1-q)} - K_0^{(1-q)} / (q-1)$
0	16.37	
5	15.41	2.3902E-13
10	15.07	3.68208E-13
30	13.99	1.06272E-12
60	13.13	2.19655E-12

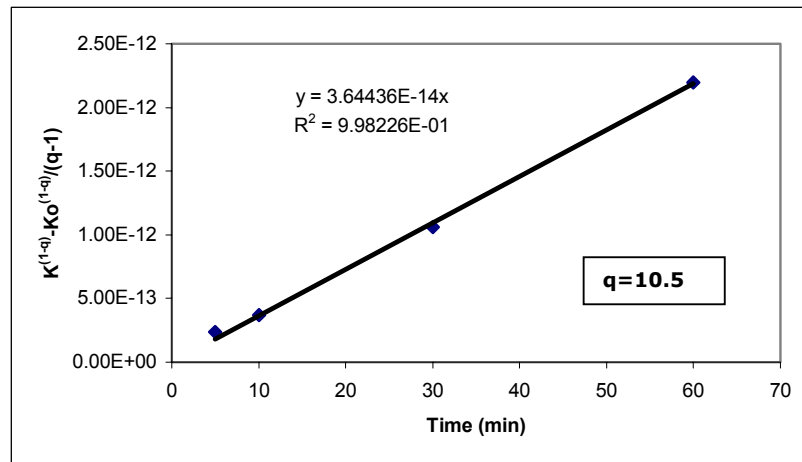


Figure B.37. Estimation of q and k for 6.5 bar, 0.05 g/L NaOH and 90 °C experiment using the integral method

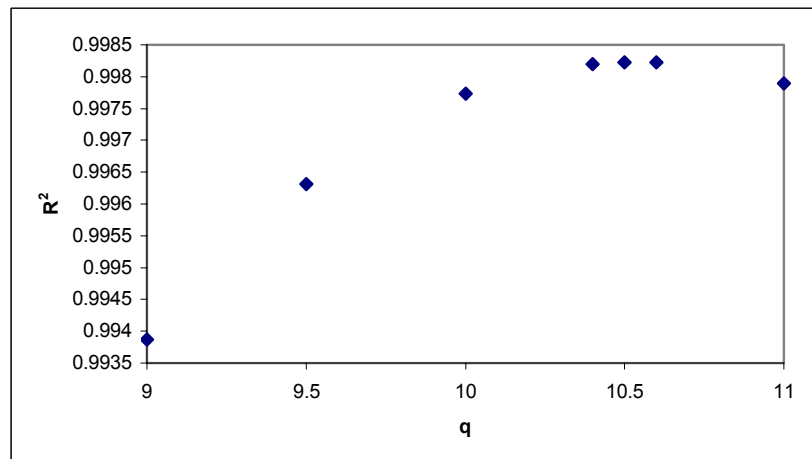


Figure B.38. Value of R^2 plotted versus q for 6.5 bar, 0.05 g/L NaOH and 90 °C

Table B.20 Value for q and k estimated from the integral method for 6.5 bar, 0.15 g/L NaOH and 90 °C experiment

Time (min)	Kappa Number	$K^{(1-q)} - K_0^{(1-q)} / (q-1)$
0	15.81	
5	14.66	3.48717E-11
10	14.22	5.59962E-11
30	13.07	1.49481E-10
60	12.08	3.15395E-10

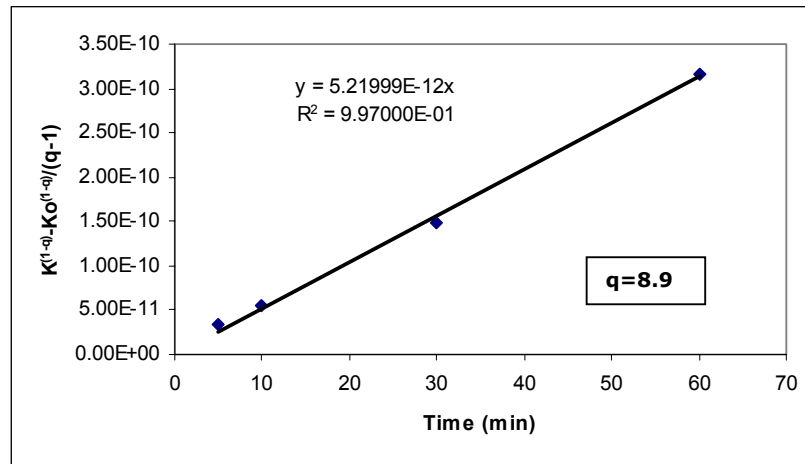


Figure B.39. Estimation of q and k for 6.5 bar, 0.15 g/L NaOH and 90 °C experiment using the integral method

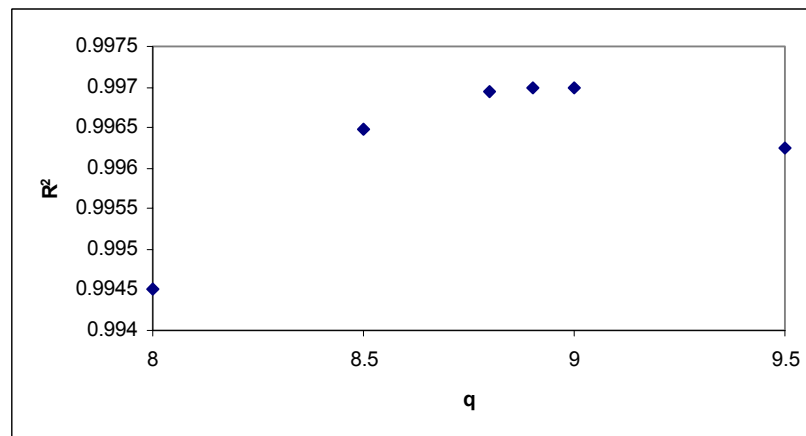


Figure B.40. Value of R² plotted versus q for 6.5 bar, 0.15 g/L NaOH and 90 °C

Table B.21 Value for q and k estimated from the integral method for 6.5 bar, 0.25 g/L NaOH and 90 °C experiment

Time (min)	Kappa Number	$K^{(1-q)} - K_0^{(1-q)} / (q-1)$
0	15.45	
5	14.03	1.00117E-10
10	13.39	1.82774E-10
30	12.35	4.19181E-10
60	11.29	9.27101E-10

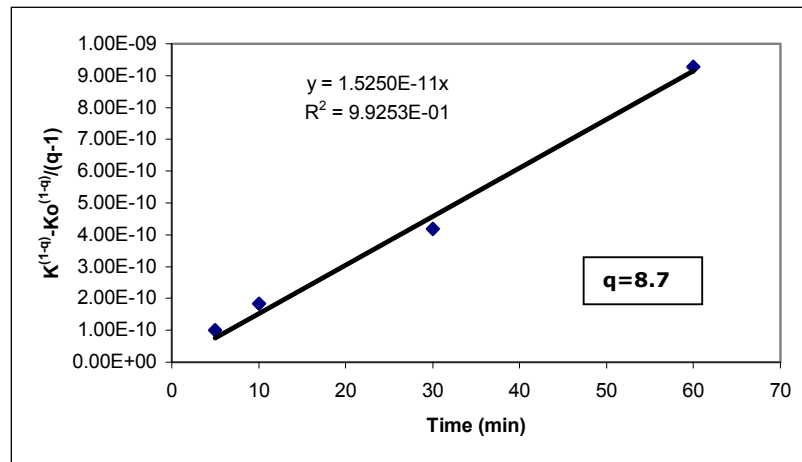


Figure B.41. Estimation of q and k for 6.5 bar, 0.25 g/L NaOH and 90 °C experiment using the integral method

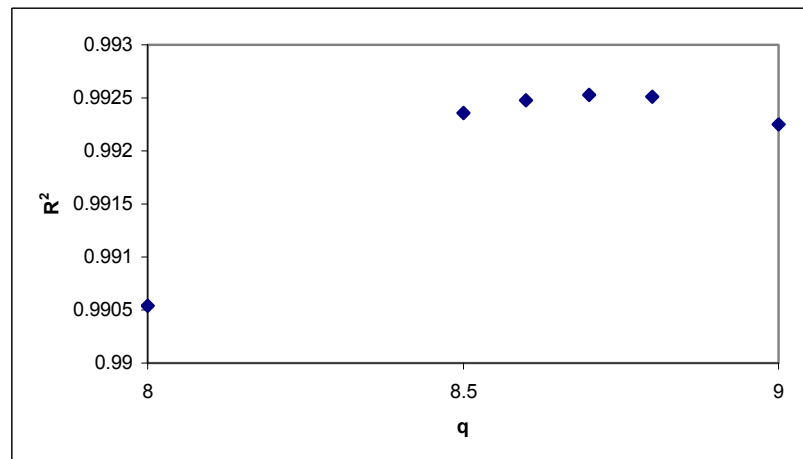


Figure B.42. Value of R² plotted versus q for 6.5 bar, 0.25 g/L NaOH and 90 °C

Table B.22 Value for q and k estimated from the integral method for 6.5 bar, 0.05 g/L NaOH and 100 °C experiment

Time (min)	Kappa Number	$K^{(1-q)} - K_0^{(1-q)} / (q-1)$
0	16.34	0
5	14.94	2.18167E-12
10	14.61	3.05498E-12
30	13.43	8.46099E-12
60	12.47	1.80442E-11

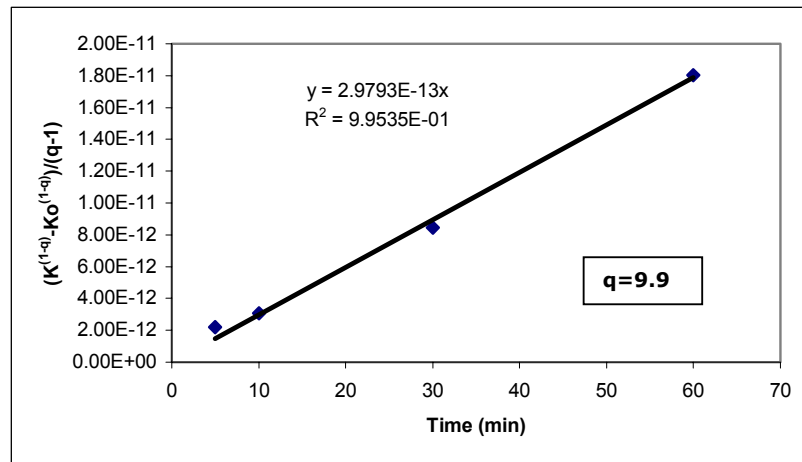


Figure B.43. Estimation of q and k for 6.5 bar, 0.05 g/L NaOH and 100 °C experiment using the integral method

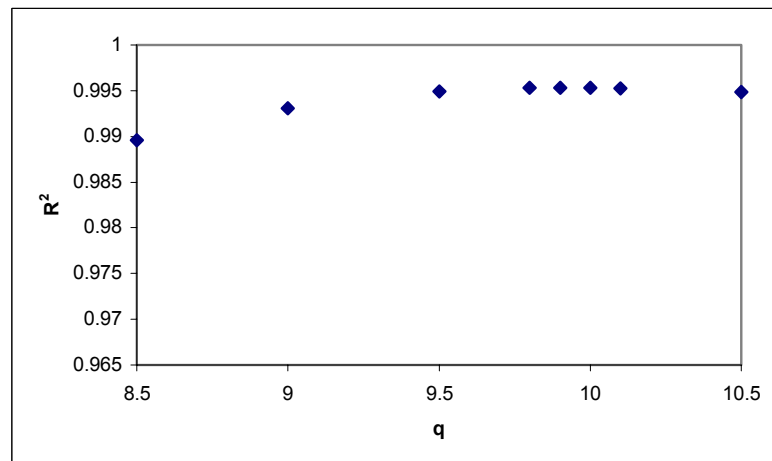


Figure B.44. Value of R^2 plotted versus q for 6.5 bar, 0.05 g/L NaOH and 100 °C

Table B.23 Value for q and k estimated from the integral method for 6.5 bar, 0.15 g/L NaOH and 100 °C experiment

Time (min)	Kappa Number	$K^{(1-q)} - K_0^{(1-q)} / (q-1)$
0	16.03	
5	14.3	1.65905E-10
10	13.85	2.44049E-10
30	12.62	6.13752E-10
60	11.51	1.34606E-09

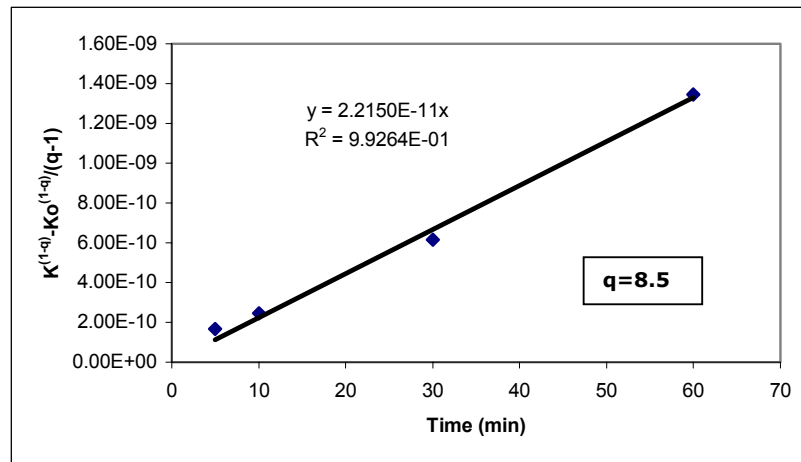


Figure B.45. Estimation of q and k for 6.5 bar, 0.15 g/L NaOH and 100 °C experiment using the integral method

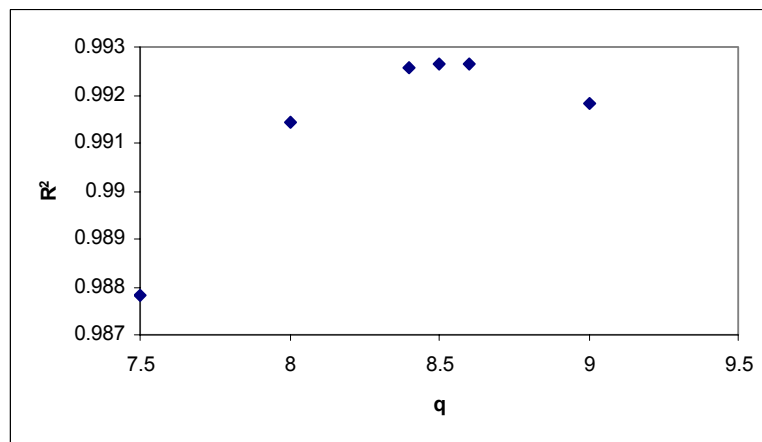


Figure B.46. Value of R^2 plotted versus q for 6.5 bar, 0.15 g/L NaOH and 100 °C

Table B.24 Value for q and k estimated from the integral method for 6.5 bar, 0.25 g/L NaOH and 100 °C experiment

Time (min)	Kappa Number	$K^{(1-q)} - K_o^{(1-q)} / (q-1)$
0	15.74	
5	13.92	9.49429E-11
10	12.95	2.11465E-10
30	11.39	6.77185E-10
60	10.51	1.31944E-09

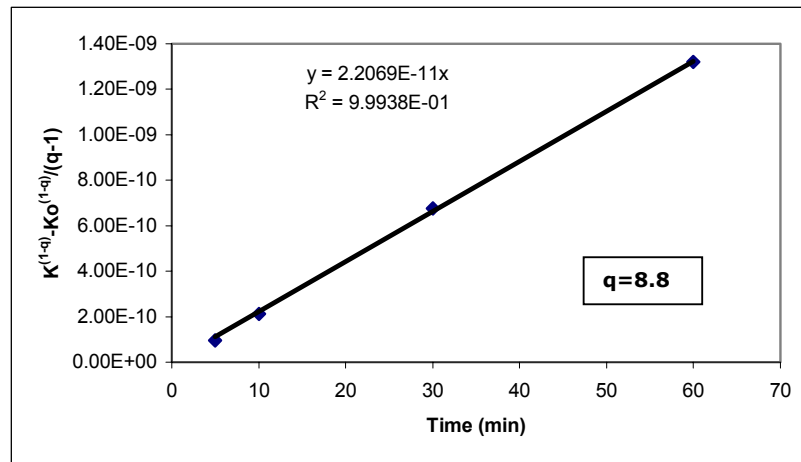


Figure B.47. Estimation of q and k for 6.5 bar, 0.25 g/L NaOH and 100 °C experiment using the integral method

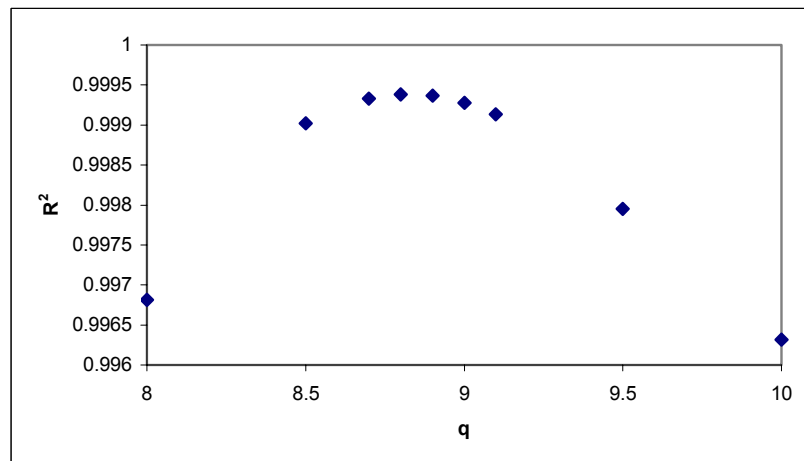


Figure B.48. Value of R^2 plotted versus q for 6.5 bar, 0.25 g/L NaOH and 100 °C

Table B.25 Value for q and k estimated from the integral method for 6.5 bar, 0.05 g/L NaOH and 110 °C experiment

Time (min)	Kappa Number	$K^{(1-q)} - K_0^{(1-q)} / (q-1)$
0	15.92	
5	14.8	3.79646E-08
10	14.18	6.81074E-08
30	12.61	1.96221E-07
60	11.37	3.98412E-07

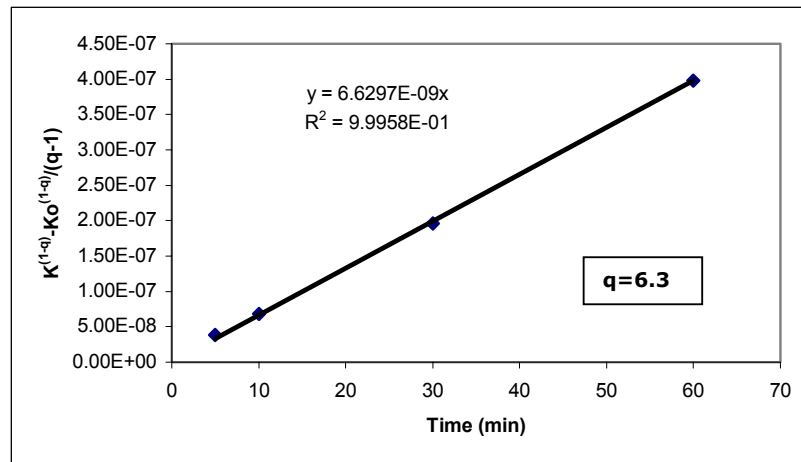


Figure B.49. Estimation of q and k for 6.5 bar, 0.05 g/L NaOH and 110 °C experiment using the integral method

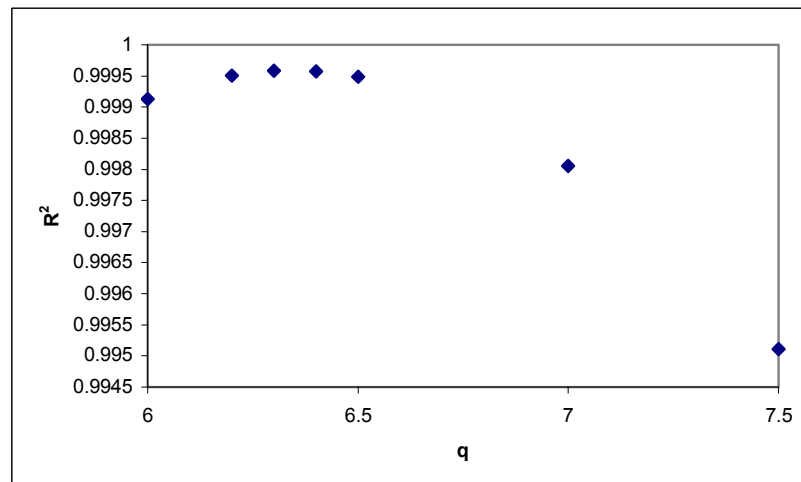


Figure B.50. Value of R^2 plotted versus q for 6.5 bar, 0.05 g/L NaOH and 110 °C

Table B.26 Value for q and k estimated from the integral method for 6.5 bar, 0.15 g/L NaOH and 110 °C experiment

Time (min)	Kappa Number	$K^{(1-q)} - K_0^{(1-q)} / (q-1)$
0	15.63	
5	14.02	2.35597E-08
10	13.44	3.74496E-08
30	11.65	1.19126E-07
60	10.49	2.39054E-07

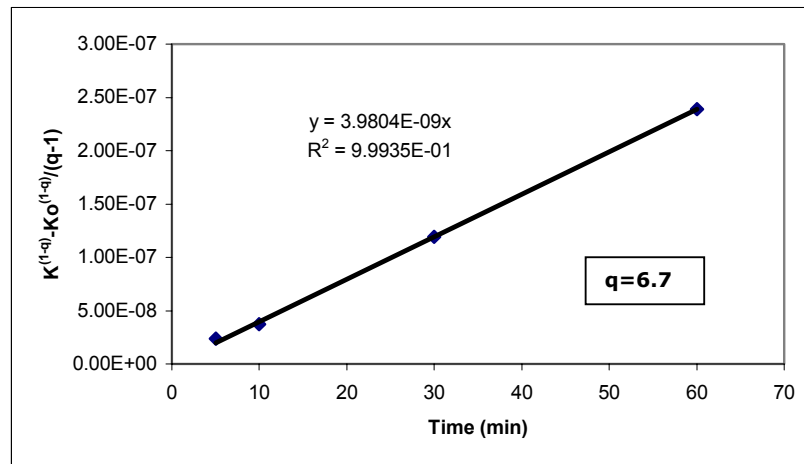


Figure B.51. Estimation of q and k for 6.5 bar, 0.15 g/L NaOH and 110 °C experiment using the integral method

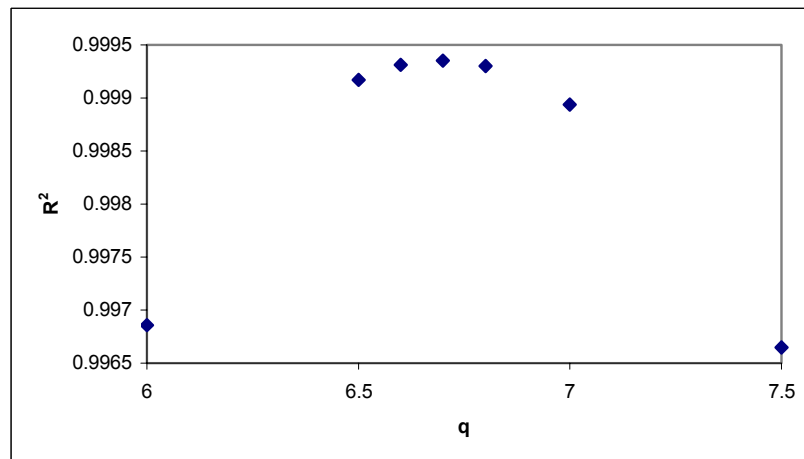


Figure B.52. Value of R^2 plotted versus q for 6.5 bar, 0.15 g/L NaOH and 110 °C

Table B.27 Value for q and k estimated from the integral method for 6.5 bar, 0.25 g/L NaOH and 110 °C experiment

Time (min)	Kappa Number	$K^{(1-q)} - K_0^{(1-q)} / (q-1)$
0	15.32	
5	13.23	5.674E-07
10	12.69	8.1386E-07
30	10.62	2.62803E-06
60	9.33	5.30937E-06

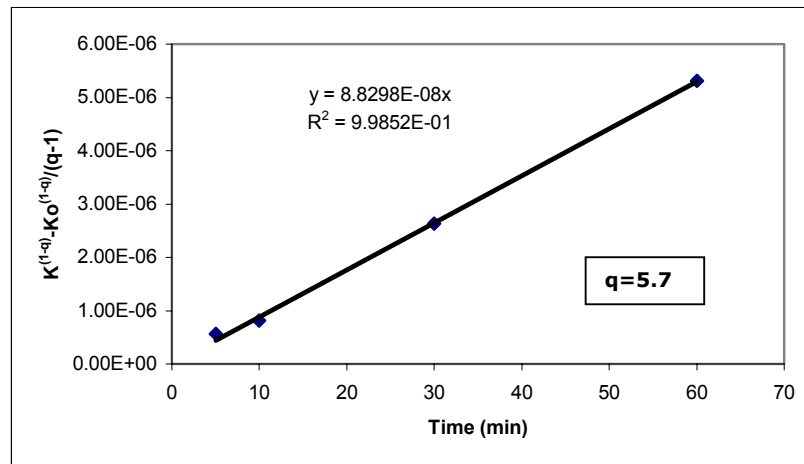


Figure B.53. Estimation of q and k for 6.5 bar, 0.25 g/L NaOH and 110 °C experiment using the integral method

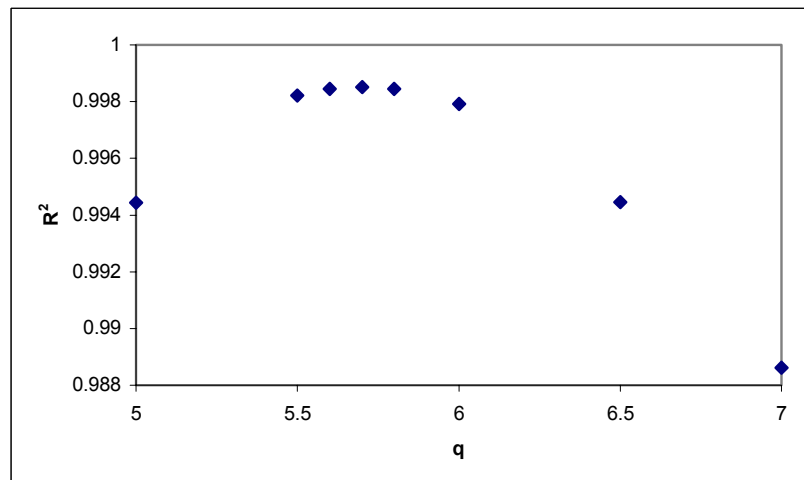


Figure B.54. Value of R^2 plotted versus q for 6.5 bar, 0.25 g/L NaOH and 110 °C

Table B.28 Best values of k and q for 27 set of experiments

Experiment	k	q
0.5 bar, 90 °C, 1% NaOH	1.3748E-10	7.1
0.5 bar, 90 °C, 3% NaOH	3.4267E-10	7
0.5 bar, 90 °C, 5% NaOH	2.1912E-11	8.2
0.5 bar, 100 °C, 1% NaOH	1.8628E-11	8
0.5 bar, 100 °C, 3% NaOH	9.0765E-12	8.5
0.5 bar, 100 °C, 5% NaOH	6.9641E-10	7.1
0.5 bar, 110 °C, 1% NaOH	9.8345E-11	7.6
0.5 bar, 110 °C, 3% NaOH	1.5491E-08	5.9
0.5 bar, 110 °C, 5% NaOH	8.7277E-09	6.3
3.5 bar, 90 °C, 1% NaOH	6.1444E-15	11
3.5 bar, 90 °C, 3% NaOH	4.4843E-12	8.8
3.5 bar, 90 °C, 5% NaOH	4.6047E-11	8.1
3.5 bar, 100 °C, 1% NaOH	4.1129E-11	7.9
3.5 bar, 100 °C, 3% NaOH	1.3261E-10	7.7
3.5 bar, 100 °C, 5% NaOH	3.1332E-10	7.6
3.5 bar, 110 °C, 1% NaOH	9.3891E-11	7.8
3.5 bar, 110 °C, 3% NaOH	1.0984E-09	7.1
3.5 bar, 110 °C, 5% NaOH	1.3301E-08	6.3
6.5 bar, 90 °C, 1% NaOH	3.6444E-14	10.5
6.5 bar, 90 °C, 3% NaOH	5.2200E-12	8.9
6.5 bar, 90 °C, 5% NaOH	1.5250E-11	8.7
6.5 bar, 100 °C, 1% NaOH	2.9793E-13	9.9
6.5 bar, 100 °C, 3% NaOH	2.2150E-11	8.5
6.5 bar, 100 °C, 5% NaOH	2.2069E-11	8.8
6.5 bar, 110 °C, 1% NaOH	6.6297E-09	6.3
6.5 bar, 110 °C, 3% NaOH	3.9804E-09	6.7
6.5 bar, 110 °C, 5% NaOH	8.8298E-08	5.7
Mean	5.1684E-09	7.9

Table B.29 Values of k for q= 7.9

Experiment	k (q=7.9)
0.5 bar, 90 °C, 1% NaOH	1.5311E-11
0.5 bar, 90 °C, 3% NaOH	3.0535E-11
0.5 bar, 90 °C, 5% NaOH	4.8440E-11
0.5 bar, 100 °C, 1% NaOH	2.4421E-11
0.5 bar, 100 °C, 3% NaOH	4.4567E-11
0.5 bar, 100 °C, 5% NaOH	8.7970E-11
0.5 bar, 110 °C, 1% NaOH	4.4342E-11
0.5 bar, 110 °C, 3% NaOH	8.7265E-11
0.5 bar, 110 °C, 5% NaOH	1.5353E-10
3.5 bar, 90 °C, 1% NaOH	2.6303E-11
3.5 bar, 90 °C, 3% NaOH	4.8185E-11
3.5 bar, 90 °C, 5% NaOH	7.7295E-11
3.5 bar, 100 °C, 1% NaOH	4.1129E-11
3.5 bar, 100 °C, 3% NaOH	7.8887E-11
3.5 bar, 100 °C, 5% NaOH	1.4670E-10
3.5 bar, 110 °C, 1% NaOH	7.2365E-11
3.5 bar, 110 °C, 3% NaOH	1.4494E-10
3.5 bar, 110 °C, 5% NaOH	2.5711E-10
6.5 bar, 90 °C, 1% NaOH	3.7337E-11
6.5 bar, 90 °C, 3% NaOH	7.0237E-11
6.5 bar, 90 °C, 5% NaOH	1.1664E-10
6.5 bar, 100 °C, 1% NaOH	5.7206E-11
6.5 bar, 100 °C, 3% NaOH	1.0333E-10
6.5 bar, 100 °C, 5% NaOH	2.0667E-10
6.5 bar, 110 °C, 1% NaOH	1.0961E-10
6.5 bar, 110 °C, 3% NaOH	1.9945E-10
6.5 bar, 110 °C, 5% NaOH	4.4875E-10

B.2 Estimation of A, E_A, m and n

Knowing the value of k, the values of A, E_A, m and n were estimated by applying Equation B.2.

For the calculation of E_A, Equation B.2, can be written as :

$$k = k_2 \exp\left(\frac{-E_A}{RT}\right) \quad (\text{B.4})$$

where $k_2 = A[\text{OH}^-]^m P_{\text{O}_2}^n$ was assumed to be constant for a particular sodium hydroxide concentration and oxygen partial pressure. Equation B.4 can be written as

$$\ln(k) = \ln(k_2) - \frac{E_A}{RT} \quad (\text{B.5})$$

Thus, the value of E_A was estimated from a regression analysis for ln(k) versus [-1/(RT)] for the different sodium hydroxide concentrations. The average of the values obtained in this manner was 64504 J/gmol.

To get m, Equation B.4 can be written as

$$\ln(k) = \ln(k_3) + m \ln[\text{OH}^-] \quad (\text{B.6})$$

where $k_3 = A \exp[-E_A/(RT)][P_{\text{O}_2}]^n$ is a constant for a particular temperature and oxygen pressure. The average value of m obtained was 0.74.

Similarly, to get n, Equation B.4 can be written as :

$$\ln(k) = \ln(k_4) + n \ln[P_{\text{O}_2}] \quad (\text{B.7})$$

where $k_4 = A \exp[-E_A/(RT)][\text{OH}^-]^m$ is a constant for a particular temperature and alkali concentration. The average value of n obtained was 0.32.

Knowing E_{A_r} , m and n Equation B.4 can be solved for A for different sodium hydroxide concentrations and temperatures. The average value of A obtained was 0.3.

APPENDIX C

CARBOHYDRATE DEGRADATION KINETICS CALCULATION

PROCEDURE

C.1 Estimation of Rate Constant k_1 and k_2

The general equation for two stage zero order power law model for carbohydrate degradation kinetics as viscosity is

$$-\frac{d\eta}{dt} = k_1(u(t) - u(t-10)) + k_2u(t-10) \quad (C.1)$$

$$k_1 = A_1 \exp\left[\frac{-E_{A1}}{RT}\right] [\text{OH}^-]^a [\text{PO}_2]^b \quad (C.2)$$

$$k_2 = A_2 \exp\left[\frac{-E_{A2}}{RT}\right] [\text{OH}^-]^c [\text{PO}_2]^d \quad (C.3)$$

where $u(t)$ is the unity function which was used to imply that in the first 10 min of reaction time, the kinetic equation was described by the first term and during the rest of the reaction time was described by the second term. Thus, the constants A_1 , E_{A1} , a , b , A_2 , E_{A2} , c and d are calculated separately for each stage by integral method of analysis. For the first 10 minute stage a zero order power model is

$$-\frac{d\eta}{dt} = k_1 \quad (C.4)$$

Integrating between $\eta = \eta_0$ at $t=0$ min and $t=10$, the equation is obtained as

$$y = \eta_0 - \eta = k_1 t \quad (C.5)$$

The plot of y with respect to time is a linear line passing through zero with slope k_1 . Also for the second stage of Equation C.1 the same procedure is applied. The zero order power model for the second stage is

$$-\frac{d\eta}{dt} = k_2 \quad (C.6)$$

Integrating between $\eta = \eta_{10}$ at $t=10$ min and t , the equation is obtained as

$$y = \eta_{10} - \eta = k_2 (t - 10) \quad (C.7)$$

Thus, the slope of the plot y with respect to time gives the k_2 . The calculations of k_1 and k_2 for each experiment is presented in Table C.1 through C.54. Figures C.1 through C.54 plot the data graphically. Table C.55 summarizes the k_1 and k_2 values for the 27 set of experiments.

Table C.1 Value of k_1 0.5 bar, 0.05 g/L NaOH and 90 °C experiment

Time (min)	Intrinsic Viscosity (dL/g)	$\eta_0 - \eta$
0	8.50	0.00
5	8.40	0.10
10	8.31	0.19

Table C.2 Value of k_2 0.5 bar, 0.05 g/L NaOH and 90 °C experiment

Time (min)	Intrinsic Viscosity (dL/g)	$\eta_{10} - \eta$
0	8.31	0.00
20	8.14	0.17
50	7.85	0.46

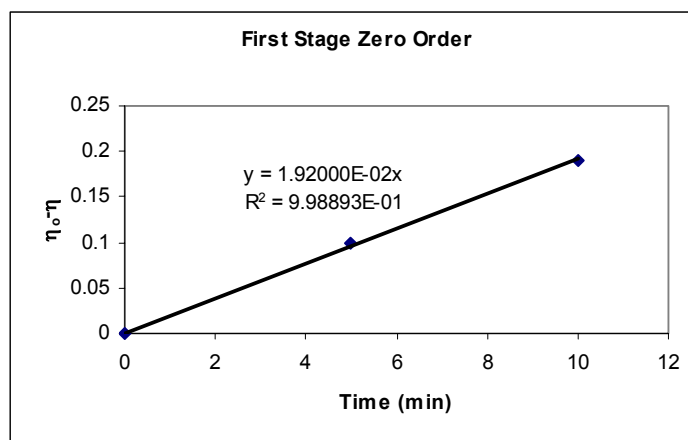


Figure C.1 Value of k_1 for 0.5 bar, 0.05 g/L NaOH and 90 °C experiment

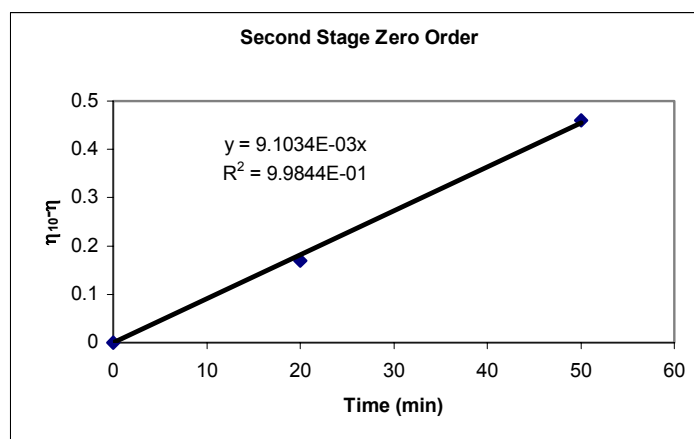


Figure C.2 Value of k_2 for 0.5 bar, 0.05 g/L NaOH and 90 °C experiment

Table C.3 Value of k_1 for 0.5 bar, 0.15 g/L NaOH and 90 °C experiment

Time (min)	Intrinsic Viscosity (dL/g)	$\eta_0 - \eta$
0	8.48	0.00
5	8.34	0.14
10	8.22	0.26

Table C.4 Value of k_2 for 0.5 bar, 0.15 g/L NaOH and 90 °C experiment

Time (min)	Intrinsic Viscosity (dL/g)	$\eta_{10} - \eta$
0	8.22	0.00
20	8.02	0.20
50	7.75	0.47

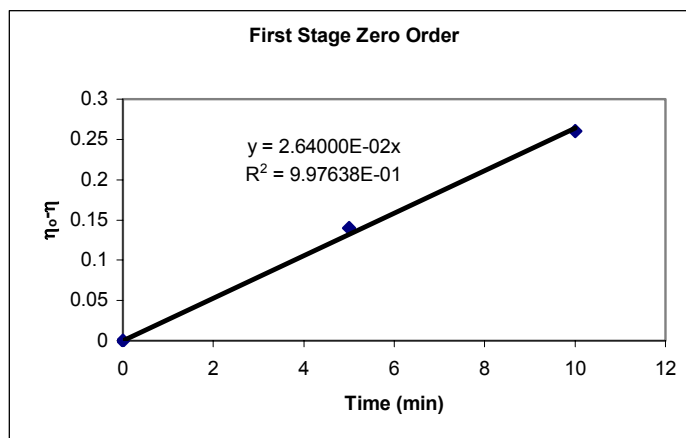


Figure C.3 Value of k_1 for 0.5 bar, 0.15 g/L NaOH and 90 °C experiment

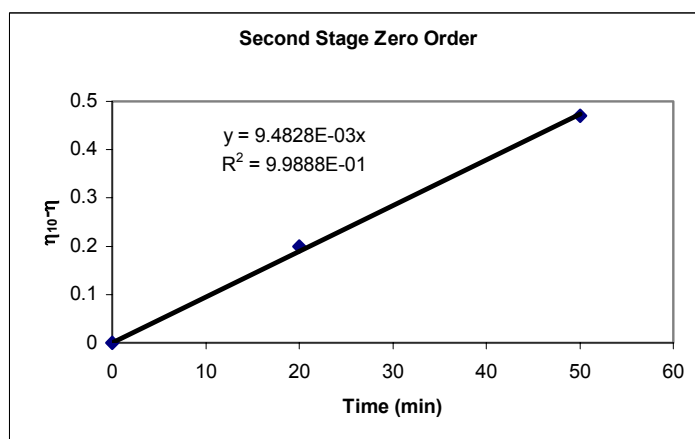


Figure C.4 Value of k_2 for 0.5 bar, 0.15 g/L NaOH and 90 °C experiment

Table C.5 Value of k_1 for 0.5 bar, 0.25 g/L NaOH and 90 °C experiment

Time (min)	Intrinsic Viscosity (dL/g)	$\eta_0 - \eta$
0	8.48	0.00
5	8.35	0.13
10	8.19	0.29

Table C.6 Value of k_2 for 0.5 bar, 0.25 g/L NaOH and 90 °C experiment

Time (min)	Intrinsic Viscosity (dL/g)	$\eta_{10} - \eta$
0	8.19	0.00
20	7.94	0.25
50	7.63	0.56

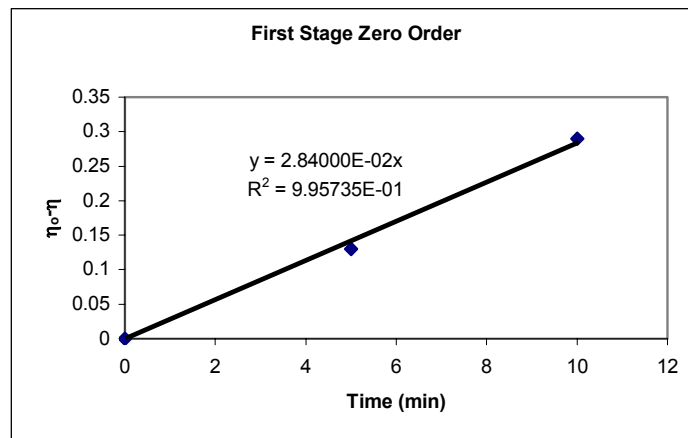


Figure C.5 Value of k_1 for 0.5 bar, 0.25 g/L NaOH and 90 °C experiment

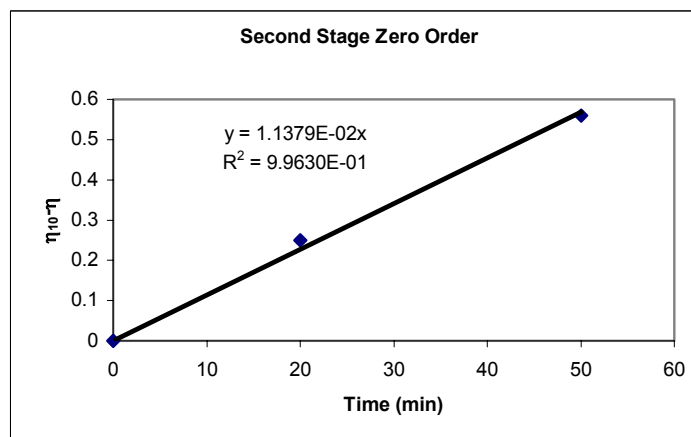


Figure C.6 Value of k_2 for 0.5 bar, 0.25 g/L NaOH and 90 °C experiment

Table C.7 Value of k_1 for 0.5 bar, 0.05 g/L NaOH and 100 °C experiment

Time (min)	Intrinsic Viscosity (dL/g)	$\eta_0 - \eta$
0	8.48	0
5	8.38	0.1
10	8.26	0.2

Table C.8 Value of k_2 for 0.5 bar, 0.05 g/L NaOH and 100 °C experiment

Time (min)	Intrinsic Viscosity (dL/g)	$\eta_{10} - \eta$
0	8.26	0
20	8.09	0.17
50	7.72	0.54

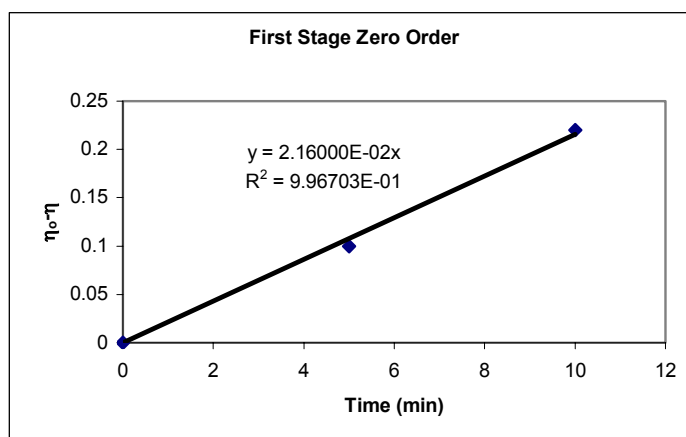


Figure C.7 Value of k_1 for 0.5 bar, 0.05 g/L NaOH and 100 °C experiment

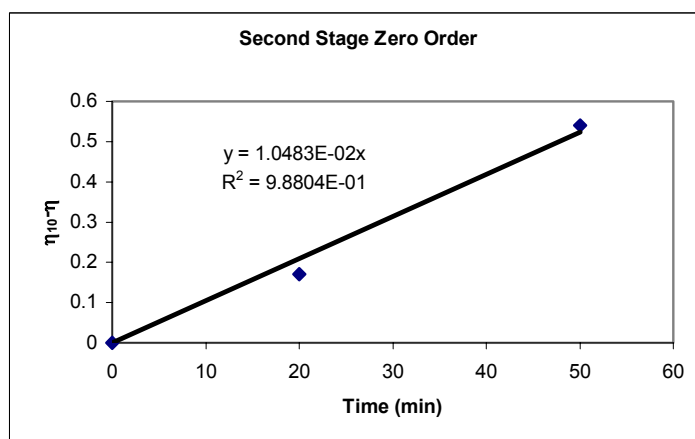


Figure C.8 Value of k_2 for 0.5 bar, 0.05 g/L NaOH and 100 °C experiment

Table C.9 Value of k_1 for 0.5 bar, 0.15 g/L NaOH and 100 °C experiment

Time (min)	Intrinsic Viscosity (dL/g)	$\eta_0 - \eta$
0	8.47	0
5	8.35	0.1
10	8.17	0.3

Table C.10 Value of k_2 for 0.5 bar, 0.15 g/L NaOH and 100 °C experiment

Time (min)	Intrinsic Viscosity (dL/g)	$\eta_{10} - \eta$
0	8.17	0
20	8.01	0.16
50	7.55	0.62

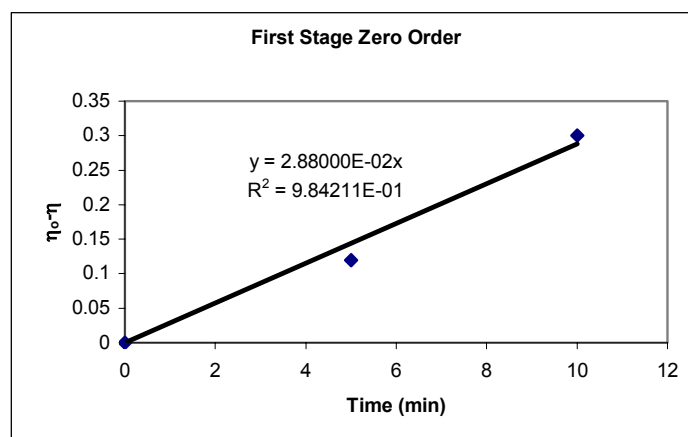


Figure C.9 Value of k_1 for 0.5 bar, 0.15 g/L NaOH and 100 °C experiment

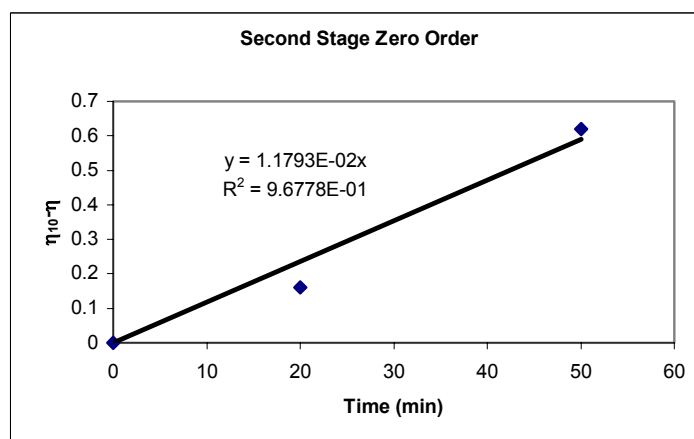


Figure C.10 Value of k_2 for 0.5 bar, 0.15 g/L NaOH and 100 °C experiment

Table C.11 Value of k_1 for 0.5 bar, 0.25 g/L NaOH and 100 °C experiment

Time (min)	Intrinsic Viscosity (dL/g)	$\eta_0 - \eta$
0	8.46	0.00
5	8.31	0.15
10	8.10	0.36

Table C.12 Value of k_2 for 0.5 bar, 0.25 g/L NaOH and 100 °C experiment

Time (min)	Intrinsic Viscosity (dL/g)	$\eta_{10} - \eta$
0	8.10	0.00
20	7.79	0.31
50	7.50	0.60

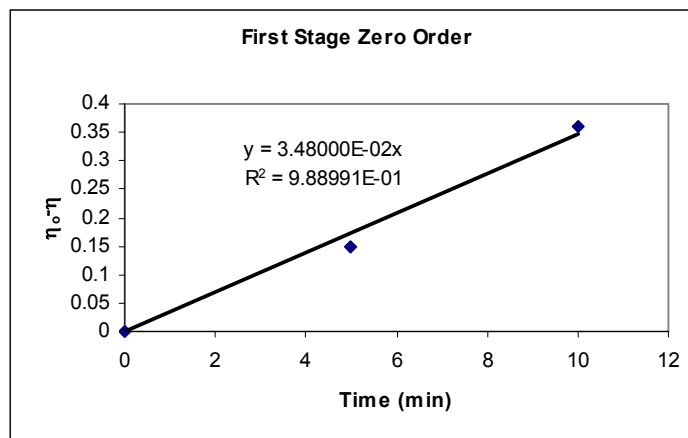


Figure C.11 Value of k_1 for 0.5 bar, 0.25 g/L NaOH and 100 °C experiment

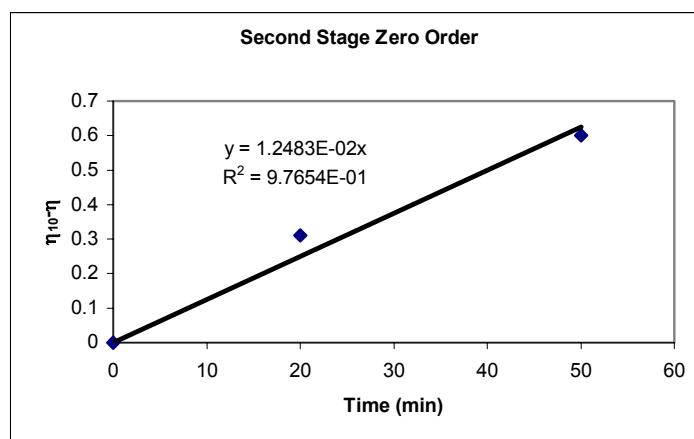


Figure C.12 Value of k_2 for 0.5 bar, 0.25 g/L NaOH and 100 °C experiment

Table C.13 Value of k_1 for 0.5 bar, 0.05 g/L NaOH and 110 °C experiment

Time (min)	Intrinsic Viscosity (dL/g)	$\eta_0 - \eta$
0	8.46	0.00
5	8.35	0.11
10	8.20	0.26

Table C.14 Value of k_2 for 0.5 bar, 0.05 g/L NaOH and 110 °C experiment

Time (min)	Intrinsic Viscosity (dL/g)	$\eta_{10} - \eta$
0	8.20	0.00
20	7.98	0.22
50	7.67	0.53

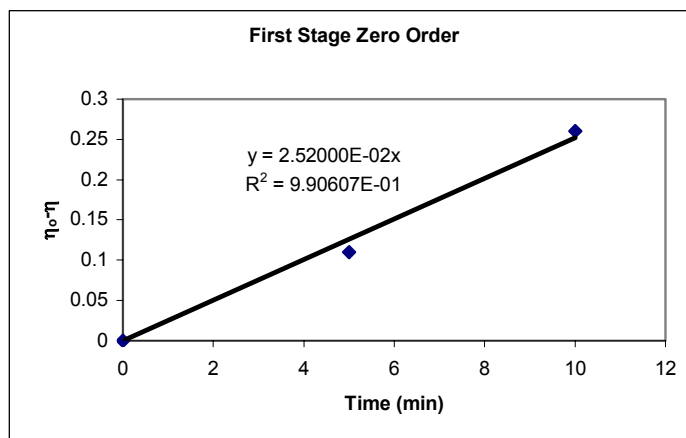


Figure C.13 Value of k_1 for 0.5 bar, 0.05 g/L NaOH and 110 °C experiment

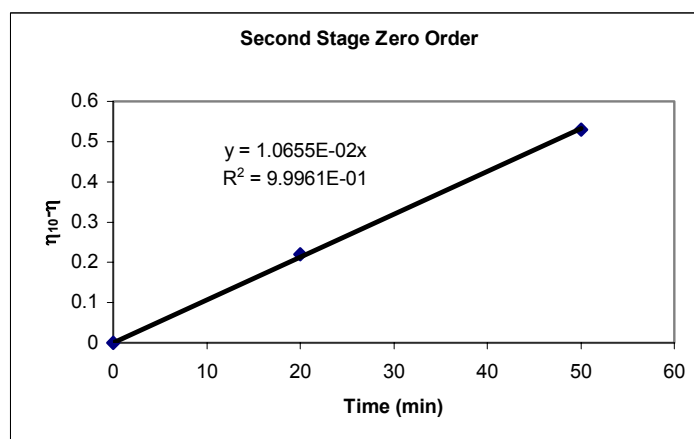


Figure C.14 Value of k_2 for 0.5 bar, 0.05 g/L NaOH and 110 °C experiment

Table C.15 Value of k_1 for 0.5 bar, 0.15 g/L NaOH and 110 °C experiment

Time (min)	Intrinsic Viscosity (dL/g)	$\eta_0 - \eta$
0	8.45	0.00
5	8.29	0.16
10	8.11	0.34

Table C.16 Value of k_2 for 0.5 bar, 0.15 g/L NaOH and 110 °C experiment

Time (min)	Intrinsic Viscosity (dL/g)	$\eta_{10} - \eta$
0	8.11	0.00
20	7.80	0.31
50	7.49	0.62

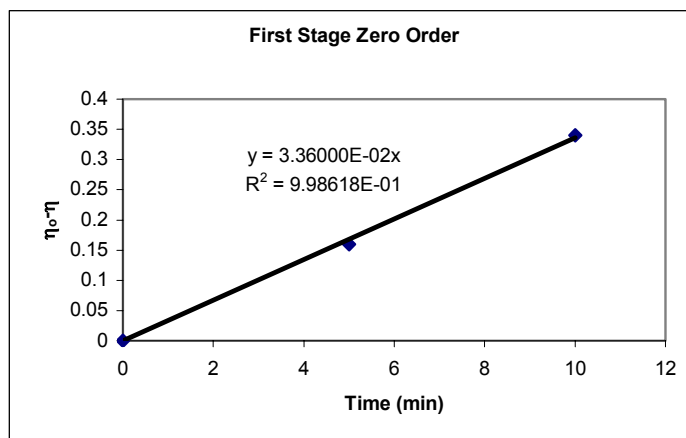


Figure C.15 Value of k_1 for 0.5 bar, 0.15 g/L NaOH and 110 °C experiment

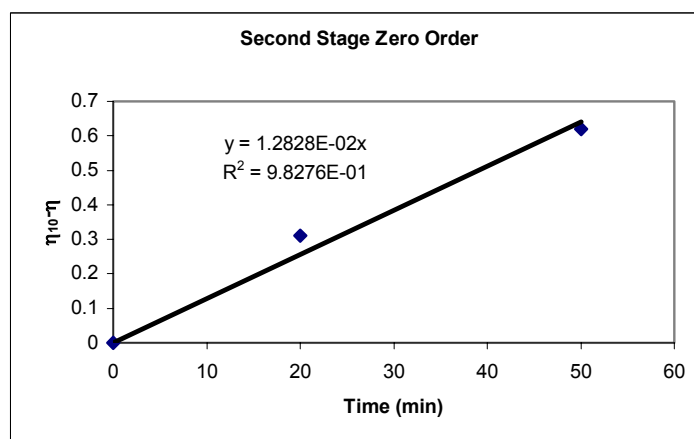


Figure C.16 Value of k_2 for 0.5 bar, 0.15 g/L NaOH and 110 °C experiment

Table C.17 Value of k_1 for 0.5 bar, 0.25 g/L NaOH and 110 °C experiment

Time (min)	Intrinsic Viscosity (dL/g)	$\eta_0 - \eta$
0	8.43	0.00
5	8.21	0.22
10	8.02	0.41

Table C.18 Value of k_2 for 0.5 bar, 0.25 g/L NaOH and 110 °C experiment

Time (min)	Intrinsic Viscosity (dL/g)	$\eta_{10} - \eta$
0	8.02	0.00
20	7.73	0.29
50	7.35	0.67

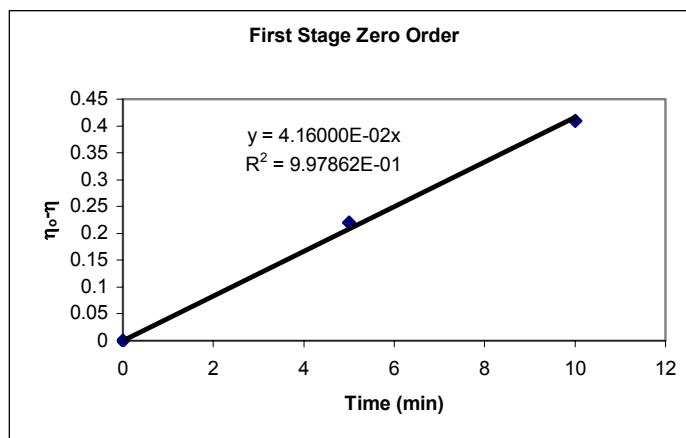


Figure C.17 Value of k_1 for 0.5 bar, 0.25 g/L NaOH and 110 °C experiment

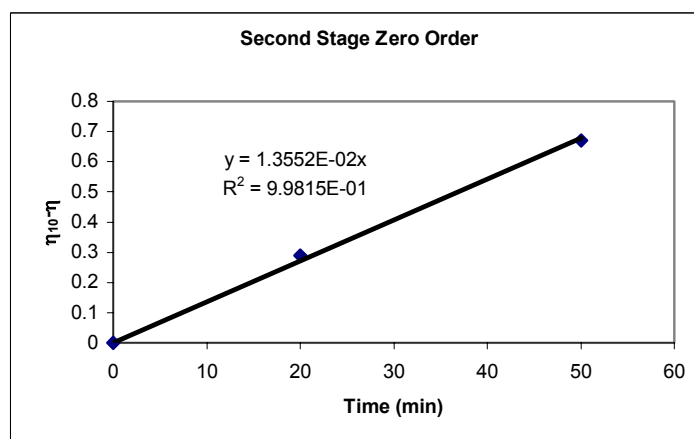


Figure C.18 Value of k_2 for 0.5 bar, 0.25 g/L NaOH and 110 °C experiment

Table C.19 Value of k_1 for 3.5 bar, 0.05 g/L NaOH and 90 °C experiment

Time (min)	Intrinsic Viscosity (dL/g)	$\eta_0 - \eta$
0	8.49	0
5	8.34	0.15
10	8.2	0.29

Table C.20 Value of k_2 for 3.5 bar, 0.05 g/L NaOH and 90 °C experiment

Time (min)	Intrinsic Viscosity (dL/g)	$\eta_{10} - \eta$
0	8.2	0.00
20	7.95	0.25
50	7.66	0.54

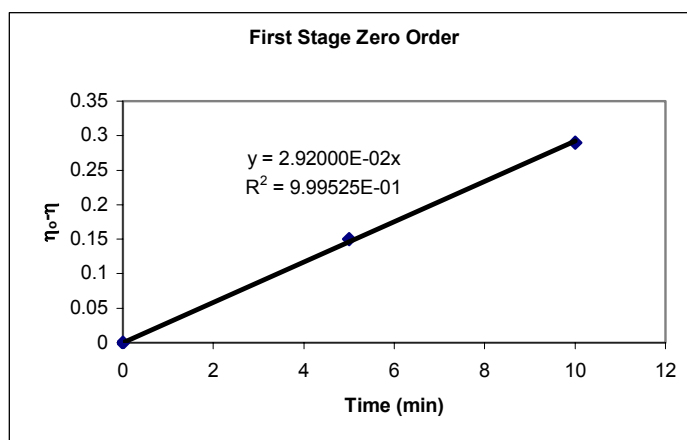


Figure C.19 Value of k_1 for 3.5 bar, 0.05 g/L NaOH and 90 °C experiment

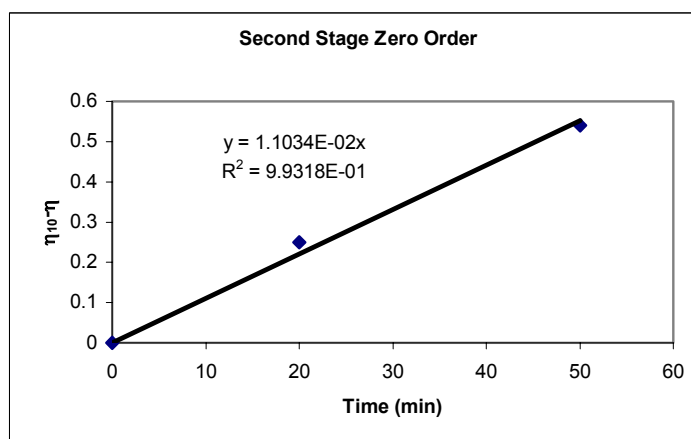


Figure C.20 Value of k_2 for 3.5 bar, 0.05 g/L NaOH and 90 °C experiment

Table C.21 Value of k_1 for 3.5 bar, 0.15 g/L NaOH and 90 °C experiment

Time (min)	Intrinsic Viscosity (dL/g)	$\eta_0 - \eta$
0	8.46	0.00
5	8.27	0.19
10	8.08	0.38

Table C.22 Value of k_2 for 3.5 bar, 0.15 g/L NaOH and 90 °C experiment

Time (min)	Intrinsic Viscosity (dL/g)	$\eta_{10} - \eta$
0	8.08	0.00
20	7.83	0.25
50	7.35	0.73

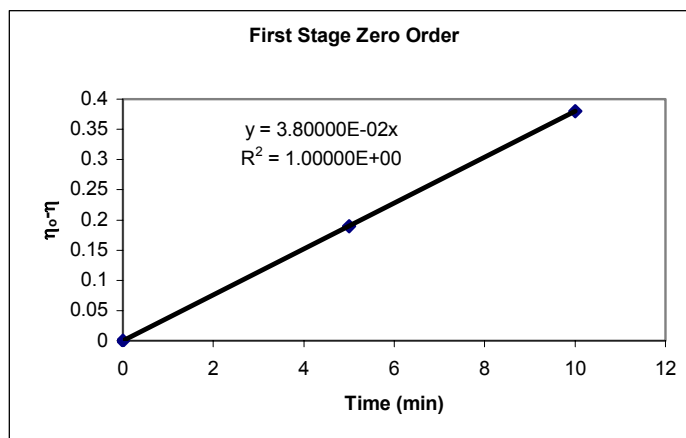


Figure C.21 Value of k_1 for 3.5 bar, 0.15 g/L NaOH and 90 °C experiment

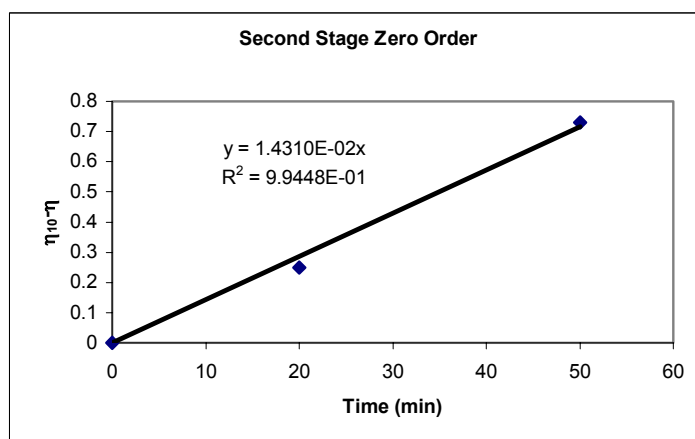


Figure C.22 Value of k_2 for 3.5 bar, 0.15 g/L NaOH and 90 °C experiment

Table C.23 Value of k_1 for 3.5 bar, 0.25 g/L NaOH and 90 °C experiment

Time (min)	Intrinsic Viscosity (dL/g)	$\eta_0 - \eta$
0	8.46	0.00
5	8.29	0.17
10	7.97	0.49

Table C.24 Value of k_2 for 3.5 bar, 0.25 g/L NaOH and 90 °C experiment

Time (min)	Intrinsic Viscosity (dL/g)	$\eta_{10} - \eta$
0	7.97	0.00
20	7.71	0.26
50	7.24	0.73

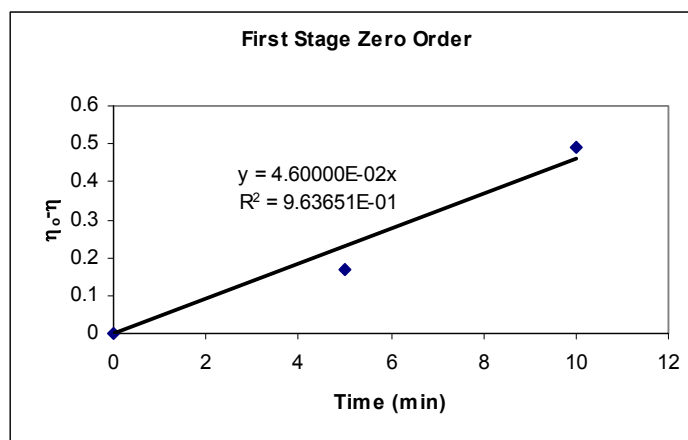


Figure C.23 Value of k_1 for 3.5 bar, 0.25 g/L NaOH and 90 °C experiment

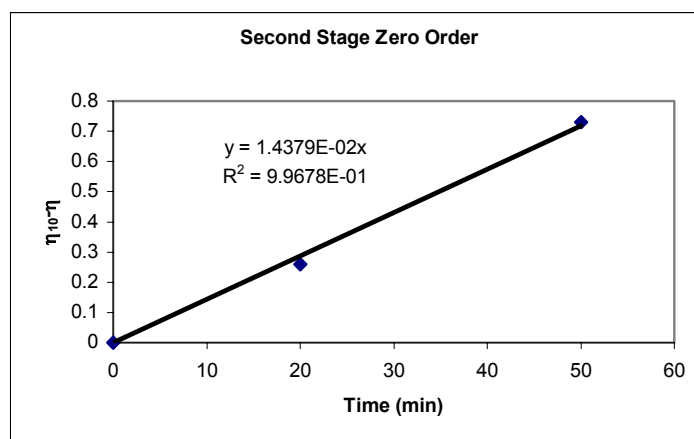


Figure C.24 Value of k_2 for 3.5 bar, 0.25 g/L NaOH and 90 °C experiment

Table C.25 Value of k_1 for 3.5 bar, 0.05 g/L NaOH and 100 °C experiment

Time (min)	Intrinsic Viscosity (dL/g)	$\eta_0 - \eta$
0	8.46	0.00
5	8.29	0.17
10	8.1	0.36

Table C.26 Value of k_2 for 3.5 bar, 0.05 g/L NaOH and 100 °C experiment

Time (min)	Intrinsic Viscosity (dL/g)	$\eta_{10} - \eta$
0	8.1	0.00
20	7.85	0.25
50	7.56	0.54

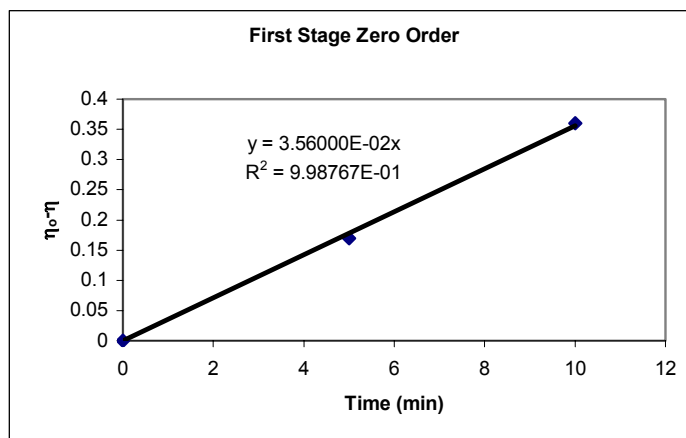


Figure C.25 Value of k_1 for 3.5 bar, 0.05 g/L NaOH and 100 °C experiment

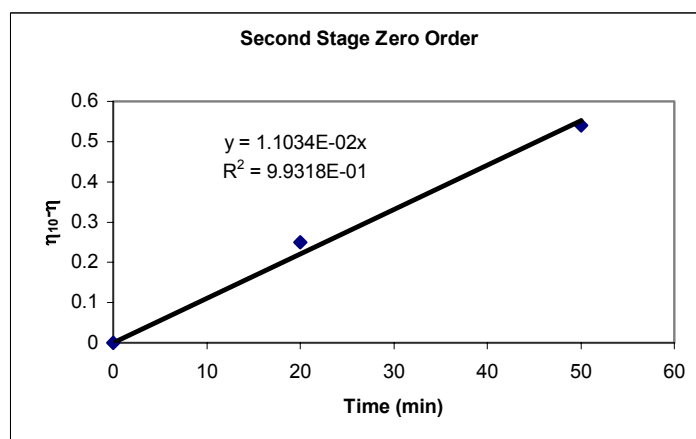


Figure C.26 Value of k_2 for 3.5 bar, 0.05 g/L NaOH and 100 °C experiment

Table C.27 Value of k_1 for 3.5 bar, 0.15 g/L NaOH and 100 °C experiment

Time (min)	Intrinsic Viscosity (dL/g)	$\eta_0 - \eta$
0	8.45	0.00
5	8.3	0.15
10	7.95	0.50

Table C.28 Value of k_2 for 3.5 bar, 0.15 g/L NaOH and 100 °C experiment

Time (min)	Intrinsic Viscosity (dL/g)	$\eta_{10} - \eta$
0	7.95	0.00
20	7.67	0.28
50	7.29	0.66

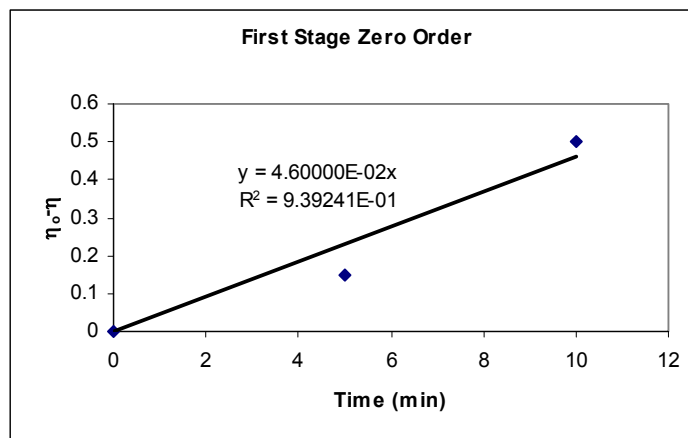


Figure C.27 Value of k_1 for 3.5 bar, 0.15 g/L NaOH and 100 °C experiment

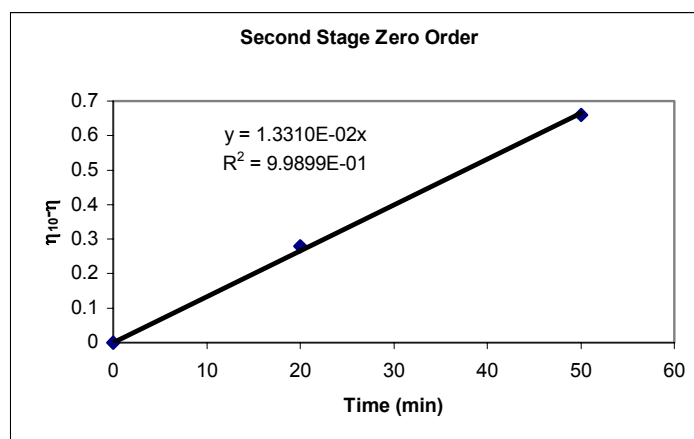


Figure C.28 Value of k_2 for 3.5 bar, 0.15 g/L NaOH and 100 °C experiment

Table C.29 Value of k_1 for 3.5 bar, 0.25 g/L NaOH and 100 °C experiment

Time (min)	Intrinsic Viscosity (dL/g)	$\eta_0 - \eta$
0	8.45	0.00
5	8.19	0.26
10	7.91	0.54

Table C.30 Value of k_2 for 3.5 bar, 0.25 g/L NaOH and 100 °C experiment

Time (min)	Intrinsic Viscosity (dL/g)	$\eta_{10} - \eta$
0	7.91	0.00
20	7.56	0.35
50	7.07	0.84

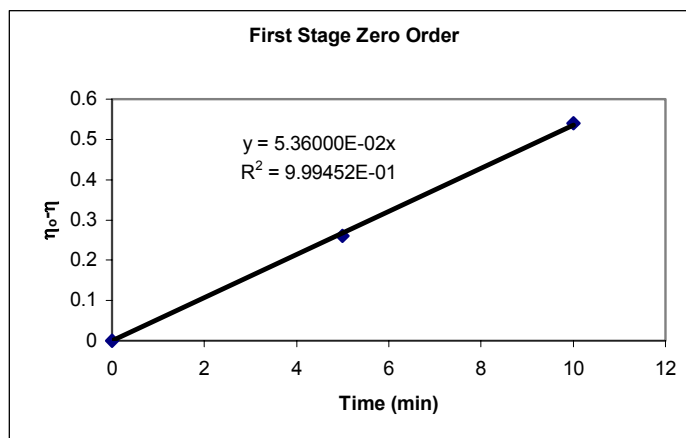


Figure C.29 Value of k_1 for 3.5 bar, 0.25 g/L NaOH and 100 °C experiment

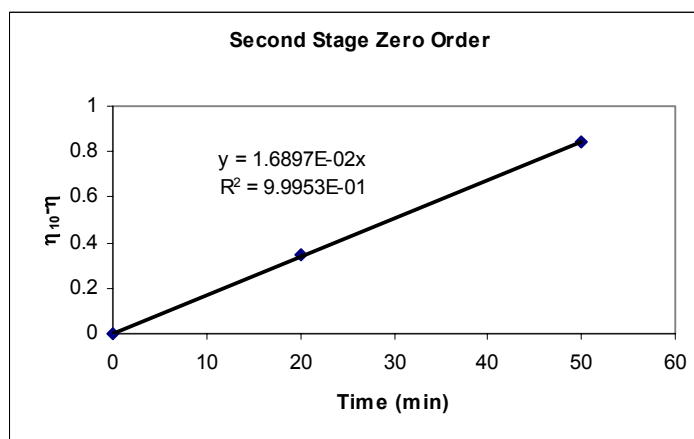


Figure C.30 Value of k_2 for 3.5 bar, 0.25 g/L NaOH and 100 °C experiment

Table C.31 Value of k_1 for 3.5 bar, 0.05 g/L NaOH and 110 °C experiment

Time (min)	Intrinsic Viscosity (dL/g)	$\eta_0 - \eta$
0	8.44	0.00
5	8.24	0.20
10	8	0.44

Table C.32 Value of k_2 for 3.5 bar, 0.05 g/L NaOH and 110 °C experiment

Time (min)	Intrinsic Viscosity (dL/g)	$\eta_{10} - \eta$
0	8	0.00
20	7.77	0.23
50	7.32	0.68

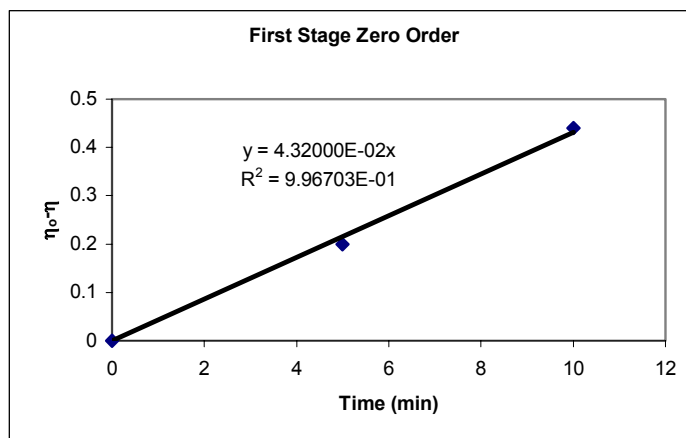


Figure C.31 Value of k_1 for 3.5 bar, 0.05 g/L NaOH and 110 °C experiment

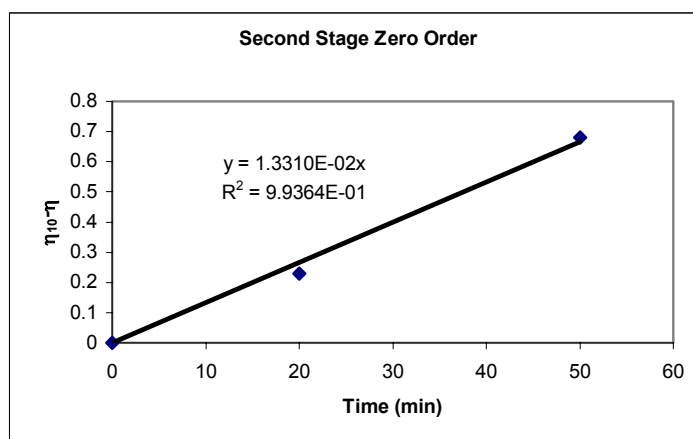


Figure C.32 Value of k_2 for 3.5 bar, 0.05 g/L NaOH and 110 °C experiment

Table C.33 Value of k_1 for 3.5 bar, 0.15 g/L NaOH and 110 °C experiment

Time (min)	Intrinsic Viscosity (dL/g)	$\eta_0 - \eta$
0	8.43	0.00
5	8.15	0.28
10	7.86	0.57

Table C.34 Value of k_2 for 3.5 bar, 0.15 g/L NaOH and 110 °C experiment

Time (min)	Intrinsic Viscosity (dL/g)	$\eta_{10} - \eta$
0	7.86	0.00
20	7.54	0.32
50	7.11	0.75

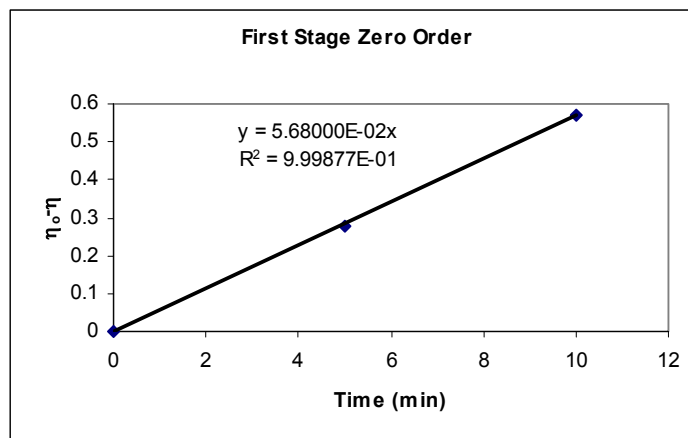


Figure C.33 Value of k_1 for 3.5 bar, 0.15 g/L NaOH and 110 °C experiment

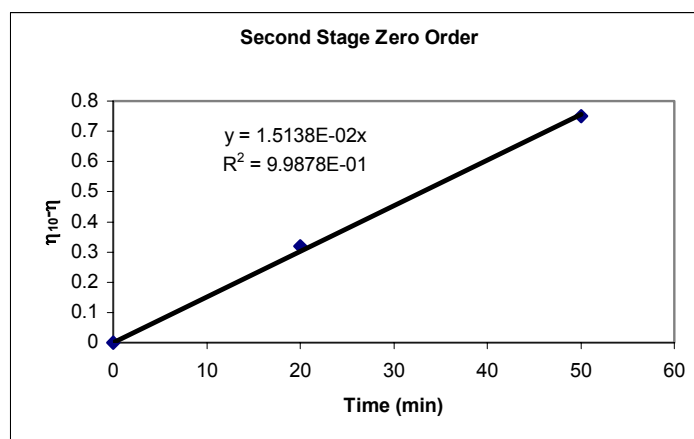


Figure C.34 Value of k_2 for 3.5 bar, 0.15 g/L NaOH and 110 °C experiment

Table C.35 Value of k_1 for 3.5 bar, 0.25 g/L NaOH and 110 °C experiment

Time (min)	Intrinsic Viscosity (dL/g)	$\eta_0 - \eta$
0	8.41	0
5	8.12	0.29
10	7.79	0.62

Table C.36 Value of k_2 for 3.5 bar, 0.25 g/L NaOH and 110 °C experiment

Time (min)	Intrinsic Viscosity (dL/g)	$\eta_{10} - \eta$
0	7.79	0.00
20	7.4	0.39
50	6.87	0.92

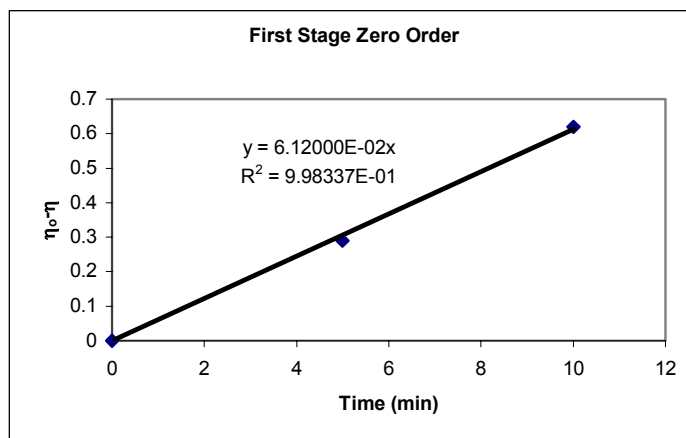


Figure C.35 Value of k_1 for 3.5 bar, 0.25 g/L NaOH and 110 °C experiment

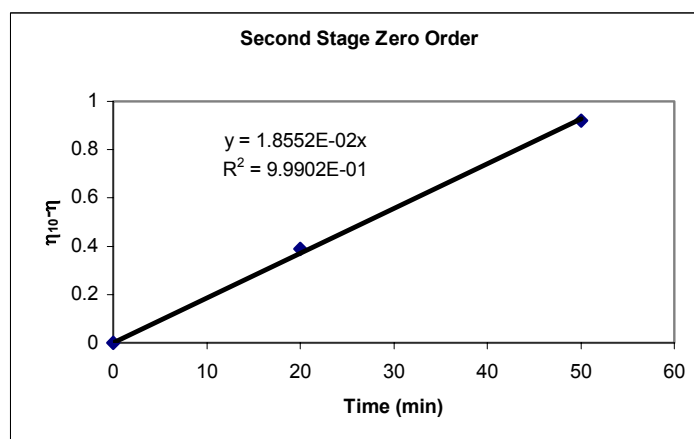


Figure C.36 Value of k_2 for 3.5 bar, 0.25 g/L NaOH and 110 °C experiment

Table C.37 Value of k_1 for 6.5 bar, 0.05 g/L NaOH and 90 °C experiment

Time (min)	Intrinsic Viscosity (dL/g)	$\eta_0 - \eta$
0	8.49	0.00
5	8.31	0.18
10	8.12	0.37

Table C.38 Value of k_2 for 6.5 bar, 0.05 g/L NaOH and 90 °C experiment

Time (min)	Intrinsic Viscosity (dL/g)	$\eta_{10} - \eta$
0	8.12	0.00
20	7.88	0.24
50	7.49	0.63

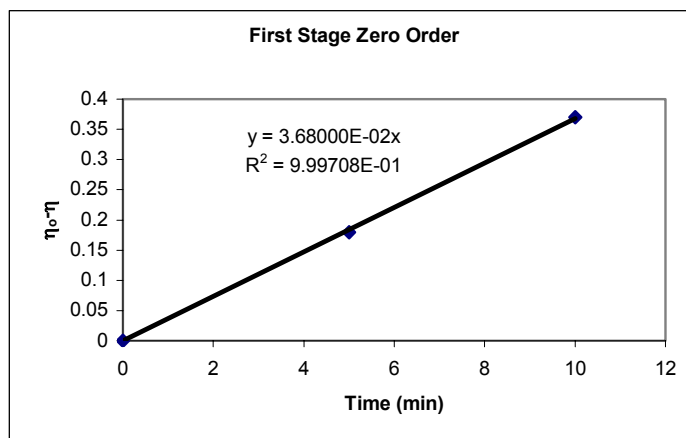


Figure C.37 Value of k_1 for 6.5 bar, 0.05 g/L NaOH and 90 °C experiment

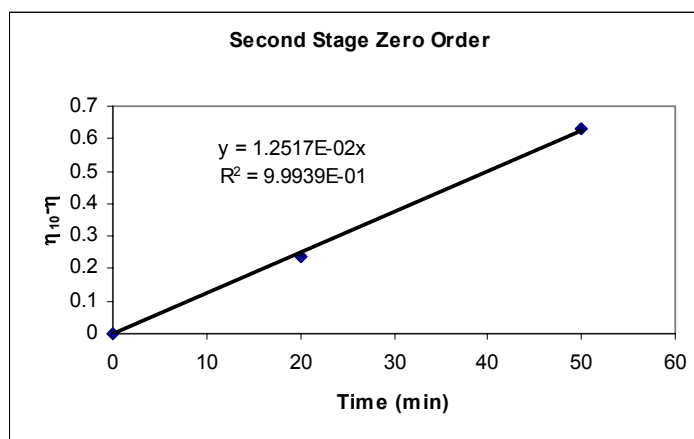


Figure C.38 Value of k_2 for 6.5 bar, 0.05 g/L NaOH and 90 °C experiment

Table C.39 Value of k_1 for 6.5 bar, 0.15 g/L NaOH and 90 °C experiment

Time (min)	Intrinsic Viscosity (dL/g)	$\eta_0 - \eta$
0	8.45	0.00
5	8.23	0.22
10	7.95	0.50

Table C.40 Value of k_2 for 6.5 bar, 0.15 g/L NaOH and 90 °C experiment

Time (min)	Intrinsic Viscosity (dL/g)	$\eta_{10} - \eta$
0	7.95	0.00
20	7.65	0.30
50	7.22	0.73

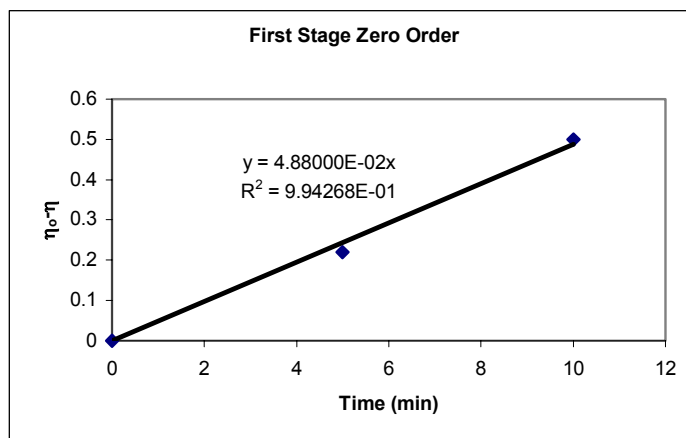


Figure C.39 Value of k_1 for 6.5 bar, 0.15 g/L NaOH and 90 °C experiment

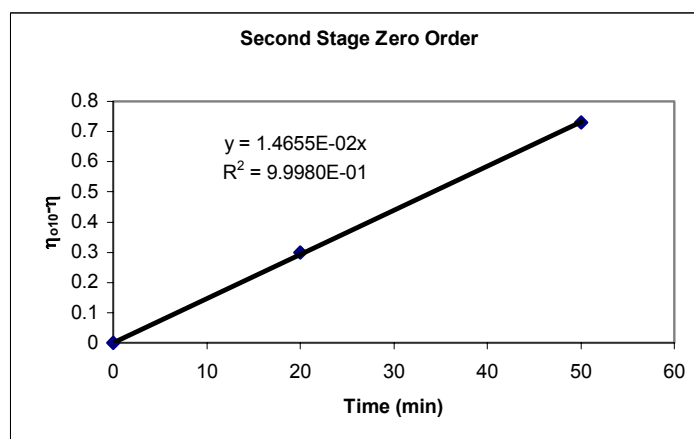


Figure C.40 Value of k_2 for 6.5 bar, 0.15 g/L NaOH and 90 °C experiment

Table C.41 Value of k_1 for 6.5 bar, 0.25 g/L NaOH and 90 °C experiment

Time (min)	Intrinsic Viscosity (dL/g)	$\eta_0 - \eta$
0	8.46	0.00
5	8.25	0.21
10	7.9	0.56

Table C.42 Value of k_2 for 6.5 bar, 0.25 g/L NaOH and 90 °C experiment

Time (min)	Intrinsic Viscosity (dL/g)	$\eta_{10} - \eta$
0	7.9	0.00
20	7.55	0.35
50	7.05	0.85

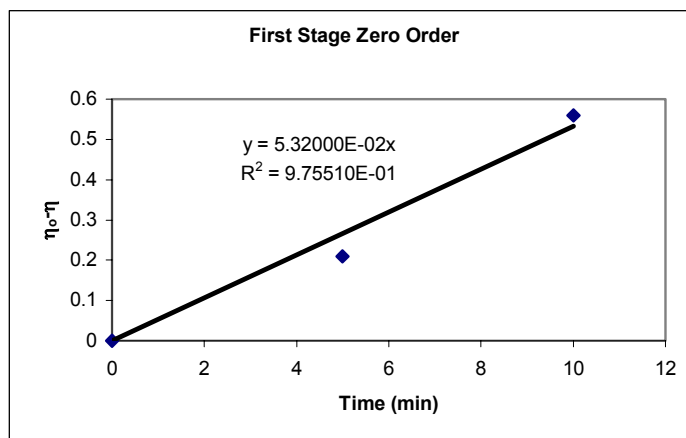


Figure C.41 Value of k_1 for 6.5 bar, 0.25 g/L NaOH and 90 °C experiment

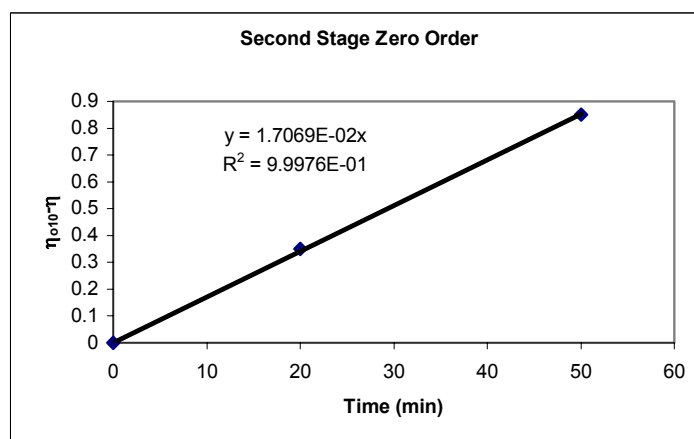


Figure C.42 Value of k_2 for 6.5 bar, 0.25 g/L NaOH and 90 °C experiment

Table C.43 Value of k_1 for 6.5 bar, 0.05 g/L NaOH and 100 °C experiment

Time (min)	Intrinsic Viscosity (dL/g)	$\eta_0 - \eta$
0	8.45	0.00
5	8.25	0.20
10	8.01	0.44

Table C.44 Value of k_2 for 6.5 bar, 0.05 g/L NaOH and 100 °C experiment

Time (min)	Intrinsic Viscosity (dL/g)	$\eta_{10} - \eta$
0	8.01	0.00
20	7.75	0.26
50	7.38	0.63

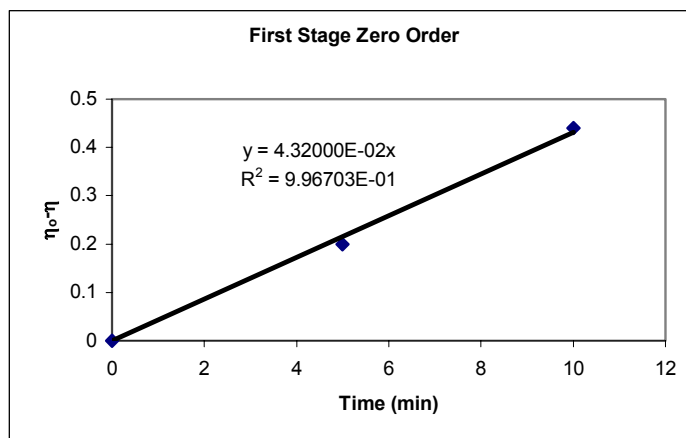


Figure C.43 Value of k_1 for 6.5 bar, 0.05 g/L NaOH and 100 °C experiment

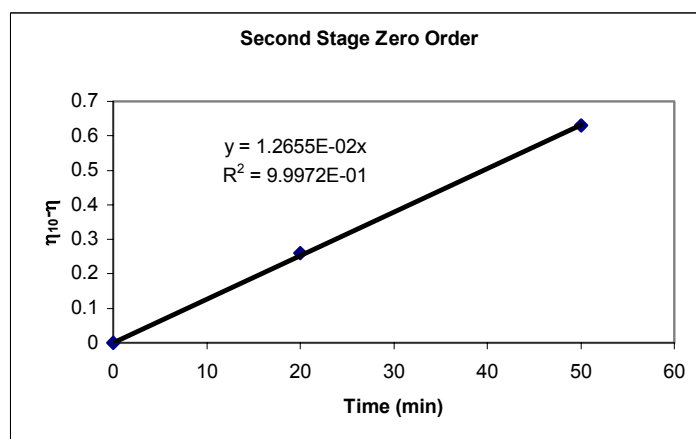


Figure C.44 Value of k_2 for 6.5 bar, 0.05 g/L NaOH and 100 °C experiment

Table C.45 Value of k_1 for 6.5 bar, 0.15 g/L NaOH and 100 °C experiment

Time (min)	Intrinsic Viscosity (dL/g)	$\eta_0 - \eta$
0	8.45	0.00
5	8.18	0.27
10	7.9	0.55

Table C.46 Value of k_2 for 6.5 bar, 0.15 g/L NaOH and 100 °C experiment

Time (min)	Intrinsic Viscosity (dL/g)	$\eta_{10} - \eta$
0	7.9	0.00
20	7.56	0.34
50	7.08	0.82

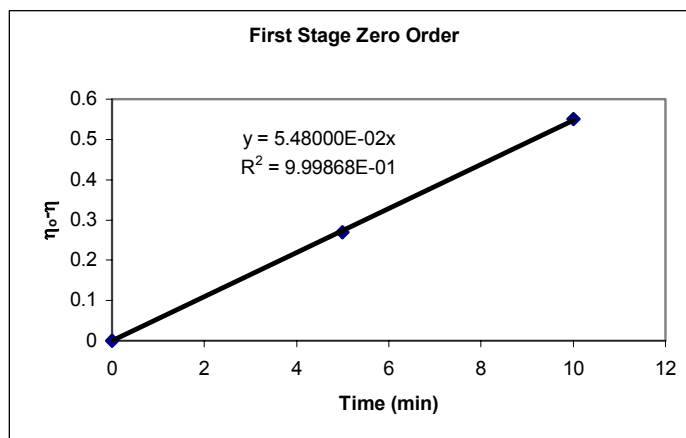


Figure C.45 Value of k_1 for 6.5 bar, 0.15 g/L NaOH and 100 °C experiment

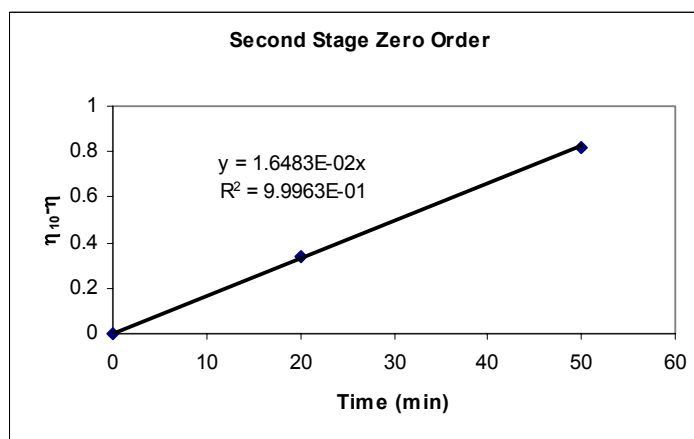


Figure C.46 Value of k_2 for 6.5 bar, 0.15 g/L NaOH and 100 °C experiment

Table C.47 Value of k_1 for 6.5 bar, 0.25 g/L NaOH and 100 °C experiment

Time (min)	Intrinsic Viscosity (dL/g)	$\eta_0 - \eta$
0	8.44	0.00
5	8.12	0.32
10	7.79	0.65

Table C.48 Value of k_2 for 6.5 bar, 0.25 g/L NaOH and 100 °C experiment

Time (min)	Intrinsic Viscosity (dL/g)	$\eta_{10} - \eta$
0	7.79	0.00
20	7.43	0.36
50	6.87	0.92

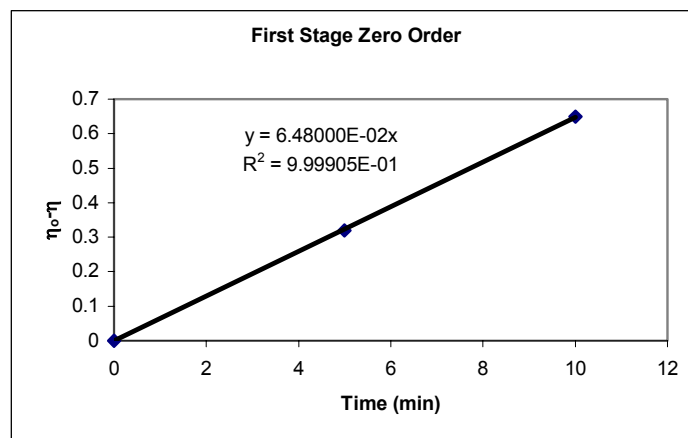


Figure C.47 Value of k_1 for 6.5 bar, 0.25 g/L NaOH and 100 °C experiment

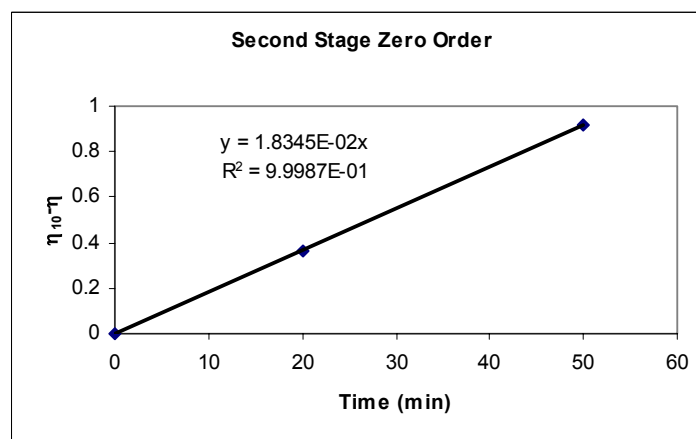


Figure C.48 Value of k_2 for 6.5 bar, 0.25 g/L NaOH and 100 °C experiment

Table C.49 Value of k_1 for 6.5 bar, 0.05 g/L NaOH and 110 °C experiment

Time (min)	Intrinsic Viscosity (dL/g)	$\eta_0 - \eta$
0	8.44	0.00
5	8.2	0.24
10	7.94	0.50

Table C.50 Value of k_2 for 6.5 bar, 0.05 g/L NaOH and 110 °C experiment

Time (min)	Intrinsic Viscosity (dL/g)	$\eta_{10} - \eta$
0	7.94	0.00
20	7.65	0.29
50	7.19	0.75

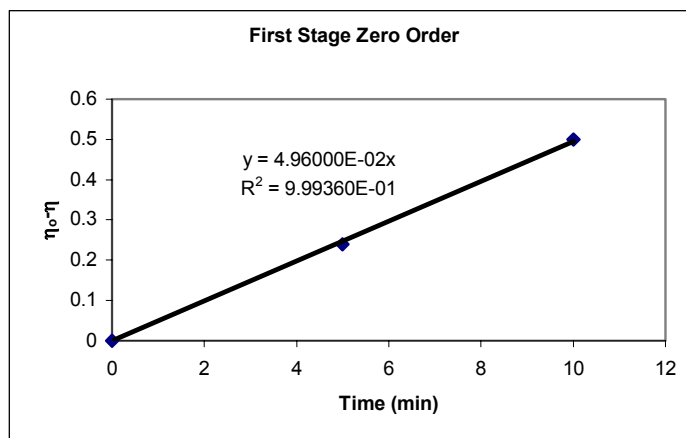


Figure C.49 Value of k_1 for 6.5 bar, 0.05 g/L NaOH and 110 °C experiment

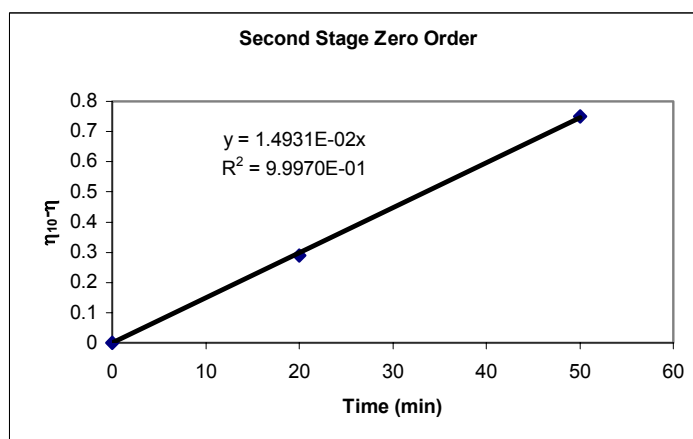


Figure C.50 Value of k_2 for 6.5 bar, 0.05 g/L NaOH and 110 °C experiment

Table C.51 Value of k_1 for 6.5 bar, 0.15 g/L NaOH and 110 °C experiment

Time (min)	Intrinsic Viscosity (dL/g)	$\eta_0 - \eta$
0	8.42	0.00
5	8.09	0.33
10	7.76	0.66

Table C.52 Value of k_2 for 6.5 bar, 0.15 g/L NaOH and 110 °C experiment

Time (min)	Intrinsic Viscosity (dL/g)	$\eta_{10} - \eta$
0	7.76	0.00
20	7.38	0.38
50	6.85	0.91

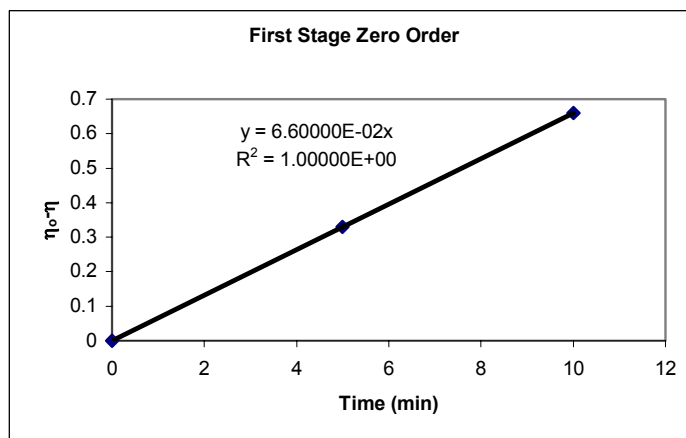


Figure C.51 Value of k_1 for 6.5 bar, 0.15 g/L NaOH and 110 °C experiment

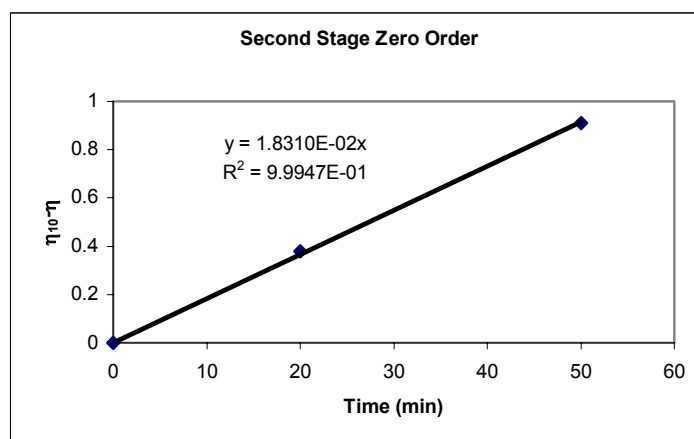


Figure C.52 Value of k_2 for 6.5 bar, 0.15 g/L NaOH and 110 °C experiment

Table C.53 Value of k_1 for 6.5 bar, 0.25 g/L NaOH and 110 °C experiment

Time (min)	Intrinsic Viscosity (dL/g)	$\eta_0 - \eta$
0	8.41	0.00
5	8.05	0.36
10	7.64	0.77

Table C.54 Value of k_2 for 6.5 bar, 0.25 g/L NaOH and 110 °C experiment

Time (min)	Intrinsic Viscosity (dL/g)	$\eta_{10} - \eta$
0	7.64	0.00
20	7.23	0.41
50	6.69	0.95

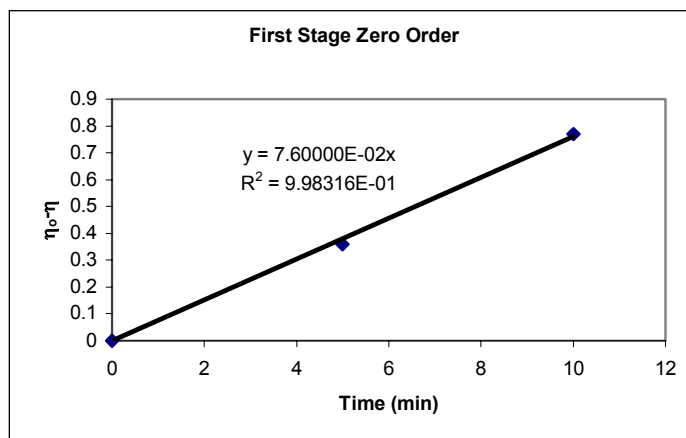


Figure C.53 Value of k_1 for 6.5 bar, 0.25 g/L NaOH and 110 °C experiment

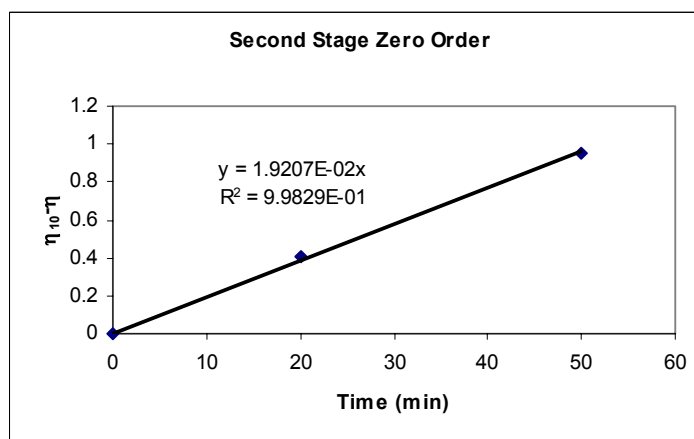


Figure C.54 Value of k_2 for 6.5 bar, 0.25 g/L NaOH and 110 °C experiment

Table C.55 Values of k_1 and k_2 for 27 set of experiments

Experiment	k_1	k_2
0.5 bar, 90 °C, 1% NaOH	1.920E-02	9.103E-03
0.5 bar, 90 °C, 3% NaOH	2.640E-02	9.483E-03
0.5 bar, 90 °C, 5% NaOH	2.840E-02	1.138E-02
0.5 bar, 100 °C, 1% NaOH	2.160E-02	1.048E-02
0.5 bar, 100 °C, 3% NaOH	2.880E-02	1.179E-02
0.5 bar, 100 °C, 5% NaOH	3.480E-02	1.248E-02
0.5 bar, 110 °C, 1% NaOH	2.520E-02	1.066E-02
0.5 bar, 110 °C, 3% NaOH	3.360E-02	1.283E-02
0.5 bar, 110 °C, 5% NaOH	4.160E-02	1.355E-02
3.5 bar, 90 °C, 1% NaOH	2.920E-02	1.103E-02
3.5 bar, 90 °C, 3% NaOH	3.800E-02	1.431E-02
3.5 bar, 90 °C, 5% NaOH	4.600E-02	1.438E-02
3.5 bar, 100 °C, 1% NaOH	3.560E-02	1.103E-02
3.5 bar, 100 °C, 3% NaOH	4.600E-02	1.331E-02
3.5 bar, 100 °C, 5% NaOH	5.360E-02	1.690E-02
3.5 bar, 110 °C, 1% NaOH	4.320E-02	1.331E-02
3.5 bar, 110 °C, 3% NaOH	5.680E-02	1.514E-02
3.5 bar, 110 °C, 5% NaOH	6.120E-02	1.855E-02
6.5 bar, 90 °C, 1% NaOH	3.680E-02	1.252E-02
6.5 bar, 90 °C, 3% NaOH	4.880E-02	1.466E-02
6.5 bar, 90 °C, 5% NaOH	5.320E-02	1.707E-02
6.5 bar, 100 °C, 1% NaOH	4.320E-02	1.266E-02
6.5 bar, 100 °C, 3% NaOH	5.480E-02	1.648E-02
6.5 bar, 100 °C, 5% NaOH	6.480E-02	1.835E-02
6.5 bar, 110 °C, 1% NaOH	4.960E-02	1.493E-02
6.5 bar, 110 °C, 3% NaOH	6.600E-02	1.831E-02
6.5 bar, 110 °C, 5% NaOH	7.600E-02	1.921E-02

C.2 Estimation of A_1 , E_{A1} , a , b , A_2 , E_{A2} , c , d

Knowing the values of k_1 , the values of A_1 , E_{A1} , a and b were estimated by applying Equation C.2.

For the calculation of E_A , Equation C.2, can be written as :

$$k_1 = k_3 \exp\left(\frac{-E_{A1}}{RT}\right) \quad (C.8)$$

where $k_3 = A_1[\text{OH}^-]^a P_{O_2}^b$ was assumed to be constant for a particular sodium hydroxide concentration and oxygen partial pressure. Equation C.8 can be written as

$$\ln(k_1) = \ln(k_3) - \frac{E_{A1}}{RT} \quad (C.9)$$

Thus, the value of E_{A1} was estimated from a regression analysis for $\ln(k_1)$ versus $[-1/(RT)]$ for the different sodium hydroxide concentrations. The average of the values obtained in this manner was 18828 J/gmol.

To get a , Equation C.8 can be written as

$$\ln(k_1) = \ln(k_4) + a \ln[\text{OH}^-] \quad (C.10)$$

where $k_4 = A_1 \exp[-E_{A1}/(RT)][P_{O_2}]^b$ is a constant for a particular temperature and oxygen pressure. The average value of a obtained was 0.26.

Similarly, to get b , Equation C.8 can be written as :

$$\ln(k_1) = \ln(k_5) + b \ln[P_{O_2}] \quad (C.11)$$

where $k_5 = A_1 \exp[-E_{A1}/(RT)][\text{OH}^-]^a$ is a constant for a particular temperature and alkali concentration. The average value of n obtained was 0.25.

Knowing E_{A1} , a and b Equation C.8 can be solved for A_1 for different sodium hydroxide concentrations and temperatures. The average value of A_1 obtained was 24.77.

Also, knowing the values of k_2 , the values of A_2 , E_{A2} , c and d were estimated by applying Equation C.3.

For the calculation of E_A , Equation C.3, can be written as :

$$k_2 = k_6 \exp\left(\frac{-E_{A2}}{RT}\right) \quad (C.12)$$

where $k_6 = A_2 [\text{OH}^-]^c P_{\text{O}_2}^d$ was assumed to be constant for a particular sodium hydroxide concentration and oxygen partial pressure. Equation C.12 can be written as

$$\ln(k_2) = \ln(k_6) - \frac{E_{A2}}{RT} \quad (C.13)$$

Thus, the value of E_{A2} was estimated from a regression analysis for $\ln(k_2)$ versus $[-1/(RT)]$ for the different sodium hydroxide concentrations. The average of the values obtained in this manner was 10592 J/gmol.

To get c, Equation C.12 can be written as

$$\ln(k_2) = \ln(k_7) + c \ln[\text{OH}^-] \quad (C.14)$$

where $k_7 = A_2 \exp[-E_{A2}/(RT)][P_{\text{O}_2}]^d$ is a constant for a particular temperature and oxygen pressure. The average value of c obtained was 0.18.

Similarly, to get d, Equation C.12 can be written as :

$$\ln(k_2) = \ln(k_8) + d \ln[P_{\text{O}_2}] \quad (C.15)$$

where $k_8 = A_2 \exp[-E_{A2}/(RT)][\text{OH}^-]^c$ is a constant for a particular temperature and alkali concentration. The average value of d obtained was 0.13.

Knowing E_{A_2} , c and d Equation C.12 can be solved for A_2 for different sodium hydroxide concentrations and temperatures. The average value of A_2 obtained was 0.542.

CURRICULUM VITAE

PERSONAL INFORMATION

Surname, Name : Dođan, İsmail
Nationality: Turkish (TC)
Date and Place of Birth: 7 January 1976, Fethiye
Marital Status: Single
Phone: +90 312 2104398
Fax: +90 312 2101264
email : idogan@metu.edu.tr

EDUCATION

Degree	Institution	Year of Graduation
MS	METU Chemical Engineering Department	2000
BS	METU Chemical Engineering Department	1998
High School	Gazi Anatolian High School, Ankara	1993

WORK EXPERIENCE

Year	Place	Enrollment
1998-Present	METU Chemical Engineering Department	Research Assistant

FOREIGN LANGUAGES

Fluency in English, Intermediate German

HONORS AND AWARDS

The Honor Award, The Foundation of Pulp and Paper of Turkish Pulp and Paper Industry, June 2000.

The Thesis of the Year Award, METU Prof. Dr. Mustafa N. Parlar Education and Research Foundation, December 2001

Middle East Technical University Chemical Engineering Department Hasan Orbey Award in Graduate Studies Ph.D., 2003

PUBLICATIONS

1. Gürüz G., Dođan İ., "Flow Sheet Optimization by the Concept of Sustainable Development in Pulp and Paper Industry", AIChE Annual Meeting 2000, Los Angeles, November 2000, Poster Presentation.
2. İ. Dođan and G. Gürüz, "Kađıt Sanayii Beyazlatma Ünitesinin Yatıřkın Durum Modellemesi", Türkiye Otomasyon Kongresi, METU, Ankara, TURKEY, 2002.
3. İ. Dođan and G. Gürüz, "Waste Minimization in a Bleach Plant", Advances in Environmental Research, Vol. 8, Iss. 3-4, pp. 359-369, 2003.
4. İ. Dođan and G. Gürüz, "Oxygen Delignification Kinetics at Ultra-Low Consistency", AIChE Annual Meeting 2003, San Francisco, November 2003, Poster Presentation.

HOBBIES

Tennis, Skiing, Reading Book, Movies